VOLUME 10 NUMBER 1 2019 ISSN 2218-7987
eISSN 2409-5508

International Journal of Mathematics and Physics

Al-Farabi Kazakh National University

The International Journal of Mathematics and Physics is a peer-reviewed international journal covering all branches of mathematics and physics. The Journal welcomes papers on modern problems of mathematics and physics, in particular, Applied Mathematics, Algebra, Mathematical Analysis, Differential Equations, Mechanics, Informatics, Mathematical Modeling, Applied Physics, Radio Physics, Thermophysics, Nuclear Physics, Nanotechnology, and etc.

International Journal of Mathematics and Physics is published twice a year by al-Farabi Kazakh National University, 71 al-Farabi ave., 050040, Almaty, Kazakhstan
website: http://ijmph.kaznu.kz/

Any inquiry for subscriptions should be send to:
Prof. Tlekkabul Ramazanov, al-Farabi Kazakh National University
71 al-Farabi ave., 050040, Almaty, Kazakhstan
e-mail: Tlekkabul.Ramazanov@kaznu.kz

EDITORIAL

The most significant scientific achievements are attained through joint efforts of different sciences, mathematics and physics are among them. Therefore publication of the Journal, which shows results of current investigations in the field of mathematics and physics, will allow wider exhibition of scientific problems, tasks and discoveries.

One of the basic goals of the Journal is to promote extensive exchange of information between scientists from all over the world. We propose publishing service for original papers and materials of Mathematical and Physical Conferences (by selection) held in different countries and in the Republic of Kazakhstan.

Creation of the special International Journal of Mathematics and Physics is of great importance because a vast amount of scientists are willing to publish their articles and it will help to widen the geography of future dissemination. We will also be glad to publish papers of scientists from all the continents.

The Journal will publish experimental and theoretical investigations on Mathematics, Physical Technology and Physics. Among the subject emphasized are modern problems of Applied Mathematics, Algebra, Mathematical Analysis, Differential Equations, Mechanics, Informatics, Mathematical Modeling, Astronomy, Space Research, Theoretical Physics, Plasma Physics, Chemical Physics, Radio Physics, Thermophysics, Nuclear Physics, Nanotechnology, and etc.

The Journal is issued on the base of al-Farabi Kazakh National University. Leading scientists from different countries of the world agreed to join the Editorial Board of the Journal.

The Journal is published twice a year by al-Farabi Kazakh National University. We hope to receive papers from many laboratories which are interested in applications of the scientific principles of mathematics and physics and are carrying out researches on such subjects as production of new materials or technological problems.

This issue of the journal is dedicated to the memory of the outstanding scientist, teacher, organizer of science and education of the Republic of Kazakhstan, doctor of physical and mathematical sciences, professor, academician of the Engineering Academy of the Republic of Kazakhstan Shaltai Smagulov. The issue of the journal contains selected scientific reports of the expanded city scientific seminar dedicated to the 70-th anniversary of Shaltai Smagulov.

IRSTI 27.41.41

The report is dedicated to the memory of my close friend and classmate D. SC.MD, Professor Smagulov S.S.

Abylkairov U.U.

al-Farabi Kazakh National University, Almaty, Kazakhstan
e-mail: U.Abylkairov@gmail.com

The Problem of Single – Determinability Equations of Navier-Stokes

Abstract. The Navier-Stokes equations describing a viscous incompressible fluid have for many decades attracted the attention of scientists working on the problem of solvability of partial differential equations and specialists in the field of numerical analysis due to numerous applications. Despite such interest, the question of the existence and uniqueness of the "on the whole" solution of the non-stationary Navier-Stokes equations in the case of three spatial variables still remains open. S. Smagulov made a great contribution to the development of the theory and numerical methods for solving initial-boundary value problems for the Navier-Stokes equations. The situation with the numerical solution of these equations is more complex. The fact is that numerical methods that have proven themselves in solving one class of problems are ineffective in solving another class. From the point of view of justification of numerical methods, there is no possibility of using a number of results. The theory of the equation of mathematical physics, since, as mentioned above, they are open to the Navier-Stokes system.
Therefore, the young scientist S. Smagulov of the 1970s of the last century, in order to work successfully in this field of mathematics, combined in himself a specialist in differential equations and also in computational mathematics.
Key words: Navier-Stokes equations, regularization, E-approximation, initial-boundary problem.

1.1. **Problem statement**. The systems of Navier-Stokes, which describes motion of viscous incompressible fluid, have the following form

$$\overrightarrow{u_t} - v\Delta\vec{u}+\nabla p + u_k\vec{u}_{x_k} = \vec{f}$$

$$div\vec{u} = 0, \vec{u}(x,0) = \vec{u}_0(x), \vec{u}|_{\partial\Omega} = 0$$

Here $\vec{u} = (u_1, u_2, u_3)$-velocity vector, p-function of hydrostatic pressure, and $\vec{f}$=(f_1, f_2, f_3)-vector-fucntion of sources, $div\, u_0$ =0, v- viscosity coefficient (value inversely proportional to the Reynolds number), solution is sought in a limited area Ω with Lipshitz border $\partial\Omega$ three-dimensional spaceR^3.

S. Smagulov, already studying at the NSU at the 4th year under the guidance of Ph.D., associate professor B.G. Kuznetsova, began to study methods for the numerical analysis of problems in hydrodynamics. Academician N.N. Yanenko closely followed his scientific growth, posed fundamental problems for solving boundary value problems for the Navier – Stokes system of equations, namely, questions of the approximation of the Navier-Stokes equations by evolutionary type equations and the substantiation of a number of difference methods for solving stationary and nonstationary hydrodynamic

equations. According to the proposed schemes, numerical calculations were carried out, the results of which were published and transferred to practical application. One of the directions of the study of approximate solutions of the Navier-Stokes equations is based on the use of difference schemes for which the difference energy a priori estimates are valid. In this case, estimates are used for the equations themselves, as well as for some of their ε-approximations.

1.2. The currently known approximations of the Navier-Stokes equations can be mainly divided into two types:

- approximations of the continuity equation (moreover, for the correctness of the approximating problem, it is necessary to make adjustments to the equations of motion)
- approximation (regularization) of only one equation of motion

ε-approximations of the Navier-Stokes equations for a viscous incompressible fluid, which were derived from physical considerations, were proposed in the papers of academician of N.N. Yanenko (by the way the author of the method of fractional steps), B.G. Kuznecov, N.N. Vladimirov [1],[2]. This idea was quickly picked up by prominent French mathematicians Jacques-Louis Lyons, Roger Themes and others. R. Temam [3],[4] proposed a different method of ε-approximation of the Navier-Stokes equations. For these equations, he studied the behavior of the solution at $\varepsilon \longrightarrow 0$, a difference scheme was constructed, for which it was shown that, under certain conditions on $\Delta t, \square, \varepsilon$ the solution of the difference problem converges to the solution of the Navier-Stokes equations. An attempt was made in [5] to substantiate difference schemes like fractional steps. We also note other regularizations of the Navier-Stokes equations.

We present an ε-approximation of the Navier-Stokes equations.

$$\frac{\partial v^\varepsilon}{\partial t} - v\Delta v^\varepsilon + v_k^\varepsilon \frac{\partial v^\varepsilon}{\partial x_k} + \frac{1}{2} v^\varepsilon div\, v^\varepsilon = f - \nabla p, \quad (1)$$

$$\varepsilon \frac{\partial p^\varepsilon}{\partial t} + \varepsilon_1 p^\varepsilon + div\, v^\varepsilon = 0. \quad (2)$$

At $\varepsilon_1 = 0$ the convergence of difference schemes for the two-dimensional case is proved under the assumption, that $\Delta t, \square, \varepsilon, \frac{\Delta t}{\varepsilon} \to 0$ and

$$\frac{\Delta t}{\sqrt{\varepsilon}\square^2} \to 0. \quad (3)$$

This restrictive condition has been removed by O.A. Ladyzhenskii [6].

We also note other regularizations of the Navier-Stokes equations, for example, E.G.Dyakonova, D.P.Kaushilayte, V.Ya.Rivkind, A.P.Oskolkov and etc.

Since 1975, a series of papers began to appear, then still a young graduate student THE VC SOAN SSSR S.Smagulov [7],[8],[9]. Two explicit finite-difference schemes are proposed that approximate a quasilinear parabolic system with a small parameter ε, which when ε = 0 degenerates into a non-stationary non-linear Navier-Stokes system. The conditions under which the solutions of these finite-difference problems converge to the exact (fairly smooth) solution of the Navier-Stokes equations are clarified. The conditions obtained are less restrictive than the similar conditions given in the papers [6],[10]. The convergence of difference schemes is investigated by the method of energy estimates. S.Smagulov in 1975 proposes an approximation of the Navier-Stokes equations, which is obtained by replacing the continuity equation with another equation. The convergence of the approximate solution that is obtained by solving the replacing system of equations, to solving the Navier-Stokes equations with the speed

$$\| v^\varepsilon - v \|^2_{V_2^1(Q_T)} = \| v^\varepsilon - v \|^2_{L^\infty\left(0,T;\, L^2(\Omega)\right)} +$$

$$+ \int_0^T \| v^\varepsilon - v \|^2_{W_2^1(\Omega)} dt \le c\varepsilon \quad (4)$$

If the solution of the Navier-Stokes equation has the following property

$$vc_\Omega - m > \delta > 0, \quad (5)$$

where m- the exact lower bound of the eigenvalues of the matrix of the strain rate tensor matrix, then the estimate (5) is uniform.

Apparently, for the first time the behavior of a strong solution of problem (1), (2) with $\varepsilon = 0$, $\varepsilon_1 > 0$ was considered in the works of S.Smagulov [11], [12] and at the same time in work P.E. Sobolevskii and V.V. Vasilev [13]

Sh. Smagulov introduced the following system:

$$v_t^\varepsilon + (v^\varepsilon \cdot \nabla) v^\varepsilon + \frac{1}{2} v^\varepsilon div v^\varepsilon = v\Delta v^\varepsilon - \nabla p^\varepsilon - \nabla Q^m, \quad (6)$$

$$\varepsilon p_t^{\varepsilon} + divv^{\varepsilon} = 0, \quad (7)$$

$$v^{\varepsilon}|_{t=0} = v_0(x),\ p^{\varepsilon}|_{t=0} = p_0(x),\ v^{\varepsilon}|_{\gamma_T}=0 \quad (8)$$

Where $Q_m = \sum_{k=1}^{m} \frac{\alpha^k p_k(x)}{k!}, \alpha(t) -$ a smooth characteristic function on (0, -∞), $p_k(x) = \frac{\partial^k p}{\partial t^k}\Big|_{t=0} -$ is found from the Navier-Stokes equation (unperturbed).

Using the obtained a priori estimates for the higher derivatives and for other structural elements of the problem, we proved the following.

Theorem. Let $f_t \epsilon L^{\infty}\left(0,T;\ L^2(\Omega)\right), f_{tt}\epsilon L^2\left(0,T;\ W_2^{-1}(\Omega)\right), \gamma \epsilon c^3$. Then there is a strong solution to problem (6) – (8) and for this solution the following estimate takes place:

$$\| v_t^{\varepsilon} \|_{L^2(0,T;\, W_2^2 \cap \dot{W}_2^1(\Omega))} + \frac{1}{\varepsilon} \| \nabla divv^{\varepsilon} \|_{L^2(Q_T)} \leq c < \infty$$

By introducing an auxiliary function $Q_m(x)$ which provides the conditions for matching at the initial time the solution of the Navier-Stokes equations and the solution of a parabolic system degenerate at ε = 0. That is, ensures equality:

$$\frac{\partial^k v^{\varepsilon}}{\partial t^k}\Big|_{t=0} = \frac{\partial^k v}{\partial t^k}\Big|_{t=0},\ \frac{\partial^k (q^{\varepsilon}+Q_m)}{\partial t^k}\Big|_{t=0} = \frac{\partial^k q}{\partial t^k}\Big|_{t=0}$$

Next, we study the internal smoothness of spatial variables.

Sh. Smagulov in 1976-1977, together with Professor Kasimov A.V. the strongest result was obtained on the unambiguous generalized and strong solvability of the diffusion model of an inhomogeneous fluid, which was later called the Kazhikhov-Smagulov equation.

We formulate the initial-boundary problem for this system:

$$\rho\left[\frac{\partial v}{\partial t} + (v \cdot \nabla)\right] -$$

$$-\lambda[(\nabla\rho \cdot \nabla)v + (v \cdot \nabla)\nabla\rho] = \mu\Delta v - \nabla p + \rho f, \quad (9)$$

$$div\ \vec{v} = 0;\ \frac{\partial \rho}{\partial t} + (v \cdot \nabla)\rho = \lambda\Delta\beta \quad (10)$$

Let the mixture move in a limited area $\Omega \subset R^3$ with a fairly smooth border Y (for example, twice continuously differentiable). For simplicity, let us assume that the boundary Y is impenetrable and there is no mass transfer between the solution and the external medium:

$$v|_{\mathrm{Y}} = 0;\ \frac{\partial \rho}{\partial \vec{n}}\Big|_{\mathrm{Y}} = 0;\ t\epsilon[0,T], \quad (11)$$

where $\vec{n} = n_1, n_2, n_3$- unit vector of external normal Y. Along with the task of mass flow through the boundary Y, another physically reasonable condition can also be considered, when the density values are known on Y:

$$\rho|_{\mathrm{Y}} = \rho_{\mathrm{Y}}(x,t);\ x\epsilon\ \gamma;\ t\epsilon[0,T]$$

In addition to the boundary conditions, we supplement the problem with the given by Cauchy:

$$v|_{t=0} = v_0(x);\ \rho|_{t=0} = \rho_0(x);\ x\epsilon\ \Omega \quad (12)$$

Regarding $\rho_0(x)$ (also $\rho_{\mathrm{Y}}(x,t)$) we will assume that this is a positive bounded function:

$$0 < vraimin\ \rho_0(x) = \underset{\Omega}{} = m \leq \rho_0(x) \leq M = \underset{\Omega}{vraimax}\ \rho_0(x) < \infty \quad (13)$$

We formulate the main results for this problem obtained by Sh. Smagulov

Theorem 1. Let $v_0(x)\epsilon H;\ \rho_0(x)\epsilon W_2^1(\Omega), m \leq \rho_0(x) \leq M;$

$$f(t) = f(x,t) \in L^p\left(0,T;L^q(\Omega)\right), \text{ где}$$

$$p\epsilon[1,2];\ q\ \epsilon\left[\frac{6}{5}, 2\right];\ \frac{1}{P} + \frac{3}{2q} \leq \frac{7}{4}$$

Then there is at least one weak solution to problem (9) – (13) if the constants M, m, μ and λ satisfy

$$\lambda \leq 2\mu(M-m)^{-1} \quad (14)$$

Theorem 2.

If $v_0(x)\epsilon V;\ \rho_0(x)\epsilon W_2^1(\Omega), f(t)\epsilon L^2(Q_T)$ and flow is plane-parallel, i.e. $x = (x_1, x_2), v = (v_1, v_2)$ then, if condition (14) is fulfilled on any finite time interval (0, T), there is a unique strong solution to problem (9) – (13).

And this task is brought by Shaltay Smagulovich to practical results, i.e an approximation of the problem (9) – (13) is proposed, the theorems of convergence, the stability of difference schemes are proved.

1.3. The important step in the scientific career of Sh.Smagulov is an adoptation of ideas of fictitious area method for the first time for nonlinear equations of mathematical physics, namely for the Navier-Stokes system of equations during 1978-1979 in papers [14]-[15]. Fictitious areas method (briefly f.a.m.) are pioneers for simple models (Saulev1963 г; lebedev 1964 y, and etc.) reduces the solution of the boundary in regions of complex shape to the solution of boundary-value problems in regions of simple shape (for example, a rectangle or parallelepiped). The reduction is due to the fact that in the domains of simple form, boundary value problems and / or their grid analogues can be solved by efficient, cost-effective methods. There are several fundamentally different approaches for such information. The method of fictitious areas for the nonlinear Navier-Stokes system. Consider a boundary value problem for a nonlinear equation.$(u^\varepsilon \cdot \nabla)u^\varepsilon = v\Delta u^\varepsilon - \nabla p^\varepsilon + f$ в Ω_1

$$div\, u^\varepsilon = 0 \qquad (15)$$

$$(u^\varepsilon \cdot \nabla)u^\varepsilon = v\Delta u^\varepsilon - \frac{1}{2}\, u^\varepsilon div\, u^\varepsilon - \frac{1}{\varepsilon}\, u^\varepsilon \text{ в } \Omega_2$$

$$u^\varepsilon|_{\gamma^+} = u^\varepsilon|_{\gamma^-}, u^\varepsilon|_r = 0,$$

$$v\frac{\partial u^\varepsilon}{\partial \vec{n}} - p^\varepsilon \delta_1 \vec{n}|_{\gamma^+} = v\frac{\partial u^\varepsilon}{\partial \vec{n}}\Big|_{\gamma^-}.$$

The behavior of the solution of problem (15) is investigated as ε → 0. An a priori estimate of the solution to the problem (15) was obtained :

$$v\|u_x^\varepsilon\|_\Omega^2 + \frac{1}{\varepsilon}\,||u^\varepsilon||_{\Omega_2}^2 \le \|f\|_{W_2^{-1}(\Omega)} \qquad (16)$$

Further, the existence of at least one generalized solution of problem (15) and its weak convergence in $W_2^1(\Omega)$ to a generalized solution of the stationary Navier – Stokes equation is proved. The rationale for the method of fictitious domains for the Navier-Stokes equations and equations for the current function and velocity vortex with inhomogeneous boundary conditions is carried out for the first time. The obtained estimates of the convergence of the solution of the auxiliary problem to the solution of the original problem.

Professor Sh. Smagulov and his students for the first time used the method of fictitious areas to describe incompressible fluid flows in multiply connected areas based on the equations for the current function and velocity vortex, which is a fundamentally new approach to solving the problem of setting boundary conditions for the current function. For the first time carried out the substantiation mf. for problems of flow of a viscous incompressible fluid with inhomogeneous boundary conditions in regions with curvilinear boundaries and complex geometry.

Numerical algorithms based on the method of fictitious areas were developed, which allow studying the flow characteristics of a viscous incompressible fluid around an obstacle in a channel with curvilinear boundaries, characteristics of a convective motion of a viscous incompressible fluid in areas of complex geometry [16-18].

1.4 The next stage of scientific research of Smagulov Shaltay is the problem of the existence of global solutions of the Navier-Stokes equation of compressible continuous media.

The first theorem on the existence of a solution for the Navier-Stokes equations of compressible viscous fluid was obtained by John Nash [19] in 1962, the future winner of the Nobel Prize in economics. He proved the existence theorem for the classical solution of the Cauchy problem “in the small” in time. Somewhat different methods his result was repeated and summarized in the works N. Itay [20], A.I. Wolpert, S.I. Hudyaev [21]

Significant development of non-local theory received in the works A.V. Kozhihov [22-23] and his students V.V. Sheluhin [24], V.A. Vaigant [25] и др.

The first theorems of solvability “on the whole” with respect to time for the model of magnetic gas dynamics were obtained in the work of Sh. Smagulov [26] in the case of a barotropic motion of a viscous gas. In the work of his student A.A.Durmagambetov [27], [28], [29], essential results on the solvability of boundary value problems and the Cauchy problem for degenerate equations of a viscous heat-conducting gas have been obtained. Also, another talented student of Smagulova, Sh. Z.E. Konysbaev, proved the correctness of the initial-boundary value problem for a system of equations of a viscous barotropic gas with an initial density that has degeneracy and takes the magnetic field into account [30–32].

1.4.1 Formulation of the problem. The equations of magnetic gas dynamics in Lagrangian coordinates are:

$$\frac{\partial v}{\partial t} - \frac{\partial u}{\partial x} = 0, v = \frac{\rho^0}{\rho},$$

$$\rho^0 \frac{\partial u}{\partial t} = \mu \frac{\partial}{\partial x}\left(\frac{1}{v}\frac{\partial u}{\partial x}\right) - \frac{\partial p}{\partial x} - \mu_e H \frac{\partial H}{\partial x},$$

$$p = k\rho^0 \frac{\theta}{v},$$

$$\rho^0 \frac{\partial \theta}{\partial t} = \lambda \frac{\partial}{\partial x}\left(\frac{1}{v}\frac{\partial \theta}{\partial x}\right) -$$

$$-p\frac{\partial u}{\partial x} + \frac{\mu}{v}\left(\frac{\partial u}{\partial x}\right)^2 + \frac{\mu_e \mu_H}{v}\left(\frac{\partial H}{\partial x}\right)^2 \qquad (17)$$

$$\frac{\partial}{\partial t}(v\mathrm{H}) = \mu_H \frac{\partial}{\partial x}\left(\frac{1}{v}\frac{\partial H}{\partial x}\right).$$

Initially, Cauchy data is known:

$$u|_{t=0} = u^0(x);\ \theta|_{t=0} = \theta^0(x);\ H|_{t=0} =$$

$$= H^0(x);\ v|_{t=0} = 1;\ x\epsilon\ [0,1], \qquad (18)$$

where $(\rho^0, u^0, \theta^0, H^0)$ – continuous, (ρ^0, θ)-limited, non-negative and ρ^0 has degeneration when x=1, i.e. $\rho^0(1) = 0$

$$0 \le \rho^0(\mathrm{x}) \le c < \infty, 0 < m_0 \le \theta^0(\mathrm{x}) \le M_0 < \infty$$

The required functions satisfy the boundary conditions:

$$u|_{x=0} = u|_{x=1} = \left.\frac{\partial \theta}{\partial x}\right|_{x=0} = \left.\frac{\partial \theta}{\partial x}\right|_{x=1} =$$

$$= H|_{x=0} = H|_{x=1} = 0 \qquad (19)$$

and the conditions of approval are met.

Theorem. Let the initial data (18) has the following properties of smoothness:

$$(\rho^0(x), u^0(x), \theta^0(x))\epsilon W_2^1(\Omega),$$

$$\frac{p_x^0(x)}{(p^0)^{\frac{3}{4}}(x)}\epsilon\ L^2(\Omega),$$

$$\frac{p^0(x)}{\inf p^0(s)} <$$

$$c, \left(\sqrt{p^0}u_t\Big|_{t=0}, \sqrt{p^0}\theta_t\Big|_{t=0}\right)\epsilon\ L^2(\Omega), H^0(x)\epsilon W_2^2(\Omega).$$

$$0 \le s \le x$$

Then there is a unique generalized solution to the problem (17)-(19), where $v(x,t)$ strictly positive, bounded function, $\rho^0(x)\ \theta(x,t)$-limited function.

The proof of the theorem is carried out by the method of regularizations. An interesting issue is the study of the correctness of difference schemes of the model of magnetic gas dynamics in Euler variables. In the one-dimensional case, the correctness of difference schemes in Lagrange variables is well studied in the work of Sh. Smagulov and B. Rysbayev [33].

Conclusion

Scientific works of Sh.S.Smagulova are devoted to the creation and study of efficient algorithms of computational mathematics, the development of numerical methods for the Navier-Stokes equations of great practical and theoretical value, a rigorous mathematical analysis of the solvability of initial-boundary value problems for nonlinear equations of composite, non-classical, degenerate types mathematical physics. Sh.S.Smagulov paid much attention to the problems of mathematical modeling and computer technologies in oil production, information technologies for solving practical problems of science and technology.

In the field of computational mathematics, Sh.S.Smagulov made a significant contribution to the development of difference schemes. He constructed and investigated difference schemes for classes of equations:Для стационарных и нестационарных уравнений навье-Стокса

- For heat convection system
- For equations of gas dynamics and magnetic gas dynamics.

Sh. Smagulov is the author of the method of fictitious domains for the non-linear Navier-Stokes equation. For the first time, the method of fictitious regions was applied to describe incompressible fluid flows in one or multiply connected domains, and the method of fictitious domains with non-uniform boundary in regions with curvilinear boundaries was substantiated.

Developed numerical algorithms based on the method of fictitious areas.

- Sh. Smagulov made a great contribution to the development of the theory of solvability of the non-linear Navier-Stokes equations, the equations of thermal convection, magnetic gas dynamicsю
- The correctness of the problems of degenerate equations of magnetic gas dynamics

- The correctness of the problems of degenerate equations of a reacting mixture of gases

Solvability and convergence of the ε-approximation of the Navier-Stokes equations, the temperature model of homogeneous and inhomogeneous liquids; and taking into account the dissipation of energy.

References

1. N.N. Yanenko. The method of fractional steps for solving multidimensional problems of mathematical physics, Novosibirsk, Science (1967): 225.
2. N.N. Vladimirova, B.G. Kuznecov, N.N. Yanenko. Numerical calculation of symmetric flow of a plate around a plane flow of a viscous incompressible fluid. Some questions of computational and applied mathematics. Novosibirsk (1966): 29-35.
3. Temam R. "Une method d'approximation dela solution des-equations de Navier-Stokes." Bull.Soc.Math.France 96 (1968): 115-152.

4-5. Temam R. Sur l'approximation de la solution des equations de Navier-Stokes parla method de pas fractionnaries (I)(II),Arzhive Rat.mech.Anal.,32.

6. O.A. Ladyzhenskaya. Mathematical problems of the dynamics of a viscous incompressible fluid. Science (1970): 288.
7. A. Smagulova. "On a non-linear equation approximating the Navier-Stokes equation." Proceedings of the Vth All-Union Seminar on Numerical Methods of Viscous Fluid Mechanics Novosibirsk (1975): 123-134.
8. B.G. Kuznecov, Sh. Smagulov. "On difference schemes with a small parameter approximating the Navier-Stokes equations." Proceedings of the Vth All-Union Seminar on Numerical Methods of Viscous Fluid Mechanics, Novosibirsk (1975): 109-122.
9. B.G. Kuznecov, Sh. Smagulov. Approximation of the hydrodynamic equation. " Numerical Methods of Continuum Mechanics" no. 2, (1975): 158-175.
10. A.P. Oskolkov. "On some convergent difference schemes for the Navier-Stokes equations." Proceedings of the Steklov mathematical Institute 125 (1973): 164-172.
11. B.G. Kuznecov, Sh. Smagulov. "On the rate of convergence of solutions of a single system of equations with a small parameter to the solution of the Navier-Stokes equations." Mathematical models of fluid flow. ITAM SB AS USSR Novosibirsk (1978): 158-175.
12. Sh. Smagulov. "On parabolic approximation of the Navier-Stokes equations." Numerical Methods of Continuum Mechanics, VTS and ITPM of Soan USSR vol. 10, no. 1979: 137-149.
13. P.E. Sobolevskii, V.V. Vasilev. On one E-approximation of the Navier-Stokes equations. "Numerical Methods of Continuum Mechanics" vol. 9, no. 5 (1978): 115-139.
14. A.N. Bugrov, Sh. Smagulov. "The method of fictitious domains in boundary value problems for the Navier-Stokes equations." Mathematical models of fluid flow (1978): 79-90.
15. Sh. Smagulov. "The method of fictitious domains for boundary value problems of the Navier-Stokes equations." VTS SO AN USSR. Preprint. 68: 22.
16. A.V. Kazhihov, Sh. Smagulov. "On the correctness of boundary problems of a diffusion model of an inhomogeneous fluid." DAN SSSR vol. 234, no. 2 (1377): 330-332.
17. Sh. Smagulov. "Approximation of the equations of one model of an inhomogeneous fluid." Numerical Methods of Continuum Mechanics vol. 8, no. 2 (1977): 112-124.
18. Sh. Smagulov. "On a variant of approximation of the Navier-Stokes equations." Partial differential equations, Novosibirsk (1980): 57-62.
19. J. Nesh. "The problem de Cauchy pour les equation diffeentielles d'un fluide general." Bull.Soc.Math.France vol. 90, no.4 (1962): 487-497.
20. Itaya N. "The existence and uniqueness of the solution of the equations describing compressible viscous fluid flow." proc. Jap. Acad. vol. 46, no. 4 (1970): 379-382.
21. Wolpert A.I., Hudlev S.I. "On the Cauchy problem for composite systems of nonlinear differential equations." Mathematical collection vol.87, no.4 (1972): 504-528.
22. Kazhihov A.V. "The correctness "on the whole" of mixed boundary value problems for a model system of equations of a viscous gas." Dynamics of continuous media no. 21(1975): 18-47.
23. Kajihov A.V. On the Cauchy problem for viscous gas equations." Siberian mathematical journal vol. 23, no.1 (1982): 60-64.
24. Kajihov A.V., Sheluhin V.V. "Unambiguous solvability of the initial-boundary value problems for the one-dimensional viscous gas equations." Applied mathematics and mechanics vol. 41, no. 2 (1977): 282-291.

25. Vaigant V.A., Kazhihov A.V. “On the existence of global solutions of the two-dimensional Navier-Stokes equations compressible viscous fluid” Siberian mathematical journal vol. 36, no.6 (1995): 1283-1316.

26. Smagulov Sh. “On the correctness of some problems for the equations of magnetic hydrodynamics.” Mate.models of fluid flows. Novosibirsk : In-t Theor. And PM .mechanics of USSR Academy of Sciences (1978): 257-266.

27. Durmaganbetov A.A. Solvability of some nonlinear problems of gas dynamics: Thesis of candidate of Phys.-math. sciences': 01.01.02. Almaty (1987): 75.

28. Smagulov Sh., Durmaganbetov A.A., Iskenderova D.A. “The Cauchy problem for the equations of magnetic gas dynamics.” Differential equations vol. 29, no.2 (1993): 337-348.

29. Smagulov Sh., Iskenderova D.A. The Cauchy problem for the equations of a viscous heat-conducting gas with a degenerate density // Journal of Computational Mathematics and Mathematical Physics. – 1993. – T. 33, no. 8. – C. 1251-1259.

30. Smagulov Sh., Konysbaev Zh.E. “On the correctness of the initial-boundary value problem for the equations of a viscous heat-conducting gas with a degenerate density.” Continuum dynamics vol. 93 (1989):119-130.

31. Smagulov Sh. Iskenderova J.A. “The Caushy problem for the equations of a viscous heat – conducting gas with degenerate density.” Comput.math.and math.phys vol 29, no.8 (1993): 1109-1117.

32. Smagulov Sh., Ourmaganbetov A.A., Iskenderova J.A. “The Caushy problem for the equations of magnetic-gas dynamics.” Different. Equations vol. 29, no. 2 (1993): 278-288.

33. Smagulov Sh., Rysbaev B.R. “On convergent difference schemes for viscous gas equations.” Doc.USSR ACADEMY OF SCIENCES vol. 287, no. 3 (1988): 558-559.

IRSTI 27.31.15

[1,*]S. Aisagaliev, [1]Zh. Zhunussova, [2]H. Akca

[1]Al-Farabi Kazakh National University, Almaty, Kazakhstan
[*]e-mail: Serikbai.Aisagaliev@kaznu.kz,
[2]Professor of Applied Mathematics, Abu-Dhabi University, Abu-Dhabi, UAE
e-mail: Haydar.Akca@adu.ac.ae

Construction of a solution for optimal control problem with phase and integral constraints

Abstract. A method for solving the Lagrange problem with phase restrictions for processes described by ordinary differential equations without involvement of the Lagrange principle is supposed. Necessary and sufficient conditions for existence of a solution of the variation problem are obtained, feasible control is found and optimal solution is constructed by narrowing the field of feasible controls. The basis of the proposed method for solving the variation problem is an immersion principle. The essence of the immersion principle is that the original variation problem with the boundary conditions with phase and integral constraints is replaced by equivalent optimal control problem with a free right end of the trajectory. This approach is made possible by finding the general solution of a class of Fredholm integral equations of the first order. The scientific novelty of the results is that: there is no need to introduce additional variables in the form of Lagrange multipliers; proof of the existence of a saddle point of the Lagrange functional; the existence and construction of a solution to the Lagrange problem are solved together.

Key words: immersion principle, feasible control, integral equations, optimal control, optimal solution, minimizing sequence.

Introduction

One of the methods for solving the variational calculus problem is the Lagrange principle. The Lagrange principle makes it possible to reduce the solution of the original problem to the search for the extremum of the Lagrange functional obtained by introducing auxiliary variables (Lagrange multipliers).

The Lagrange principle is the statement about the existence of Lagrange multipliers, satisfying a set of conditions when the original problem has a weak local minimum. The Lagrange principle gives the necessary condition for a weak local minimum and it does not exclude the existence of other methods for solving variational calculus problems unrelated to the Lagrange functional.

The Lagrange principle is devoted to the works [1-3]. A unified approach to different extremum problems based on the Lagrange principle is described in [4].

In the classical variational calculus, it is assumed that the solution of the differential equation belongs to the space $C^1(I,R^n)$, and the control $u(t)$, $t \in I$ is from the space $C^1(I,R^m)$, in optimal control problems [5] the solution $x(t) \in KC^1(I,R^n)$, and the control $u(t) \in KC(I,R^m)$. In this work, the control $u(t)$, $t \in I$ is chosen from $L_2(I,R^m)$ and the solution $x(t)$, $t \in I$ is an absolutely continuous function on the interval $I = [t_0, t_1]$. For this case solvability and uniqueness of the initial problem for differential equation are given in [4, 6-8].

The purpose of this work is to create a method for solving the variational calculus problem for the processes described by ordinary differential equations with phase and integral constraints that

differ from the known methods based on the Lagrange principle. It is a continuation of the research outlined [9-10].

Problem statement

We consider the following problem: minimize the functional

$$J(u(\cdot),x_0,x_1)= \\ =\int_{t_0}^{t_1} F_0(x(t),u(t),x_0,x_1,t)dt \to inf \quad (1.1)$$

at conditions

$$\dot{x} = A(t)x + B(t)f(x,u,t),\ \ t \in I = [t_0,t_1] \quad (1.2)$$

with boundary conditions

$$(x(t_0)) = x_0, x(t_1) = x_1) \in S_0 \times S_1 = S \subset R^{2n} \quad (1.3)$$

in the presence of phase constraints

$$x(t) \in G(t) : G(t) = \\ = \{x \in R^n \,/\, \omega(t) \le Q(x,t) \le \phi(t),\ \ t \in I\},$$

and integral constraints

$$g_j(u(\cdot),x_0,x_1) \le 0,$$

$$j = \overline{1,m_1};\ \ g_j(u(\cdot),x_0,x_1) = 0, \quad (1.4)$$

$$j = \overline{m_1+1,m_2},$$

$$g_j(u(\cdot),x_0,x_1) = \\ =\int_{t_0}^{t_1} f_{0j}(x(t),u(t),x_0,x_1,t)dt, \quad (1.5)$$

$$j = \overline{1,m_2}.$$

where the control

$$u(\cdot) \in L_2(I,R^m). \quad (1.6)$$

Here $A(t)$, $B(t)$ are matrices with piecewise-continuous elements of orders $n \times n$, $n \times r$, respectively, a vector function $f(x,u,t) = (f_1(x,u,t),\ldots,f_r(x,u,t))$ is continuous with respect to the variables $(x,u,t) \in R^n \times R^m \times I$, satisfies the Lipschitz condition by x, i.e.

$$|f(x,u,t) - f(y,u,t)| \le l(t)|x-y|, \\ \forall (x,u,t),(y,u,t) \in R^n \times R^m \times I \quad (1.7)$$

and the condition

$$|f(x,u,t)| \le c_0(|x| + |u|^2) + c_1(t), \\ \forall (x,u,t), \quad (1.8)$$

where $l(t) \ge 0$, $l(t) \in L_1(I,R^1)$, $c_0 = const > 0$, $c_1(t) \ge 0$, $c_1(t) \in L_1(I,R^1)$.

The vector function $F(x,t) = (F_1(x,t),\ldots,F_s(x,t))$ is continuous with respect to the variables $(x,t) \in R^n \times I$. Function $f_0(x,u,x_0,x_1,t) = (f_{01}(x,u,x_0,x_1,t),\ldots \\ \ldots, f_{0m_2}(x,u,x_0,x_1,t))$ satisfies the condition

$$|f_0(x,u,x_0,x_1,t)| \le c_2(|x| + |u|^2 + |x_0| + |x_1|) + \\ + c_3(t),$$

$$\forall (x,u,x_0,x_1,t),(y,u,x_0,x_1,t) \in R^n \times \\ \times R^m \times R^n \times R^n \times I,$$

$$c_2 = const \ge 0,\ \ c_3(t) \ge 0,\ \ c_3(t) \in L_1(I,R^1).$$

Scalar function $F_0(x,u,x_0,x_1,t)$ is defined and continuous with respect to the variables together with partial derivatives by variables (x,u,x_0,x_1), $\omega(t)$, $\varphi(t)$, $t \in I$ – are given s– dimensional functions. S is given bounded convex closed set of R^{2n}, the time moments t_0,t_1 are fixed.

In particular, the set $S = \{(x_0,x_1) \in R^{2n} / H_j(x_0,x_1) \le 0, \quad j = \overline{1,p_1}; \\ < a_j,(x_0,x_1) >= 0, \quad j = \overline{p_1+1,p_2}\}$, where $H_j(x_0,x_1)$, $j = \overline{1,p_1}$ are convex functions, $a_j \in R^{2n}$, $j = \overline{p_1+1,p_2}$ are given vectors.

Note, that if the conditions (1.7), (1.8) are satisfied for any control $u(\cdot) \in L_2(I,R^m)$ and the initial condition $x(t_0) = x_0$ of the differential

equation (1.2) has a unique solution. $x(t),\ t \in I$. This solution has derivative $\dot{x} \in L_2(I, R^n)$ and satisfies equation (1.2) for almost all $t \in I$.

It should be noted that integral constraints

$$g_j(u(\cdot), x_0, x_1) = \int_{t_0}^{t_1} f_{0j}(x(t), u(t), x_0, x_1, t)dt \le 0, \quad j = \overline{1, m_1}, \tag{1.9}$$

by introducing additional variables $d_j \ge 0$, $j = \overline{1, m_1}$, can be written in the form

$$g_j(u(\cdot), x_0, x_1) = -d_j, \quad j = \overline{1, m_1}.$$

Let the vector be $\bar{c} = (-d_1, \ldots, -d_{m_1}, 0, 0, \ldots, 0) \in R^{m_2}$, where $d_j \ge 0$, $j = \overline{1, m_1}$. Let a set be $Q = \{\bar{c} \in R^{m_2} / d_j \ge 0,\ j = \overline{1, m_1}\}$, where $d_j \ge 0$, $j = \overline{1, m_1}$ are unknown numbers.

Definition 1.1. The triple $(u_*(t), x_0^*, x_1^*) \in U \times S_0 \times S_1$ is called by admissible control for the problem (1.1) – (1.6), if the boundary problem (1.2) – (1.6) has a solution. A set of all admissible controls is denote by Σ, $\Sigma \subset U \times S_0 \times S_1$.

From this definition it follows that for each element of the set Σ the following properties are satisfied: 1) the solutions $x_*(t),\ t \in I$ of the differential equation (1.2), issuing from the point $x_0^* \in S_0$, satisfy the condition $x_*(t_1) = x_1^* \in S_1$, and also $(x_0^*, x_1^*) \in S_0 \times S_1 = S$; 2) the inclusion $x_*(t) \in G(t),\ t \in I$ holds; 3) for each element of the set Σ we have the equality $g(u(\cdot), x_0, x_1) = \bar{c}$, where

$$g(u_*(\cdot), x_0^*, x_1^*) = (g_1(u_*(\cdot), x_0^*, x_1^*), \ldots, g_{m_2}(u_*(\cdot), x_0^*, x_1^*)).$$

The following problems are set:

Problem 1.2. *Find the necessary and sufficient conditions for the existence of a solution of the boundary value problem (1.2) – (1.6).*

Note, that the optimal control problem (1.1) – (1.6) has a solution if and only if the boundary value problem (1.2) – (1.6) has a solution.

Problem 1.3. *Find an admissible control* $(u_*(t), x_0^*, x_1^*) \in \Sigma \subset U \times S_0 \times S_1$.

If problem 1.2. has a solution, then there exists an admissible control.

Problem 1.4. *Find the optimal control* $\bar{u}_*(t) \in U(t)$, *the point* $(\bar{x}_0^*,\ \bar{x}_1^*) \in S_0 \times S_1 = S$ *and the optimal trajectory* $\bar{x}_*(t; t_0, \bar{x}_0^*),\ t \in I$, where $\bar{x}_*(t) \in G(t),\ t \in I,\ \bar{x}_*(t_1) = \bar{x}_1^* \in S_1$, $g_j(\bar{u}_*(\cdot), \bar{x}_0^*, \bar{x}_1^*) \le 0,\ j = \overline{1, m_1},\ g_j(\bar{u}_*(\cdot), \bar{x}_0^*, \bar{x}_1^*) = 0,$ $j = \overline{m_1 + 1, m_2},\ J(\bar{u}_*(\cdot), \bar{x}_0^*, \bar{x}_1^*) = \inf J(\bar{u}(\cdot), \bar{x}_0, \bar{x}_1),$ $\forall (\bar{u}(\cdot), \bar{x}_0, \bar{x}_1) \in L_2(I, R^m) \times S_0 \times S_1$.

One of the methods for solving the problem of variation calculus is the Lagrange principle. The Lagrange principle allows to reduce the solution of the original problem to the search for an extremum of the Lagrange functional obtained by introducing auxiliary variables (Lagrange multipliers).

In the classical variation calculus, it is assumed that the solution of the differential equation (1.2) belongs to the space $C^1(I, R^n)$ and the control *u(t), t* $\in I$ of the space $C(I, R^m)$ in the optimal control problems [5], the solution $x \in KC^l(I, R^n)$ and control $u(t) \in KC^l(I, R^m)$. In this paper, the control *u(t), t* $\in I$ is chosen from $L_2(I, R^m)$, and the solution *x(t), t* $\in I$ is an absolutely continuous function on the interval $I = [t_0, t_1]$. For this case, the existence and uniqueness of the solutions of the initial problem for equation (1.2) are presented in the references [4, 6, 7, 8].

The purpose of this paper is to create a method for solving the problem of the variation calculus for processes described by ordinary differential equations with phase and integral constraints that differ from the known methods based on the Lagrange principle. It is a continuation of the scientific research presented in [9-16].

Existence of a solution

We consider the following optimal control problem: minimize the functional

$$I_1(u(\cdot), p(\cdot), v_1(\cdot), v_2(\cdot), x_0, x_1, d) = \int_{t_0}^{t_1} F_1(q(t), t) \to \inf \tag{2.1}$$

$$\dot{z} = A_1(t)z + B_1(t)v_1(t) + B_2v_2(t),\ z(t_0) = 0,\ t \in I \quad (2.2)$$

$$v_1(\cdot) \in L_2(I, R^r),\ v_2(\cdot) \in L_2(I, R^{m_2}), \quad (2.3)$$

$$p(t) \in V(t),\ u(\cdot) \in L_2(I, R^m),\ (x_0, x_1) \in S_0 \times S_1 = S,\ d \in \Gamma. \quad (2.4)$$

We introduce the following notations: $H = L_2(I, R^m) \times L_2(I, R^s) \times L_2(I, R^r) \times \times L_2(I, R^{m_2}) \times R^n \times R^n \times R^{m_1}$, $X = L_2(I, R^m) \times V \times L_2(I, R^r) \times \times L_2(I, R^{m_2}) \times S_0 \times S_1 \times \Gamma \subset H$, vector function $\theta(t) = (u(t), p(t), v_1(t), v_2(t), x_0, x_1, d) \in X \subset H$, $q(t) = (z(t), z(t_1), \theta(t))$.

The optimization problem (2.3) – (2.6) can be represented in the form:

$$I_1(\theta(\cdot)) = \int_{t_0}^{t_1} F_1(q(t), t) \to \inf,\ \theta(\cdot) \in X \subset H.$$

Let the set be

$$X_* = \{\theta_*(\cdot) \in X \mid I_1(\theta_*(\cdot)) = \inf_{\theta \in X} I_1(\theta(\cdot))\}.$$

Lemma 2.1. *Let the matrix be positive definite* $T(t_0, t_1) > 0$. *In order to the boundary value problem (1.2) – (1.6) have a solution, it is necessary and sufficient that* $\lim_{n\to\infty} I_1(\theta_n) = I_{1*} = \inf_{\theta \in X} I_1(\theta) = 0$, *where* $\{\theta_n(\cdot)\} \subset X$ *is a minimizing sequence in the problem (2.1) – (2.4).*

Proof of the lemma follows from Theorem 2.3. and Lemmas 2.4. and 2.5. [9].

Theorem 2.2. *Let the matrix be* $T(t_0, t_1) > 0$, *the function* $F_1(q,t)$ *be defined and continuous in the set of variables* (q,t) *together with the partial derivatives with respect to* q *and satisfies the Lipschitz conditions*

$$| F_{1q}(q + \Delta q, t) - F_{1q}(q, t) | \le l\, | \Delta q |,\ t \in I, \quad (2.5)$$

where

$$F_{1q}(q,t) = (F_{1z}(q,t), F_{1z(t_1)}(q,t), F_{1u}(q,t), F_{1p}(q,t), F_{1v_1}(q,t), F_{1v_2}(q,t), F_{1x_0}(q,t), F_{1x_1}(q,t), F_{1d}(q,t)),$$

$$q = (z, z(t_1), u, p, v_1, v_2, x_0, x_1, d) \in R^{n+m_2} \times R^{n+m_2} \times \times R^m \times R^s \times R^r \times R^{m_2} \times R^n \times R^n \times R^{m_1},$$

$$\Delta q = (\Delta z, \Delta z(t_1), \Delta u, \Delta p, \Delta v_1, \Delta v_2, \Delta x_0, \Delta x_1, \Delta d),\ l = const > 0.$$

Then the functional (2.1) under the conditions (2.2) – (2.4) is continuously Frechet differentiable, the gradient $I_1'(\theta) = (I_{1u}'(\theta), I_{1p}'(\theta), I_{1v_1}'(\theta), I_{1v_2}'(\theta), I_{1x_0}'(\theta), I_{1x_1}'(\theta), I_{1d}'(\theta)) \in H$ *at any point* $\theta \in X$ *is calculated by the formula*

$$I_{1u}'(\theta) = F_{1u}(q(t),t),\ I_{1p}'(\theta) = F_{1p}(q(t),t),\ I_{1v_1}'(\theta) = = F_{1v_1}(q(t),t) - B_1^*(t)\psi(t),$$

$$I_{1v_2}'(\theta) = F_{1v_2}(q(t),t) - B_2^*\psi(t),\ I_{1x_0}'(\theta) = \int_{t_0}^{t_1} F_{1x_0}(q(t),t)dt,$$

$$I_{1x_1}'(\theta) = \int_{t_0}^{t_1} F_{1x_1}(q(t),t)dt,\ I_{1d}'(\theta) = \int_{t_0}^{t_1} F_{1d}(q(t),t)dt, \quad (2.6)$$

where $z(t)$, $t \in I$ is the solution of the differential equation (2.2), and the function $\psi(t)$, $t \in I$ is the solution of the conjugate system

$$\dot{\psi} = F_{1z}(q(t),t) - A_1^*(t)\psi,\ \psi(t_1) = = -\int_{t_0}^{t_1} F_{1z(t_1)}(q(t),t)dt. \quad (2.7)$$

In addition, the gradient $I_1'(\theta)$, $\theta \in X$ *satisfies the Lipschitz condition*

$$\| I_1'(\theta_1) - I_1'(\theta_2) \| \le K \| \theta_1 - \theta_2 \|, \forall \theta_1, \theta_2 \in X, \quad (2.8)$$

where $K = const > 0$.

Proof. Let $\theta(t), \theta(t) + \Delta\theta(t) \in X$, $z(t, v_1, v_2)$, $z(t, v_1 + \Delta v_1, v_2 + \Delta v_2)$, $t \in I$ be a solution of the system (2.2), (2.3). Let $z(t, v_1 + \Delta v_1, v_2 + \Delta v_2) = z(t, v_1, v_2) + \Delta z(t)$, $t \in I$. Then

$$|\Delta z(t)| \le C_1 \|\Delta v_1\| + C_2 \|\Delta v_2\|. \quad (2.9)$$

The increment of the functional (see (2.5))

$$\Delta I_1 = I_1(\theta+\Delta\theta) - I_1(\theta) =$$
$$= \int_{t_0}^{t_1} [F_1(q(t)+\Delta q(t),t) - F_1(q(t),t)]dt =$$
$$= \int_{t_0}^{t_1} [\Delta u^*(t)F_{1u}(q(t),t) + \Delta p^*(t)F_{1p}(q(t),t) +$$
$$+\Delta v_1^*(t)F_{1v_1}(q(t),t) +$$
$$+\Delta v_2^*(t)F_{1v_2}(q(t),t) + \Delta x_0^* F_{1x_0}(q(t),t) +$$
$$+\Delta x_1^* F_{1x_1}(q(t),t) + \Delta d^* F_{1d}(q(t),t) +$$
$$+\Delta z^*(t)F_{1z}(q(t),t) + \Delta z^*(t_1)F_{1z(t_1)}(q(t),t)]dt +$$
$$+\sum_{i=1}^{9} R_i, \quad (2.10)$$

where $|R_1| \le l_1 \int_{t_0}^{t_1} |\Delta u(t)|\,|\Delta q(t)|\,dt,$

$$|R_2| \le l_2 \int_{t_0}^{t_1} |\Delta p(t)|\,|\Delta q(t)|\,dt,$$
$$|R_3| \le l_3 \int_{t_0}^{t_1} |\Delta v_1(t)|\,|\Delta q(t)|\,dt,$$
$$|R_4| \le l_4 \int_{t_0}^{t_1} |\Delta v_2(t)|\,|\Delta q(t)|\,dt,$$
$$|R_5| \le l_5 \int_{t_0}^{t_1} |\Delta x_0|\,|\Delta q(t)|\,dt,$$
$$|R_6| \le l_6 \int_{t_0}^{t_1} |\Delta x_1|\,|\Delta q(t)|\,dt,$$
$$|R_7| \le l_7 \int_{t_0}^{t_1} |\Delta d|\,|\Delta q(t)|\,dt,$$
$$|R_8| \le l_8 \int_{t_0}^{t_1} |\Delta z(t)|\,|\Delta q(t)|\,dt,$$

$|R_9| \le l_9 \int_{t_0}^{t_1} |\Delta z(t_1)|\,|\Delta q(t)|\,dt$ by the Lipschitz condition (2.5). We note that (see (2.7), (2.9))

$$\int_{t_0}^{t_1} \Delta z^*(t_1)F_{1z(t_1)}(q(t),t)dt =$$
$$= -\int_{t_0}^{t_1} [\Delta v_1^*(t)B_1^*(t) + \Delta v_2^*(t)B_2^*]\psi(t)dt - \quad (2.11)$$
$$-\int_{t_0}^{t_1} \Delta z^*(t)F_{1z}(q(t),t)dt.$$

From (2.10) and (2.11) we get

$$\Delta I_1 = \int_{t_0}^{t_1} \{\Delta u^*(t)F_{1u}(q(t),t) + \Delta p^*(t)F_{1p}(q(t),t) +$$
$$+\Delta v_1^*(t)[F_{1v_1}(q(t),t) - B_1^*(t)\psi(t)] +$$
$$+\Delta v_2^*(t)[F_{1v_2}(q(t),t) - B_2^*\psi(t)] +$$
$$+\Delta x_0^* F_{1x_0}(q(t),t) + \Delta x_1^* F_{1x_1}(q(t),t) +$$
$$+\Delta d^* F_{1d}(q(t),t)\}dt + \sum_{i=1}^{9} R_i = <I_1'(\theta), \Delta\theta>_H + R,$$

where $R = \sum_{i=1}^{9} R_i$, $|R| \le C_3 \|\Delta\theta\|^2$, $\frac{|R|}{\|\Delta\theta\|} \to 0$, *at* $\|\Delta\theta\| \to 0$.

This implies the relation (2.6). Let

$$\theta_1 = (u+\Delta u, p+\Delta p, v_1+\Delta v_1, v_2 +$$
$$+\Delta v_2, x_0+\Delta x_0, x_1+\Delta x_1, d+\Delta d),$$

$\theta_2 = (u, p, v_1, v_2, x_0, x_1, d) \in X$. Since

$$|I_1'(\theta_1) - I_1'(\theta_2)|^2 \le l_{10}|\Delta q(t)|^2 + l_{11}|\Delta\psi(t)|^2 + l_{12}|\Delta\theta|^2,$$

$$|\Delta q(t)| \le l_{13}\|\Delta\theta\|, |\Delta\psi(t)| \le l_{14}\|\Delta\theta\|,$$

that

$$\|I_1'(\theta_1) - I_1'(\theta_2)\|^2 =$$
$$= \int_{t_0}^{t_1} |I_1'(\theta_1) - I_1'(\theta_2)|^2\,dt \le l_{15}\|\Delta\theta\|^2,$$

where $l_i = const > 0$, $i = \overline{10,15}$. This implies the estimation (2.8), where $K = \sqrt{l_{15}}$. The theorem is proved.

Lemma 2.3. *Let the matrix be* $T(t_0,t_1) > 0$, *the function* $F_1(q,t)$ *be convex, with respect to the variable* $q \in R^N$, $N = 4n+m+s+r+m_1$, i.e.

$$F_1(\alpha q_1 + (1-\alpha)q_2) \le \alpha F_1(q_1,t) + (1-\alpha)F_1(q_2,t),$$
$$\forall q_1, q_2 \in R^N, \forall \alpha, \alpha \in [0,1]. \tag{2.12}$$

Then the functional (2.1) under the conditions (2.2) – (2.4) is convex.

Proof. Let $\theta_1, \theta_2 \in X$, $\alpha \in [0,1]$. It can be shown, that

$$z(t, \alpha v_1 + (1-\alpha)\bar{v}_1, \alpha v_2 + (1-\alpha)\bar{v}_2) =$$
$$= \alpha z(t, v_1, v_2) + (1-\alpha) z(t, \bar{v}_1, \bar{v}_2),$$

$$\forall (v_1, v_2), (\bar{v}_1, \bar{v}_2) \in L_2(I, R^{r+m_2}).$$

Then

$$I_1(\alpha\theta_1 + (1-\alpha)\theta_2) = \int_{t_0}^{t_1} F_1(\alpha q_1(t) +$$
$$+(1-\alpha)q_2(t))dt \le \alpha I_1(\theta_1) + (1-\alpha) I_1(\theta_2),$$

$$\forall \theta_1, \theta_2 \in X, \theta_1 = (u_1, p_1, v_1, v_2, x_0, x_1, d),$$
$$\theta_2 = (\bar{u}_1, \bar{p}_1, \bar{v}_1, \bar{v}_2, \bar{x}_0, \bar{x}_1, \bar{d}).$$

The lemma is proved.

The initial optimal control problem (2.1) – (2.4) can be solved by numerical methods for solving extremal problems [9,10]. We introduce the following sets $U = \{u(\cdot) \in L_2(I, R^m) / \| u \| \le \beta\}$,

$$V_1(I, R^r) = \{v_1(\cdot) \in L_2(I, R^r) / \| v_1 \| \le \beta\},$$

$$V_2(I, R^{m_2}) = \{v_2(\cdot) \in L_2(I, R^{m_2}) / \| v_2 \| \le \beta\}),$$

$$\Gamma_1 = \{d \in R^{m_1} / d \ge 0, | d | \le \beta\},$$

$\beta > 0$ is a sufficiently large number. We construct sequences
$\{\theta_n\} = \{u_n, p_n, v_1^n, v_2^n, x_0^n, x_1^n, d_n\} \subset X_1$,
$n = 0,1,2,\ldots$ by the algorithm

$$u_{n+1} = P_U[u_n - \alpha_n I'_{1u}(\theta_n)],\ p_{n+1} = P_V[p_n - \alpha_n I'_{1p}(\theta_n)],$$

$$v_1^{n+1} = P_{V_1}[v_1^n - \alpha_n I'_{1v_1}(\theta_n)], v_2^{n+1} = P_{V_2}[v_2^n - \alpha_n I'_{1v_2}(\theta_n)],$$

$$x_0^{n+1} = P_{S_0}[x_0^n - \alpha_n I'_{1x_0}(\theta_n)],\ x_1^{n+1} = P_{S_1}[x_1^n - \alpha_n I'_{1x_1}(\theta_n)],$$

$$d_{n+1} = P_{\Gamma_1}[d_n - \alpha_n I'_{1d}(\theta_n)],\ n = 0,1,2,\ldots,$$
$$0 < \varepsilon_0 \le \alpha_n \le \frac{2}{K + 2\varepsilon},\ \varepsilon > 0, \tag{2.13}$$

where $P_\Omega[\cdot]$ is the projection of the point on the set Ω, $K = const > 0$ from (2.8).

Theorem 2.4. *Let the conditions of Theorem 2.2. be satisfied, in addition, the function* $F_1(q,t)$ *be convex with respect to the variable* $q \in R^N$ *and the sequence* $\{\theta_n\} \subset X_1$ *be determined by formula (2.13). Then:*

1) the lower bound of the functional (2.1) is reached under the conditions (2.2) – (2.4)

$$\inf_{\theta \in X_1} I_1(\theta) = I_1(\theta_*) = \min_{\theta \in X_1} I_1(\theta),\ \theta_* \in X_1;$$

2) the sequence $\{\theta_n\} \subset X_1$ *is minimizing* $\lim_{n\to\infty} I_1(\theta_n) = I_{1*} = \inf_{\theta \in X_1} I_1(\theta)$;

3) the sequence $\{\theta_n\} \subset X_1$ *weakly converges to the point* $\theta_* \in X_1$, $u_n \longrightarrow u_*$, $p_n \longrightarrow p_*$, $v_1^n \longrightarrow v_1^*$, $v_2^n \longrightarrow v_2^*$, $x_0^n \to x_0^*$, $x_1^n \to x_1^*$, $d_n \to d_*$ *at* $n \to \infty$, *where* $\theta_* = (u_*, p_*, v_1^*, v_2^*, x_0^*, x_1^*, d_*) \in X_1$;

4) in order to the problem (1.2) – (1.6) have a solution, it is necessary and sufficient that $\lim_{n\to\infty} I_1(\theta_n) = I_{1*} = 0$;

5) the following estimation of the rate of convergence holds

$$0 \le I_1(\theta_n) - I_{1*} \le \frac{C_0}{n},\ n = 1,2,\ldots, \tag{2.14}$$
$$C_0 = const > 0.$$

Proof. Since the function $F_1(q,t)$, $t \in I$ is convex, it follows from Lemma 3.3. that the

functional $I_1(\theta)$, $\theta \in X_1$ is convex on a weekly bicompact set X_1. Consequently, $I_1(\theta) \in C^1(X_1)$ is weakly lower semicontinuous on a weakly bicompact set and reaches the lower bound on X_1. This implies the first statement of the theorem.

Using the properties of the projection of a point on a convex closed set X_1 and taking into account that $I_1(\theta) \in C^{1,1}(X_1)$ it can be shown that $I_1(\theta_n) - I_1(\theta_{n+1}) \geq \varepsilon \| \theta_n - \theta_{n+1} \|^2$, $n = 0,1,2,..$, $\varepsilon > 0$. It follows that: 1) the numerical sequence $\{I_1(\theta_n)\}$ strictly decreases; 2) $\| \theta_n - \theta_{n+1} \| \to 0$ at $n \to \infty$.

Since the functional is convex and the set X_1 is bounded, the inequality holds

$$0 \leq I_1(\theta_n) - I_1(\theta_*) \leq C_1 \| \theta_n - \theta_{n+1} \|, \quad C_1 = const > 0, n = 0,1,2,.... \tag{2.15}$$

Hence, taking into account that $\| \theta_n - \theta_{n+1} \| \to 0$ at $n \to \infty$,, we have: the sequence $\{\theta_n\}$ is minimizing. $\lim\limits_{n\to\infty} I_1(\theta_n) = I_1(\theta_*) = \inf\limits_{\theta \in X_1} I_1(\theta)$.

Since $\{\theta_n\} \subset X_1$, X_1 is weakly bicompact, that, $\theta_n \xrightarrow{weakly} \theta_*$ *at* $n \to \infty$.

As it follows from Lemma 3.1., if the value $I_1(\theta_*) = 0$, then the problem of optimal control (1.1) – (1.6) has a solution.

The estimation (2.14) follows directly from the inequalities (2.15),

$I_1(\theta_n) - I_1(\theta_{n+1}) \geq \varepsilon \| \theta_n - \theta_{n+1} \|^2$.

We briefly outlined above, the main steps in proof of the theorem. Detailed proof of an analogous theorem is given in [16]. The theorem is proved.

For the case when the function $F_1(q,t)$ is not convex with respect to the variable q, the following theorem is true.

Theorem 2.5. *It is supposed, that the conditions of Theorem 2.2. are satisfied, the sequence* $\{\theta_n\} \subset X_1$ *is determined by formula (2.13). Then: 1) the value of the functional* $I_1(\theta_n)$ *strictly decreases for* $n = 0,1,2,..$; *2)* $\| \theta_n - \theta_{n+1} \| \to 0$ *at* $n \to \infty$.

Proof of the theorem follows from Theorem 2.4.

From the results it follows that 1) if $\theta_* = (u_*, p_*, v_1^*, v_2^*, x_0^*, x_1^*, d_*) \in X_1$ is the solution of optimal control problem (2.1) – (2.4), for which $I_1(\theta_*) = 0$, then $(u_* = u_*(t), x_0^*, x_1^*) \in \Sigma \subset U \times S_0 \times S_1$ is admissible control; 2) the function $x_*(t; t_0, x_0^*)$, $t \in I$ is the solution of differential equation (1.2), satisfies the conditions: $x(t_1; t_0, x_0^*) = x_1^*$, $x_*(t; t_0, x_0^*) \in G(t)$, $t \in I$, the functionals $g_j(u_*(\cdot), x_0^*, x_1^*) \leq 0$, $j = \overline{1, m_1}$, $g_j(u_*(\cdot), x_0^*, x_1^*) = 0$, $j = \overline{m_1 + 1, m_2}$; 3) the necessary and sufficient condition for the existence of a solution of the boundary value problem (1.2) – (1.6) is $I_1(\theta_*) = 0$ where $\theta_* \in X_1$ is the solution of problem (2.1) – (2.4); 4) for the admissible control, the value of the functional (1.1) equals to

$$J(u_*(\cdot), x_0^*, x_1^*) = \int_{t_0}^{t_1} F_0(x_*(t), u_*(t), x_0^*, x_1^*, t)dt = \gamma_*, \tag{2.16}$$

where $x_*(t) = x_*(t; t_0, x_0^*)$, $t \in I$. In the general case, the value

$$J(u_*(\cdot), x_0^*, x_1^*) \neq J(\overline{u}_*, \overline{x}_0^*, \overline{x}_1^*) = \inf J(u(\cdot), x_0, x_1),$$
$$(u(\cdot), x_0, x_1) \in L_2(I, R^m) \times S_0 \times S_1.$$

Construction of an optimal solution

We consider the optimal control problem (1.1) – (1.6). We define a scalar function $\sigma(t)$, $t \in I$ as:

$$\sigma(t) = \int_{t_0}^{t} F_0(x(\tau), u(\tau), x_0, x_1, \tau)d\tau, t \in I.$$

Then $\dot{\sigma}(t) = F_0(x(t), u(t), x_0, x_1, t)$, $\sigma(t_0) = 0$, $\sigma(t_1) = \gamma = I(u(\cdot), x_0, x_1) \in \Omega$, $\Omega = \{\gamma \in R^1 / \gamma \geq \gamma_0, \gamma_0 > -\infty\}$, *where* $\gamma = \inf I(u(\cdot), x_0, x_1) \geq \gamma_0$, the value γ_0 is bounded from below, in particular $\gamma_0 = 0$, if $F_0 \geq 0$.

Now the problem of optimal control (1.1) – (1.6) can be written in the form (see (2.1))

$$\sigma(t_1) = \gamma = I(u(\cdot), x_0, x_1) \to \inf \tag{3.1}$$

at conditions

$$\begin{gathered} \dot{\boldsymbol{\sigma}}(t) = F_0(x(t), u(t), x_0, x_1, t), \\ \boldsymbol{\sigma}(t_0) = 0, \boldsymbol{\sigma}(t_1) = \boldsymbol{\gamma}, \end{gathered} \tag{3.2}$$

$$\begin{gathered} \dot{x} = A(t)x + B(t)f(x, u, t), (x(t_0) = x_0, \\ x(t_1) = x_1) \in S_0 \times S_1, \end{gathered} \tag{3.3}$$

$$\begin{gathered} \dot{\boldsymbol{\eta}} = f_0(x(t), u(t), x_0, x_1, t), \\ \boldsymbol{\eta}(t_0) = 0, \boldsymbol{\eta}(t_1) = \bar{c} \in Q, \end{gathered} \tag{3.4}$$

$$x(t) \in G(t), u(\cdot) \in L_2(I, R^m), t \in I. \tag{3.5}$$

We introduce the notations

$$\boldsymbol{\mu}(t) = \begin{pmatrix} \boldsymbol{\sigma}(t) \\ x(t) \\ \boldsymbol{\eta}(t) \end{pmatrix},$$

$$A_2(t) = \begin{pmatrix} O_{1,1} & O_{1,n} & O_{1,m_2} \\ O_{n,1} & A(t) & O_{n,m_2} \\ O_{m_2,1} & O_{m_2,n} & O_{m_2,m_2} \end{pmatrix},$$

$$B_0 = \begin{pmatrix} 1 \\ O_{n,1} \\ O_{m_2,1} \end{pmatrix},$$

$$C_0(t) = \begin{pmatrix} O_{1,r} \\ B(t) \\ O_{m_2,r} \end{pmatrix}, D_0(t) = \begin{pmatrix} O_{1,m_2} \\ O_{n,m_2} \\ I_{m_2} \end{pmatrix},$$

$$P_0 = \begin{pmatrix} 1, & O_{1,n}, & O_{1,m_2} \end{pmatrix}, P_1 = \begin{pmatrix} O_{n,1}, & I_n, & O_{n,m_2} \end{pmatrix},$$

where $P_0\mu(t_1) = \sigma(t_1)$, $P_1\mu = x$.

Then the optimal control problem (3.1) – (3.5) has the form:

$$P_0\mu(t_1) = \gamma = I(u(\cdot), x_0, x_1) \to \inf, \tag{3.6}$$

at conditions

$$\begin{gathered} \dot{\boldsymbol{\mu}} = A_2(t)\boldsymbol{\mu} + B_0F_0(P_1\boldsymbol{\mu}, u, x_0, x_1, t) + \\ + C_0(t)f(P_1\boldsymbol{\mu}, u, t) + D_0f_0(P_1\boldsymbol{\mu}, u, x_0, x_1, t), \end{gathered} \tag{3.7}$$

$$\begin{gathered} \boldsymbol{\mu}(t_0) = \boldsymbol{\mu}_0 = \begin{pmatrix} \boldsymbol{\sigma}(t_0) \\ x(t_0) \\ \boldsymbol{\eta}(t_0) \end{pmatrix} = \\ = \begin{pmatrix} O_{1,1} \\ x_0 \\ O_{m_2,1} \end{pmatrix} \in O_{1,1} \times S_0 \times O_{m_2,1} = T_0, \end{gathered} \tag{3.8}$$

$$\begin{gathered} \boldsymbol{\mu}(t_1) = \boldsymbol{\mu}_1 = \begin{pmatrix} \boldsymbol{\sigma}(t_1) \\ x(t_1) \\ \boldsymbol{\eta}(t_1) \end{pmatrix} = \\ = \begin{pmatrix} \boldsymbol{\gamma} \\ x_1 \\ \bar{c} \end{pmatrix} \in \boldsymbol{\Omega} \times S_1 \times Q = T_1, \end{gathered} \tag{3.9}$$

$$P_1\mu(t) \in G(t), u(\cdot) \in L_2(I, R^m), d \in \Gamma, \tag{3.10}$$

where $x(t) = P_1\mu(t)$, $\sigma(t) = P_0\mu(t)$, $t \in I$, γ is determined by formula (3.6).

The immersion principle. We consider the boundary value problem (3.7) – (3.10). The corresponding linear controlled system has the form

$$\begin{gathered} \dot{\boldsymbol{\zeta}} = A_2(t)\boldsymbol{\zeta} + B_0\overline{w}_1(t) + C_0(t)\overline{w}_2(t) + \\ + D_0\overline{w}_3(t), t \in I, \end{gathered} \tag{3.11}$$

$$\begin{gathered} \overline{w}_1(\cdot) \in L_2(I, R^1), \ \overline{w}_2(\cdot) \in L_2(I, R^r), \\ \overline{w}_3(\cdot) \in L_2(I, R^{m_2}), \end{gathered} \tag{3.12}$$

$$\zeta(t_0) = \mu_0 \in T_0, \quad \zeta(t_1) = \mu_1 \in T_1. \tag{3.13}$$

We introduce the following notations:

$$\begin{gathered} \overline{B}_0(t) = (B_0, C_0(t), D_0), \overline{w}(t) = \\ = (\overline{w}_1(t), \overline{w}_2(t), \overline{w}_3(t)), \boldsymbol{\Psi}(t, \tau) = K(t)K^{-1}(\tau), \\ \overline{a} = \boldsymbol{\Psi}(t_0, t_1)\boldsymbol{\mu}_1 - \boldsymbol{\mu}_0, R(t_0, t_1) = \\ = \int_{t_0}^{t_1} \boldsymbol{\Psi}(t_0, t)\overline{B}_0(t)\overline{B}_0^*(t)\boldsymbol{\Psi}^*(t_0, t)dt, \end{gathered}$$

$$R(t_0,t)=\int_{t_0}^{t}\Psi(t_0,\tau)\overline{B}_0(\tau)\overline{B}_0^*(\tau)\Psi^*(t_0,\tau)d\tau,$$

$$R(t_0,t_1)=R(t_0,t)+R(t,t_1),$$

$$\overline{\Lambda}_1(t,\mu_0,\mu_1)=\overline{B}_0^*(t)\Psi^*(t_0,t)R^{-1}(t_0,t_1)a=$$

$$=\begin{pmatrix}B_0^*\Psi^*(t_0,t)R^{-1}(t_0,t_1)\overline{a}\\ C_0^*\Psi^*(t_0,t)R^{-1}(t_0,t_1)\overline{a}\\ D_0^*\Psi^*(t_0,t)R^{-1}(t_0,t_1)\overline{a}\end{pmatrix}=\begin{pmatrix}\overline{\Lambda}_{11}(t,\mu_0,\mu_1)\\ \overline{\Lambda}_{12}(t,\mu_0,\mu_1)\\ \overline{\Lambda}_{13}(t,\mu_0,\mu_1)\end{pmatrix},$$

$$K_1(t)=-\overline{B}_0^*\Psi^*(t)(t_0,t)R^{-1}(t_0,t_1)\Psi(t_0,t_1)=$$

$$=\begin{pmatrix}-B_0^*\Psi^*(t_0,t)R^{-1}(t_0,t_1)\Psi(t_0,t_1)\\ -C_0^*\Psi^*(t_0,t)R^{-1}(t_0,t_1)\Psi(t_0,t_1)\\ -D_0^*\Psi^*(t_0,t)R^{-1}(t_0,t_1)\Psi(t_0,t_1)\end{pmatrix}=\begin{pmatrix}K_{11}(t)\\ K_{12}(t)\\ K_{13}(t)\end{pmatrix},$$

$$\overline{\Lambda}_2(t,\mu_0,\mu_1)=\Psi(t,t_0)R(t,t_1)R^{-1}(t_0,t_1)\mu_0+$$
$$+\Psi(t,t_0)R(t_0,t)R^{-1}(t_0,t_1)\Psi(t_0,t_1)\mu_1,$$

$$K_2(t)=-\Psi(t,t_0)R(t_0,t)R^{-1}(t_0,t_1)\Psi(t_0,t_1),t\in I.$$

Theorem 3.1. *Let the matrix be* $R(t_0,t_1)>0$. *Then the control* $\overline{w}(t)=(\overline{w}_1(t),\overline{w}_2(t),\overline{w}_3(t))\in L_2(I,R^{1+r+m_2})$ *transforms the trajectory of the system (3.11) – (3.13) from any initial point* $\mu_0\in R^{1+n+m_2}$ *to any given finite state* $\mu_1\in R^{1+n+m_2}$ *if and only if*

$$\overline{w}_1(t)\in\overline{W}_1=\{\overline{w}_1(\cdot)\in L_2(I,R^1)/\overline{w}_1(t)=$$
$$=\overline{v}_1(t)+\overline{\Lambda}_{11}(t,\mu_0,\mu_1)+K_{11}(t)\overline{z}(t_1,\overline{v}),$$

$$\forall\overline{v}_1(\cdot)\in L_2(I,R^1),t\in I\},\qquad(3.14)$$

$$\overline{w}_2(t)\in\overline{W}_2=\{\overline{w}_{2(\cdot)}\in L_2(I,R^r)/\overline{w}_2(t)=$$
$$=\overline{v}_2(t)+\overline{\Lambda}_{12}(t,\mu_0,\mu_1)+K_{12}(t)\overline{z}(t_1,\overline{v}),$$

$$\forall\overline{v}_2(\cdot)\in L_2(I,R^r),t\in I\},\qquad(3.15)$$

$$\overline{w}_3(t)\in\overline{W}_3=\{\overline{w}_3(\cdot)\in L_2(I,R^{m_2})/\overline{w}_3(t)=$$
$$=\overline{v}_3(t)+\overline{\Lambda}_{13}(t,\mu_0,\mu_1)+K_{13}(t)\overline{z}(t_1,\overline{v}),$$

$$\forall\overline{v}_3(\cdot)\in L_2(I,R^{m_2}),t\in I\},\qquad(3.16)$$

where $\overline{v}(t)=(\overline{v}_1(t),\overline{v}_2(t),\overline{v}_3(t)),\overline{z}(t)=\overline{z}(t,\overline{v}),t\in I$ is the solution of the differential equation

$$\dot{\overline{z}}=A_2(t)\overline{z}+B_0\overline{v}_1(t)+C_0(t)\overline{v}_2(t)+$$
$$+D_0\overline{v}_3(t),\overline{z}(t_0)=0,\qquad(3.17)$$

$$\overline{v}_1(\cdot)\in L_2(I,R^1),\overline{v}_2(\cdot)\in L_2(I,R^r),$$
$$\overline{v}_3(\cdot)\in L_2(I,R^{m_2}).\qquad(3.18)$$

Solution of the system (3.11) – (3.13) has the form

$$\zeta(t)=\overline{z}(t,\overline{v})+\overline{\Lambda}_2(t,\mu_0,\mu_1)+$$
$$+K_2(t)\overline{z}(t_1,\overline{v}),t\in I.\qquad(3.19)$$

The proof of the analogous theorem is presented in the work [10].

Lemma 3.2. *Let the matrix be* $R(t_0,t_1)>0$. *Then the boundary value problem (3.7) – (3.10) is equivalent to the following problem*

$$\overline{w}_1(t)\in\overline{W}_1,\overline{w}_1(t)=F_0(P_1\zeta,u,x_0,x_1,t),\quad t\in I,\qquad(3.20)$$

$$\overline{w}_2(t)\in\overline{W}_2,\overline{w}_2(t)=f(P_1\zeta,u,t),t\in I,\qquad(3.21)$$

$$\overline{w}_3(t)\in\overline{W}_3,\overline{w}_3(t)=f_0(P_1\zeta,u,x_0,x_1,t),\quad t\in I,\qquad(3.22)$$

$$p(t)\in V(t)=\{p(\cdot)\in L_2(I,R^s)/p(t)=$$
$$=F(P_1\zeta,t),\omega(t)\le p(t)\le\phi(t),t\in I\},\qquad(3.23)$$

$$\dot{\overline{z}}=A_2(t)\overline{z}+B_0\overline{v}_1(t)+C_0(t)\overline{v}_2(t)+$$
$$+D_0\overline{v}_3(t),\overline{z}(t_0)=0,t\in I,\qquad(3.24)$$

$$\overline{v}_1(\cdot)\in L_2(I,R^1),\overline{v}_2(\cdot)\in L_2(I,R^r),$$
$$\overline{v}_3(\cdot)\in L_2(I,R^{m_2}),\qquad(3.25)$$

$$(x_0,x_1)\in S_0\times S_1,u(\cdot)\in L_2(I,R^m),$$
$$\gamma\in\Omega,d\in\Gamma,\qquad(3.26)$$

where $\zeta(t),\ t\in I$ *is determined by formula (3.19),* $\overline{z}(t,\overline{v})$ *is the solution of system (3.17), (3.18).*

We consider the following optimal control problem: minimize the functional

$$J_2(\bar{v},u,p,x_0,x_1,d,\boldsymbol{\gamma}) = \int_{t_0}^{t_1} F_2(\bar{q}(t),t)dt =$$

$$= \int_{t_0}^{t_1} [|\,\bar{w}_1(t) - F_0(P_1\boldsymbol{\zeta}(t),u(t),x_0,x_1,t)\,|^2 +$$

$$+ |\,\bar{w}_2(t) - f(P_1\boldsymbol{\zeta}(t),u(t),t)\,|^2 +$$

$$+ |\,\bar{w}_3(t) - f_0(P_1\boldsymbol{\zeta}(t),u(t),x_0,x_1,t)\,|^2 +$$

$$+ |\,p(t) - F(P_1\zeta(t),t)\,|^2]dt \to \inf \qquad (3.27)$$

under the conditions (3.24) – (3.26), where $\bar{w}_1(t) \in \bar{W}_1$, $\bar{w}_2(t) \in \bar{W}_2$, $\bar{w}_3(t) \in \bar{W}_3$, $\bar{v} = (\bar{v}_1, \bar{v}_2, \bar{v}_3)$,

$\bar{q}(t) = (\bar{v}_1, \bar{v}_2, \bar{v}_3, u, p, x_0, x_1, d, \gamma, \bar{z}(t), \bar{z}(t_1))$.

Note, that the optimization problem (3.27), (3.24) – (3.26) is obtained on the basis of relations (3.20) – (3.23).

Theorem 3.3. *Let the matrix be, the derivative* $\dfrac{\partial F_2(\bar{q},t)}{\partial q}$ *satisfies the Lipschitz condition.*

Then:

1. The functional (3.27) under conditions (3.24) – (3.26) is continuously differentiable by Frechet, gradient of the functional

$$J_2'(\bar{\boldsymbol{\theta}}) = (J'_{2\bar{v}_1}(\bar{\boldsymbol{\theta}}), J'_{2\bar{v}_2}(\bar{\boldsymbol{\theta}}), J'_{2\bar{v}_3}(\bar{\boldsymbol{\theta}}), J'_{2u}(\bar{\boldsymbol{\theta}}), J'_{2p}(\bar{\boldsymbol{\theta}}),$$

$$J'_{2x_0}(\bar{\boldsymbol{\theta}}), J'_{2x_1}(\bar{\boldsymbol{\theta}}), J'_{2d}(\bar{\boldsymbol{\theta}}), J'_{2\boldsymbol{\gamma}}(\bar{\boldsymbol{\theta}})),$$

$$\bar{\theta} = (\bar{v}_1, \bar{v}_2, \bar{v}_3, u, p, x_0, x_1, d, \gamma) \in \bar{X},$$

$$\bar{X} = L_2(I,R^1) \times L_2(I,R^r) \times L_2(I,R^{m_2}) \times$$

$$\times L_2(I,R^m) \times V \times S_0 \times S_1 \times \boldsymbol{\Gamma} \times \boldsymbol{\Omega}$$

$$H_1 = L_2(I,R^1) \times L_2(I,R^r) \times L_2(I,R^{m_2}) \times$$

$$\times L_2(I,R^m) \times L_2(I,R^s) \times R^n \times R^n \times R^{m_1} \times R^1,$$

$$\bar{X} \subset H_1, \quad J_2'(\bar{\boldsymbol{\theta}}) \in H_1$$

for any point $\bar{\theta} \in \bar{X}$ *is calculated by the formulas*

$$J'_{2\bar{v}_1}(\bar{\boldsymbol{\theta}}) = \frac{\partial F_2(\bar{q}(t),t)}{\partial \bar{v}_1} - B_0^*\bar{\boldsymbol{\psi}}(t),$$

$$J'_{2\bar{v}_2}(\bar{\boldsymbol{\theta}}) = \frac{\partial F_2(\bar{q}(t),t)}{\partial \bar{v}_2} - C_0^*\bar{\boldsymbol{\psi}}(t),$$

$$J'_{2\bar{v}_3}(\bar{\boldsymbol{\theta}}) = \frac{\partial F_2(\bar{q}(t),t)}{\partial \bar{v}_3} - D_0^*\bar{\boldsymbol{\psi}}(t),$$

$$J'_{2u}(\bar{\boldsymbol{\theta}}) = \frac{\partial F_2(\bar{q}(t),t)}{\partial u}, \quad J'_{2p}(\bar{\boldsymbol{\theta}}) = \frac{\partial F_2(\bar{q}(t),t)}{\partial p}$$

$$J'_{2x_0}(\bar{\boldsymbol{\theta}}) = \int_{t_0}^{t_1} \frac{\partial F_2(\bar{q}(t),t)}{\partial x_0}dt,$$

$$J'_{2x_1}(\bar{\boldsymbol{\theta}}) = \int_{t_0}^{t_1} \frac{\partial F_2(\bar{q}(t),t)}{\partial x_1}dt,$$

$$J'_{2d}(\bar{\boldsymbol{\theta}}) = \int_{t_0}^{t_1} \frac{\partial F_2(\bar{q}(t),t)}{\partial d}dt,$$

$$J'_{2\boldsymbol{\gamma}}(\bar{\boldsymbol{\theta}}) = \int_{t_0}^{t_1} \frac{\partial F_2(\bar{q}(t),t)}{\partial \boldsymbol{\gamma}}dt,$$

where $\bar{\psi}(t), \ t \in I$ *is the solution of the adjoint system*

$$\dot{\bar{\psi}} = \frac{\partial F_2(\bar{q}(t),t)}{\partial \bar{z}} - A_2^*(t)\bar{\psi},$$

$$\bar{\psi}(t_1) = -\int_{t_0}^{t_1} \frac{\partial F_2(\bar{q}(t),t)}{\partial \bar{z}(t_1)}dt;$$

2. gradient $J_2'(\bar{\theta}), \bar{\theta} \in \bar{X}$ *satisfies the Lipchitz condition*

$$\| J_2'(\bar{\boldsymbol{\theta}}_1) - J_2'(\bar{\boldsymbol{\theta}}_2) \| \le l \| \bar{\boldsymbol{\theta}}_1 - \bar{\boldsymbol{\theta}}_2 \|, \qquad (3.28)$$

$$\forall \bar{\boldsymbol{\theta}}_1, \bar{\boldsymbol{\theta}}_2 \in \bar{X}.$$

The proof of the analogous theorem can be found in the work [16]. We construct the following sequences $\{\bar{\theta}_n\} = \{\bar{v}_1^n, \bar{v}_2^n, \bar{v}_3^n, u_n, p_n, x_0^n, x_1^n, d_n, \gamma_n\} \subset \bar{X}_2$ by the algorithm

$$\bar{v}_1^{n+1} = P_{\bar{V}_1}[\bar{v}_1^n - \alpha_n J'_{2\bar{v}_1}(\bar{\theta}_n)],$$

$$\bar{v}_2^{n+1} = P_{\bar{V}_2}[\bar{v}_2^n - \alpha_n J'_{2\bar{v}_2}(\bar{\theta}_n)],$$

$$\bar{v}_3^{n+1} = P_{\bar{V}_3}[\bar{v}_3^n - \alpha_n J'_{2\bar{v}_3}(\bar{\theta}_n)],$$

$$u_{n+1} = P_U[u_n - \alpha_n J'_{2u}(\bar{\theta}_n)],$$

$$p_{n+1} = P_V[p_n - \alpha_n J'_{2p}(\bar{\theta}_n)],$$

$$x_0^{n+1} = P_{S_0}[x_0^n - \alpha_n J'_{2x_0}(\bar{\theta}_n)],$$

$$x_1^{n+1} = P_{S_1}[x_1^n - \alpha_n J'_{2x_1}(\bar{\theta}_n)],$$

$$d_{n+1} = P_{\bar{\Gamma}}[d_n - \alpha_n J'_{2d}(\bar{\theta}_n)],$$

$$\gamma_{n+1} = P_{\bar{\Omega}}[\gamma_n - \alpha_n J'_{2\gamma}(\bar{\theta}_n)], \qquad n = 0,1,2,...,$$

$$0 \le \alpha_n \le \frac{2}{l+2\varepsilon}, \quad \varepsilon > 0, \quad l = const > 0, \qquad (3.29)$$

where $\bar{V}_1 = \{\bar{v}_1(\cdot) \in L_2(I, R^1) / \| \bar{v}_1 \| \le \bar{\beta}\}$,
$\bar{V}_2 = \{\bar{v}_2(\cdot) \in L_2(I, R^r) / \| \bar{v}_2 \| \le \bar{\beta}\}$,
$\bar{V}_3 = \{\bar{v}_3(\cdot) \in L_2(I, R^{m_2}) / \| \bar{v}_3 \| \le \bar{\beta}\}$,
$U = \{u(\cdot) \in L_2(I, R^m) / \| u \| \le \bar{\beta}\}$,
$\bar{\Gamma} = \{d \in R^{m_1} / d \ge 0, | d | \le \bar{\beta}\}$,
$\bar{\Omega} = \{\gamma \in R^1 \ / \ a \le \gamma \le \gamma_*\}$,
$\bar{X}_2 = \bar{V}_1 \times \bar{V}_2 \times \bar{V}_3 \times U \times V \times S_0 \times S_1 \times \bar{\Gamma} \times \bar{\Omega} \subset H_1$,
$U = \{u(\cdot) \in L_2(I, R^m) / \ \| u \| \le \bar{\beta}\}$, $\bar{\beta} > 0$ is a sufficiently large number.

Theorem 3.4. *Let the conditions of Theorem 3.3. be satisfied $\bar{X}_1$ is a bounded convex closed set, the sequence $\{\bar{\theta}_n\} \subset \bar{X}_2$ is determined by the formula (3.29). Then:*

1. the numerical sequence $\{J_2(\bar{\theta}_n)\}$ is strictly decreasing $\| \bar{\theta}_n - \bar{\theta}_{n+1} \| \to 0$, at $n \to \infty$.

If, in addition,, $F_2(\bar{q}, t)$ is a convex function with respect to a variable $\bar{q}$, then:

2. the lower bound of the functional (3.27) is obtained under the conditions (3.24) – (3.26)

$$J_2(\bar{\theta}_*) = \inf_{\bar{\theta} \in \bar{X}_2} J_2(\bar{\theta}) = \min_{\bar{\theta} \in \bar{X}_2} J_2(\bar{\theta}) = J_{2*};$$

3. the sequence $\{\bar{\theta}_n\} \subset \bar{X}_2$ is minimizing $\lim_{n \to \infty} J_2(\bar{\theta}_n) = J_{2*} = \inf_{\bar{\theta} \in \bar{X}_2} J_2(\bar{\theta})$;

4. the sequence { $\{\bar{\theta}_n\} \subset \bar{X}_1$ weakly converges to the point $\bar{\theta}_* \in \bar{X}_{1*}$, $\bar{X}_{2*} = \{\bar{\theta}_* / J_2(\bar{\theta}_*) = J_{2*} = \inf_{\bar{\theta} \in \bar{X}_1} J_2(\bar{\theta}) = \min_{\theta \in \bar{X}_1} J_2(\bar{\theta})\}$, where $\bar{v}_1^n \longrightarrow \bar{v}_1^*$, $\bar{v}_2^n \longrightarrow \bar{v}_2^*$, $\bar{v}_3^n \longrightarrow \bar{v}_3^*$, $u_n \longrightarrow \bar{u}_*$, $p_n \longrightarrow \bar{p}_*$, $x_0^n \to \bar{x}_0^*$, $x_1^n \to \bar{x}_1^*$, $d_n \to \bar{d}_*$, $\gamma_n \to \gamma_*$ at $n \to \infty$, $\bar{\theta}_* = (\bar{v}_1^*, \bar{v}_2^*, \bar{v}_3^*, \bar{u}_*, p_*, \bar{x}_0^*, \bar{x}_1^*, \bar{d}_*, \bar{\gamma}_*)$;

5. if $J_2(\bar{\theta}_*) = 0$, then the optimal control for problem (1.1) – (1.6) is $\bar{u}_* \in U$, $\bar{x}_0^* \in S_0$, $\bar{x}_1^* \in S_1$, and the optimal trajectory

$$\bar{x}_*(t) = P_1 \zeta_*(t) = P_1[\bar{z}(t, \bar{v}_*) + \bar{\Lambda}_2(t, \mu_0^*, \mu_1^*) + K_2(t)\bar{z}(t_1, \bar{v}_*)], t \in I,$$

where

$$\bar{v}_* = (\bar{v}_1^*, \bar{v}_2^*, \bar{v}_3^*), \mu_0^* = (O_{1,1}, \bar{x}_0^*, O_{m_2,1}),$$

$$\mu_1^* = (\gamma_*, \bar{x}_1^*, \bar{c}_*), \bar{c}_* \in Q = \{\bar{c}_* \in R^{m_2} / \bar{c}_{j*} = c_j - \bar{d}_j^*, \bar{d}_j^* \ge 0, j = \overline{1, m_1}; \bar{c}_{j*} = c_j, j = \overline{m_1 + 1, m_2}\},$$

the inclusion $\bar{x}_*(t) \in G(t)$ and limitations (1.4) – (1.6) $J(\bar{u}_*, \bar{x}_0^*, \bar{x}_1^*) = \bar{\gamma}_*$; hold.

6. The following estimation of the rate of convergence holds

$$0 \le J_2(\bar{\theta}_n) - J_{2*} \le \frac{\bar{c}_0}{n}, n = 1,2,...,\bar{c}_0 = const > 0.$$

Proof of the analogous theorem is given above.

A more obvious method for solving problem (1.1) – (1.6) is the method of narrowing the domain of admissible controls.

Theorem 3.5. *Let the conditions of Theorem 3.3. be satisfied,* $\overline{X}_3 = \overline{V}_1 \times \overline{V}_2 \times \overline{V}_3 \times U \times V \times S_0 \times S_1 \times \overline{\Gamma}$ *be a bounded convex closed set, the sequence* $\{\overline{\theta}_n\} \subset \overline{X}_2$ *be defined by (3.28) with the exception of the sequence* $\{\gamma_n\} \subset \Omega$. *Then:*

1. the numerical sequence $\{J_2(\overline{\theta}_n)\}$, $\{\overline{\theta}_n\} \subset X_3$ *is strictly decreasing;*

2. $\| \overline{\theta}_n - \overline{\theta}_{n+1} \| \to 0$ *at* $n \to \infty$, $\{\overline{\theta}_n\} \subset \overline{X}_3$;

If, in addition, the function $F_2(\overline{q}, t)$ *is convex with respect to a variable* $\overline{q}$ *for fixed* γ, *then:*

3. the sequence $\{\overline{\theta}_n\} \subset \overline{X}_3$, *for a fixed* $\gamma = \overline{\gamma}$ *is minimizing;*

4. $\overline{\theta}_n \longrightarrow \overline{\theta}_* \in \overline{X}_3$ *at* $n \to \infty$, $\gamma = \overline{\gamma}$;

5. $J_2(\overline{\theta}_*) = \inf\limits_{\overline{\theta}_n \in \overline{X}_3} J_2(\overline{\theta}_n) = \min\limits_{\theta_n \in X_3} J_2(\overline{\theta}_n)$;

6. the following estimation holds

$$0 \le J_2(\overline{\theta}_n) - J_2(\overline{\theta}_*) \le \frac{c_1}{n},$$

$c_1 = const > 0, n = 1, 2, ..., \{\overline{\theta}_n\} \subset \overline{X}_3$.

The proof of the analogous theorem is presented in the work [10] for a fixed $\gamma \in \Omega$, $\gamma = \overline{\gamma}$.

Let the solution of the problem be $\overline{\theta}_* \in \overline{X}_2$ (3.27), (3.24) – (3.26) with $\gamma = \gamma_* \in \Omega$. There are the possible cases:

1. the value $J_2(\overline{\theta}_*) > 0$;
2. the value $J_2(\overline{\theta}_*) = 0$.

Note, that $J_2(\overline{\theta}) \ge 0$, $\overline{\theta} \in \overline{X}_3$.

If $J_2(\overline{\theta}_*) > 0$, then a new value of γ is selected as $\gamma = 2\gamma_*$, and if $J_2(\overline{\theta}_*) = 0$, then a new value $\gamma = \frac{\gamma_*}{2}$. According to this scheme, by dividing the uncertainty segment in half, the smallest value of the functional (1.1), under the conditions (1.2) – (1.6) can be found.

Conclusion

The Lagrange problem of the variation calculus is investigated in the presence of phase and integral constraints for processes described by ordinary differential equations. The particular cases of which are the simplest problem, the Bolz problem, the isoperimetric problem, the conditional extremum problem.

In contrast to the well-known method for solving the problem of the variation calculus on the basis of the Lagrange principle, an entirely new approach an "immersion principle" is proposed. The immersion principle is based on the investigation of the Fredholm integral equation of the first kind. For the Fredholm integral equation of the first kind, the existence theorem for the solution as well as the theorem on its general solution are proved.

The main scientific results are:

- reduction of the boundary value problem connected to the conditions in the Lagrange problem to the initial optimal control problem with a specific functional;
- necessary and sufficient conditions for the existence of the admissible control;
- method of constructing an admissible control on the limit point of the minimizing sequence;
- necessary and sufficient conditions for the existence of a solution of the Lagrange problem;
- method for constructing the solution of the Lagrange problem.

References

1. Bliss Dzh. *Lectures on variation calculus*, – M.: IL (1950):348.

2. Lavrentev M.A., Lyusternik L.A. “Basics of variation calculus.” *ONTI* 1, Ch.1, 2 (1935): 148, 400.

3. Yang L. “Lectures on variation calculus and optimal control theory.” *Mir* (1974): 488.

4. Alekseev V.M., Tihomirov V.M., Fomin S.V. “Optimal control.” *Nauka* (1979): 430.

5. Pontryagin L.S., Boltyanskiy V.G., Gamkrelidze R.V., Mischenko E.F. “Mathematical theory of optimal processes.” *Nauka* (1969): 384.

6. Varga Dzh. “Optimal control by differential and functional equations.” *Nauka* (1977): 624.

7. Gamkrelidze R.V. “Basics of optimal control.” – Tbilisi: Izd-vo Tbilisskogo n-ta, (1977): 253.

8. Li Ya.B., Markus L. “Basics of the optimal control theor.” *Nauka* (1972): 574.

9. Aysagaliev S.A., Sevryugin I.V. “Controlabillity and speed of the process described by linear system of ordinary differential equations.” *Mathematical journal* 13, no. 2(4) (2013): 5–30.

10. Aysagaliev S.A., Kabidoldanova A.A. “Optimal control by dynamic systems, Palmarium Academic Publishing.” *Verlag* (2012): 288.

IRSTI 27.31.15

[3]M. Ruzhansky, [1,2]D. Serikbaev, [1,2]N. Tokmagambetov

[1]Al-Farabi Kazakh National University, Almaty, Kazakhstan
[2]Institute of Mathematics and Mathematical Modeling, Almaty, Kazakhstan
[3]Ghent University, Ghent, Belgium
e-mail: tokmagambetov@math.kz

An inverse problem for the pseudo-parabolic equation for Laplace operator

Abstract. A class of inverse problems for restoring the right-hand side of the pseudo-parabolic equation for 1D Laplace operator is considered. The inverse problem is to be well-posed in the sense of Hadamard whenever an overdetermination condition of the final temperature is given. Mathematical statements involve inverse problems for the pseudo-parabolic equation in which, solving the equation, we have to find the unknown right-hand side depending only on the space variable. We prove the existence and uniqueness of the classical solutions. The proof of the existence and uniqueness results of the solutions is carried out by using L-Fourier analysis. The mentioned results are presented as well as for the fractional time pseudo–parabolic equation. Inverse problems of identifying the coefficients of right hand side of the pseudo-parabolic equation from the local overdetermination condition have important applications in various areas of applied science and engineering, also such problems can be modeled using common homogeneous left-invariant hypoelliptic operators on common graded Lie groups.
Key words: Pseudo-parabolic equation, 1D Laplace operator, fractional Caputo derivative, inverse problem, well-posedness.

Introduction

In this paper we study inverse problem for the time-fractional pseudo-parabolic equation for one dimensional Laplace operator. We consider following equation

$$\mathcal{D}_t^{\alpha}[u(t,x)-u_{xx}(t,x)]-u_{xx}(t,x)=f(x), \quad (1)$$

for $(t,x)\in\Omega=\{(t,x)|0<t\leq T<\infty, 0\leq x\leq l\}$, where $\mathcal{D}_t^{\alpha}$ is the Caputo derivative which is defined in the next section. The operator $-\frac{d^2}{dx^2}$ which is participating in the equation(1) is the well known 1D Laplace operator and we will denote it further by $\mathcal{L}$. We know the second order differential operator in $L^2(0,l)$ generated by the differential expression

$$\mathcal{L}u(x)=-u_{xx}(x), x\in(0,l) \quad (2)$$

and boundary conditions

$$u(0)=0, u(l)=0, \quad (3)$$

is self-adjoint in $L^2(0,l)$. The problem (2)-(3) has the following eigenvalues

$$\lambda_k=\left(\frac{k\pi}{l}\right)^2, k\in\mathbb{N},$$

and the corresponding system of eigenfunctions

$$e_k(x)=\sqrt{\frac{2}{l}}\sin\frac{k\pi}{l}(x), k\in\mathbb{N}.$$

It is known that the self-adjoint problem has real eigenvalues and their eigenfunctions form a complete orthonormal basis in $L^2(0,l)$.

The study of inverse problems for pseudo parabolic equations began in the 1980s. The first result obtained by Rundell [2] refers to the inverse

identification problems for an unknown sourse function f in a following equation

$$\frac{\partial}{\partial t}[u(x,t)+\mathcal{L}u(x,t)]+\mathcal{L}u(x,t)=f. \qquad (4)$$

Where $\mathcal{L}$ is even order linear differential operator. Rundell proved global existence and uniqueness theorems for cases when f depends only x or only t. In a series of articles [6], [7], [8], [9], [10], [12], [13], [14], [15],[16],[17] some recent work has been done on inverse problems and spectral problems for the diffusion and anomalous diffusion equations.

Definitions of fractional operators

We begin this paper with a brief introduction of several concepts that are important for the further studies.

Definition 1. [5] The Riemann-Liouville fractional integral I^{α} of order $\alpha>0$ for an integrable function is defined by

$$I^{\alpha}[f](t)=\frac{1}{\Gamma(\alpha)}\int_{c}^{t}(t-s)^{\alpha-1}f(s)ds, t\in[c,d],$$

where Γ denotes the Euler gamma function.

Definition 2. [5] The Riemann-Liouville fractional derivative D^{α} of order $\alpha\in(0,1)$ of a continuous function is defined by

$$D^{\alpha}[f](t)=\frac{d}{dt}I^{\alpha}[f](t), t\in[c,d].$$

Definition 3. [5] The Caputo fractional derivative of order $0<\alpha<1$ of a differentiable function is defined by

$$\mathcal{D}_{*}^{\alpha}[f](t)=D^{\alpha}[f'(t)], t\in[c,d].$$

Definition 4.[5] (Caputo derivative). Let $f\in L^{1}[a,b], -\infty\le a<t<b\le+\infty$and $f*K_{m-\alpha}(t)\in W^{m,1}[a,b], m=[\alpha], \alpha>0$.The Caputo fractional derivative$\partial_{+a}^{\alpha}$of order$\alpha\in\mathbb{R}$ $(m-1<\alpha<m, m\in\mathbb{N})$ is defined as

$$\partial_{+a}^{\alpha}f(t)=$$
$$=D_{+a}^{\alpha}\left[f(t)-f(a)\right.$$
$$\left.-f'(a)\frac{(t-a)}{1!}-\ldots-f^{(m-1)}(a)\frac{(t-a)^{m-1}}{(m-1)!}\right].$$

If $f\in C^{m}[a,b]$ then, the Caputo fractional derivative ∂_{+a}^{α} of order $\alpha\in\mathbb{R}$ ($m-1<\alpha<m, m\in\mathbb{N}$) is defined as

$$\partial_{+a}^{\alpha}[f](t)=I_{+a}^{m-\alpha}f^{(m)}(t)=$$
$$=\frac{1}{\Gamma(m-\alpha)}\int_{a}^{t}(t-s)^{m-1-\alpha}f^{(m)}(s)ds.$$

Formulation of the problem

Problem 1. We aim to find a couple of functions $(u(t,x), f(x))$ satisfying the equation(1), under the conditions

$$u(0,x)=\varphi(x), x\in[0,l] \qquad (5)$$

$$u(T,x)=\psi(x), x\in[0,l]. \qquad (6)$$

and the homogeneous Dirichlet boundary conditions

$$u(t,0)=u(t,l)=0, t\in[0,T]. \qquad (7)$$

By using $\mathcal{L}$–Fourier analysis we obtain existence and uniqueness results for this problem.

We say a solution of Problem 1 is a pair of functions $(u(t,x), f(x))$ such that they satisfy equation(1) and conditions(5)-(7) where $u(t,x)\in C^{1}([0,T];C^{2}([0,l]))$ and $f(x)\in C([0,l])$.

Main results

For Problem 3.1, the following theorem holds.

Theorem 1. Assume that$\varphi(x),\psi(x)\in C_{0}^{3}[0,\pi]$. Then the solution $u(t,x)\in C^{1}\big([0,T],\ C^{2}([0,l])\big)$, $f(x)\in C([0,l])$ of the Problem 3.1 exists, is unique, and can be written in the form

$$u(t,x) = \varphi(x) + \sum_{k=1}^{\infty} \frac{\left(\varphi_k^{(2)} - \psi_k^{(2)}\right)\left(1 - E_{\alpha,1}\left(-\frac{\left(\frac{k\pi}{l}\right)^2}{1+\left(\frac{k\pi}{l}\right)^2} t^{\alpha}\right)\right)}{\left(\frac{k\pi}{l}\right)^2\left(1 - E_{\alpha,1}\left(-\frac{\left(\frac{k\pi}{l}\right)^2}{1+\left(\frac{k\pi}{l}\right)^2} T^{\alpha}\right)\right)} \sin\frac{k\pi}{l}(x), \tag{8}$$

$$f(x) = -\varphi''(x) + \sum_{k=1}^{\infty} \frac{\varphi_k^{(2)} - \psi_k^{(2)}}{1 - E_{\alpha,1}\left(-\frac{\left(\frac{k\pi}{l}\right)^2}{1+\left(\frac{k\pi}{l}\right)^2} T^{\alpha}\right)} \sin\frac{k\pi}{l}(x), \tag{9}$$

where $\varphi_k^{(2)} = (\varphi'', e_k)_{L^2(0,l)}, \psi_k^{(2)} = (\psi'', e_k)_{L^2(0,l)}$ and $E_{\alpha,\beta}(\lambda t)$ is the Mittag-Leffler type function (see [4]):

$$E_{\alpha,\beta}(z) = \sum_{n=0}^{\infty} \frac{z^m}{\Gamma(\alpha m + \beta)}.$$

First of all, we start by proving an existence result**.**

Proof. Let us seek functions $u(x,t)$ and $f(x)$ in the forms:

$$u(t,x) = \sum_{k=1}^{\infty} u_k(t)\sin\frac{k\pi}{l}(x), k \in \mathbb{N}, \tag{10}$$

and

$$f(x) = \sum_{k=1}^{\infty} f_k \sin\frac{k\pi}{l}(x), k \in \mathbb{N}, \tag{11}$$

where $u_k(t)$ and f_k are unknown. Substituting Equations (10) and (11) into Equation (1), we obtain the following equation for the functions $u_k(t)$ and the constants f_k:

$$D_t^{\alpha} u_k(t) + \frac{\left(\frac{k\pi}{l}\right)^2}{1+\left(\frac{k\pi}{l}\right)^2} u_k(t) = \frac{f_k}{1+\left(\frac{k\pi}{l}\right)^2}.$$

Solving these equation,we obtain

$$u_k(t) = \frac{f_k}{\left(\frac{k\pi}{l}\right)^2} + C_k E_{\alpha,1}\left(-\frac{\left(\frac{k\pi}{l}\right)^2}{1+\left(\frac{k\pi}{l}\right)^2} t^{\alpha}\right),$$

where the constants f_k and C_k are unknown. To find these constants, we use conditions(5), (6). Let φ_k and ψ_k be the coefficients of the expansions of $\varphi(x)$ and $\psi(x)$:

$$\varphi_k = \sqrt{\frac{2}{l}}\int_0^l \varphi(x)\sin\frac{k\pi}{l}(x)dx, k \in \mathbb{N},$$

$$\psi_k = \sqrt{\frac{2}{l}}\int_0^l \psi(x)\sin\frac{k\pi}{l}(x)dx, k \in \mathbb{N}.$$

We first find C_k:

$$u_k(0) = \frac{f_k}{\left(\frac{k\pi}{l}\right)^2} + C_k = \varphi_k,$$

$$u_k(T) = \frac{f_k}{\left(\frac{k\pi}{l}\right)^2} + C_k E_{\alpha,1}\left(-\frac{\left(\frac{k\pi}{l}\right)^2}{1+\left(\frac{k\pi}{l}\right)^2} T^{\alpha}\right) = \psi_k.$$

Then

$$C_k = \frac{\varphi_{1k} - \psi_{1k}}{1 - E_{\alpha,1}\left(-\frac{\left(\frac{k\pi}{l}\right)^2}{1+\left(\frac{k\pi}{l}\right)^2} T^{\alpha}\right)}.$$

The constant f_k is represented as

$$f_k = \varphi_k\left(\frac{k\pi}{l}\right)^2 - C_k\left(\frac{k\pi}{l}\right)^2.$$

Substituting $u_k(t)$ and f_k into expansion (10), we find

$$u(t,x)=\varphi(x)+\sum_{k=1}^{\infty}C_k\left(E_{\alpha,1}\left(-\frac{\left(\frac{k\pi}{l}\right)^2}{1+\left(\frac{k\pi}{l}\right)^2}t^{\alpha}\right)-1\right)\sin\frac{k\pi}{l}(x). \tag{12}$$

By the supposition of the theorem we know

$$\varphi^{(n)}(0)=0,\varphi^{(n)}(\pi)=0,n=0,1,2,$$
$$\psi^{(n)}(0)=0,\psi^{(n)}(\pi)=0,n=0,1,2.$$

then using they we have

$$C_k=\frac{\varphi_k-\psi_k}{1-E_{\alpha,1}\left(-\frac{\left(\frac{k\pi}{l}\right)^2}{1+\left(\frac{k\pi}{l}\right)^2}T^{\alpha}\right)}=-\frac{\varphi_k^{(2)}-\psi_k^{(2)}}{\left(\frac{k\pi}{l}\right)^2\left(1-E_{\alpha,1}\left(-\frac{\left(\frac{k\pi}{l}\right)^2}{1+\left(\frac{k\pi}{l}\right)^2}T^{\alpha}\right)\right)}.$$

Putting this into equations (10) and (11) we obtain

$$u(t,x)=\varphi(x)+\sum_{k=1}^{\infty}\frac{\left(\varphi_k^{(2)}-\psi_k^{(2)}\right)\left(1-E_{\alpha,1}\left(-\frac{\left(\frac{k\pi}{l}\right)^2}{1+\left(\frac{k\pi}{l}\right)^2}t^{\alpha}\right)\right)}{\left(\frac{k\pi}{l}\right)^2\left(1-E_{\alpha,1}\left(-\frac{\left(\frac{k\pi}{l}\right)^2}{1+\left(\frac{k\pi}{l}\right)^2}T^{\alpha}\right)\right)}\sin\frac{k\pi}{l}(x). \tag{13}$$

Similarly,

$$f(x)=-\varphi''(x)+\sum_{k=1}^{\infty}\frac{\varphi_k^{(2)}-\psi_k^{(2)}}{1-E_{\alpha,1}\left(-\frac{\left(\frac{k\pi}{l}\right)^2}{1+\left(\frac{k\pi}{l}\right)^2}T^{\alpha}\right)}\sin\frac{k\pi}{l}(x). \tag{14}$$

The following Mittag-Leffler function's estimate is known by [11]:

$$|E_{\alpha,\beta}(z)|\leq\frac{M}{1+|z|},arg(z)=\pi,|z|\to\infty. \tag{15}$$

Now, we show that $u(t,x)\in C^1([0,T];C^2([0,l])),\ f(x)\in C([0,l])$, that is

$$\|u\|_{C^1([0,T];C^2([0,l]))}=\max_{t\in[0,T]}\|u(t,\cdot)\|_{C^2([0,l])}+\max_{t\in[0,T]}\|\mathcal{D}_t^{\alpha}u(t,\cdot)\|_{C^2([0,l])}<\infty,$$

and

$$\|f\|_{C([0,l])}<\infty.$$

By using (15), we get following estimates

$$\begin{aligned}|u(t,x)| &\lesssim|\varphi(x)|+\sum_{k=1}^{\infty}\frac{\left|\varphi_k^{(2)}\right|+\left|\psi_k^{(2)}\right|}{\left(\frac{k\pi}{l}\right)^2\left(1-E_{\alpha,1}\left(-\frac{\left(\frac{k\pi}{l}\right)^2}{1+\left(\frac{k\pi}{l}\right)^2}T^{\alpha}\right)\right)}\\ &\lesssim|\varphi(x)|+\sum_{k=1}^{\infty}\frac{\left|\varphi_k^{(2)}\right|+\left|\psi_k^{(2)}\right|}{\left(\frac{k\pi}{l}\right)^2},\end{aligned} \tag{16}$$

$$|f(x)| \lesssim |\varphi''(x)| + \sum_{k=1}^{\infty} \frac{\left|\varphi_k^{(2)}\right|+\left|\psi_k^{(2)}\right|}{1-E_{\alpha,1}\left(-\frac{\left(\frac{k\pi}{l}\right)^2}{1+\left(\frac{k\pi}{l}\right)^2}T^{\alpha}\right)} \lesssim |\varphi''(x)| + \sum_{k=1}^{\infty} \left|\varphi_k^{(2)}\right| + \left|\psi_k^{(2)}\right|. \quad (17)$$

Where, $L \lesssim \mathrm{Q}$ \$L denotes $L \leq \mathrm{CQ}$ for some positive constant C independent of L and Q.

By supposition of the theorem we know $\varphi^{(2)}$ and $\psi^{(2)}$ are continuous on $[0, l]$.

Then by the Bessel inequality for the trigonometric series (see [1]) and by the Weierstrass M-test (see [3]), series (16) and (17) converge absolutely and uniformly in the region $\overline{\Omega}$. Now we show.

$$|u_{xx}(t,x)| \lesssim |\varphi''(x)| + \sum_{k=1}^{\infty} \frac{\left|\varphi_k^{(2)}\right| + \left|\psi_k^{(2)}\right|}{1 - E_{\alpha,1}\left(-\frac{\left(\frac{k\pi}{l}\right)^2}{1+\left(\frac{k\pi}{l}\right)^2}T^{\alpha}\right)} \lesssim |\varphi''(x)| + \sum_{k=1}^{\infty} \left|\varphi_k^{(2)}\right| + \left|\psi_k^{(2)}\right| < \infty,$$

$$|\mathcal{D}_t^{\alpha} u(t,x)| \lesssim \sum_{k=1}^{\infty} \frac{\left|\varphi_k^{(2)}\right| + \left|\psi_k^{(2)}\right|}{\left(1+\left(\frac{k\pi}{l}\right)^2\right)\left(1 - E_{\alpha,1}\left(-\frac{\left(\frac{k\pi}{l}\right)^2}{1+\left(\frac{k\pi}{l}\right)^2}T^{\alpha}\right)\right)} \lesssim \sum_{k=1}^{\infty} \frac{\left|\varphi_k^{(2)}\right| + \left|\psi_k^{(2)}\right|}{1+\left(\frac{k\pi}{l}\right)^2} < \infty,$$

$$|\mathcal{D}_t^{\alpha} u_{xx}(t,x)| \lesssim \sum_{k=1}^{\infty} \frac{\left(\frac{k\pi}{l}\right)^2\left(\left|\varphi_k^{(2)}\right| + \left|\psi_k^{(2)}\right|\right)}{\left(1+\left(\frac{k\pi}{l}\right)^2\right)\left(1 - E_{\alpha,1}\left(-\frac{\left(\frac{k\pi}{l}\right)^2}{1+\left(\frac{k\pi}{l}\right)^2}T^{\alpha}\right)\right)} \lesssim \sum_{k=1}^{\infty} \left|\varphi_k^{(2)}\right| + \left|\psi_k^{(2)}\right| + \sum_{k=1}^{\infty} \frac{\left|\varphi_k^{(2)}\right| + \left|\psi_k^{(2)}\right|}{1+\left(\frac{k\pi}{l}\right)^2} < \infty.$$

Finally, we obtain

$$\| u \|_{C^1([0,T],C^2[0,\pi])} \leq C < \infty, C = const,$$

and

$$\| f \|_{C([0,l])} < \infty.$$

Existence of the solution is proved.

Now, we start proving uniqness of the solution.Let us suppose that $\{u_1(t,x), f_1(x)\}$ and $\{u_2(t,x), f_2(x)\}$ are solution of the Problem 1. Then $u(t,x) = u_1(t,x) - u_2(t,x)$ and $f(x) = f_1(x) - f_2(x)$ are solution of following problem:

$$\mathcal{D}_t^{\alpha}[u(t,x) - u_{xx}(t,x)] - u_{xx}(t,x) = f(x), \quad (18)$$

$$u(0,x) = 0, \tag{19}$$

$$u(T,0) = 0. \tag{20}$$

By using (13) and (14) for (18)-(20) we easily see $u(x,t) \equiv 0, f(x) \equiv 0$. Uniqness of the solution of the Problem 1.

Acknowledgement

Theauthors were supported by the Ministry of Education and Science of the Republic of Kazakhstan Grant AP05130994.

References

1. Zygmund, A., "Trigonometrical Series." Cambridge (1959).

2. Rundell W. "Determination of an unknown nonhomogeneous term in a linear partial differential equation from overspecified boundary data." Appl. Anal. 10 (1980): 231-242.

3. Knopp K. "Theory of Functions Parts I and II, Two Volumes Bound as One, Part I."New York: Dover; (1996): 73.

4. Y. Luchko, R. Gorenflo. "An operational method for solving fractional differential equations with the Caputo derivatives." Acta Math. Vietnam. 24 (1999): 207–233.

5. Kilbas A.A, Srivastava H.M, Trujillo J.J. "Theory and Applications of Fractional Differential Equations." Mathematics studies 204. North-Holland: Elsevier; (2006): vii–x.

6. Kaliev I.A, Sabitova M.M. "Problems of determining the temperature and density of heat sources from the initial and final temperatures." J Appl Ind Math. 4(3) (2010): 332-339.

7. M. Kirane, A.S. Malik. "Determination of an unknown source term and the temperature distribution for the linear heat equation involving fractional derivative in time." Applied Mathematics and Computation 218(1) (2011):163–170.

8. I. Orazov, M.A. Sadybekov. "One nonlocal problem of determination of the temperature and density of heat sources." Russian Mathematics 56(2) (2012): 60–64 and Computation. 218(1):163–170, 2011.

9. Orazov I., Sadybekov M.A. "On a class of problems of determining the temperature and density of heat sources given initial and final temperature." Sib Math J. 53(1) (2012): 146-151.

10. K.M. Furati, O.S. Iyiola, M. Kirane. "An inverse problem for a generalized fractional di□usion." Applied Mathematics and Computation 249 (2014): 24–31.

11. Z. Li, Y. Liu, M. Yamamoto. "Initial – boundary value problems for multi-term time-fractional diffusion equations with positive constant coefficients." Appl. Math. Comput. 257 (2015): 381–397,.

12. H.T. Nguyen, D.L. Le, V.T. Nguyen. "Regularized solution of an inverse source problem for a time fractional di□usion equation." Applied Mathematical Modelling 40(19) (2016): 8244–8264.

13. M.I. Ismailov, M. Cicek. "Inverse source problem for a time-fractional di□usion equation with nonlocal boundary conditions." Applied Mathematical Modelling 40(7) (2016): 4891–4899.

14. M, Al-Salti N. "Inverse problems for a non-local wave equation with an involution perturbation." J Nonlinear Sci Appl. 9(3) (2016): 1243-1251.

15. N. Al-Salti, M. Kirane, B. T. Torebek. "On a class of inverse problems for a heat equation with involution perturbation." Hacettepe Journal of Mathematics and Statistics. (2017) Doi: 10.15672/HJMS.2017.538

16. M. Kirane, B. Samet, B. T. Torebek. "Determination of an unknown source term temperature distribution for the sub-diffusion equation at the initial and final data." Electronic Journal of Differential Equations (2017): 1–13.

17. B.T. Torebek, R. Tapdigoglu. "Some inverse problems for the nonlocal heat equation with Caputo fractional derivative." Mathematical Methods in the Applied Sciences 40(18) (2017): 6468–6479.

IRSTI 27.31.15

[1*]S.Ya. Serovajsky, [2]A.A. Azimov, [1]M.O. Kenzhebayeva,
[2]D.B. Nurseitov, [1]A.T. Nurseitova, [1]M.A. Sigalovskiy

[1]al-Farabi Kazakh National University, Almaty, Kazakhstan
[2]Satbayev University, Almaty, Kazakhstan
[*]e-mail: serovajskys@mail.ru

Mathematical problems of gravimetry and its applications

Abstract. Gravimetry is associated with analysis of the gravitational field. The gravitational field is characterized by its potential. This is described by the Poisson equation, the right side of which includes the density of the environment. There exists direct and inverse problems of gravimetry. Direct gravimetry problems involve the determination of the potential of the gravitational field in a given region. The inverse problems of gravimetry imply the restoration of the structure of a given area from the results of measuring the characteristics of the gravitational field. Such studies are needed to assess on the basis of gravimetric geodynamic events occurring in oil and gas fields. The relevance of such research is necessary, because with prolonged development of the oil and gas fields, negative consequences may occur. This paper discusses some of the features of direct and inverse gravimetry problems. A description of the mathematical model of the processes under consideration is given. Different direct and inverse gravimetry problems are posed. Describes the methods of its solving. Based on the analysis of the results of a computer experiment, appropriate conclusions are made.
Key words: gravimetry, inverse problems, mathematical model.

Introduction

Gravimetry is a science related to the study of gravitational fields. The gravitational field is potential, i.e. the work expended on movement in this field along a closed curve is zero. The main function characterizing a potential field is the potential. The potential of the gravitational field is described by the Poisson equation, the right-hand side of which includes the density distribution in a given region [1, 2].

Mathematical problems of gravimetry are divided into direct and inverse. Direct gravimetry problems involve finding the distribution of the potential of a gravitational field over a known density distribution in a given region. This is achieved by solving the corresponding boundary value problem for the Poisson equation. In the inverse problems of gravimetry, on the contrary, it is necessary to reconstruct the structure of the considered set by measuring the gravitational field.

The relevance of the inverse problems of gravimetry is due to the fact that in the process of long-term operation of deposits of different minerals (in particular, oil and gas), significant changes occur that have undesirable consequences [3–5]. In this regard, monitoring of existing fields is regularly conducted. In this case, we are interested in gravimetric monitoring. With the help of gravimeters, measurement of the acceleration of gravity, corresponding to the gradient of the potential of the gravitational field, is carried out [6, 7]. This experimental information can be used as a basis for the formulation of inverse problems of gravimetry.

It is known that the inverse problems are ill-posed, in principle [8]. However, the inverse problems of gravity are essentially ill-posed. In particular, the values of the acceleration of gravity determined during the measurement process may be due to various gravity anomalies. Thus, the solution of the inverse problem of gravimetry in the full formulation is not the only solution. Naturally, in

the numerical solution of such a problem, the algorithm outputs to one of these solutions. However, this result may not correspond to reality. Mathematically correct, it will have no practical meaning. In this connection, in practice, only partial inverse gravimetry problems are actually solved (see, for example, [9–18]). These works differ, firstly, in the volume of measured information, secondly, in the amount of identifiable information and, thirdly, in research methods.

In this paper, we discuss some peculiar properties of the formulation of direct and inverse gravimetry problems based on the available experimental information, as well as methods for solving these problems. We characterize some of the difficulties encountered in solving direct and inverse gravimetry problems and discuss ways to overcome.

Statement of the problem

At first, give the general direct gravimetry problem (see, for example, [1,2]). The gravitational field in the given volume is described by the Poisson equation

$$\Delta\psi(x,y,z) = -4\pi G\rho(x,y,z), \qquad (1)$$

where ψ is the gravitational potential, ρ is the density, G is the gravitational constant.

It is necessary to add the boundary conditions. In principle, we can have some results of measuring on the ground surface. Unfortunately, we do not, as a rule, any information about the gravitational field underground. However, it is known that the influence of the object to the gravitational field decreases with distance from the object and tends to zero with unlimited distance from it. Then we can extend the given set such that the gravitational potential on the boundary of the extended set will be zero. Thus, the general direct gravimetry problem is finding the gravitational potential $\psi = \psi(x,y,z)$ from the homogeneous Dirichlet problem for the Poisson equation (1), using known density distribution $\psi = \psi(x,y,z)$.

For formulating inverse problems of gravimetry, it is necessary to determine what specific information we can directly get into the process of gravimetric monitoring and what exactly we would like to find on the basis of this information. Note that when analyzing deposits, we have some territory S in the x, y plane. The terrain in this area is known. In addition, the maximum depth that is of interest to the research is usually specified. It is natural to choose it as a reference, i.e. the zero value of the vertical coordinate z. Then we can assume that the given function is $h = h(x, y)$, which characterizes the height of the terrain at the point x, y of the surface S with respect to the chosen system. Thus, the system is considered in three-dimensional volume

$$V = \{(x,y,z) \mid 0 < z < h(x,y), (x,y) \in S\}.$$

In practice, using gravimeters, the gravitational acceleration is measured, which, up to a sign, coincides with the vertical derivative of the potential of the gravitational field. Thus, the following condition holds

$$\frac{\partial\psi\left(x,y,h(x,y)\right)}{\partial z} = -g(x,y), \ (x,y) \in S, \quad (2)$$

where g is the experimentally measured value of the gravitational acceleration. This information, which is the result of gravimetric monitoring, can be used as the basis for the formulation of inverse gravimetry problems.

The purpose of the gravimetric monitoring of the existing field is largely to clarify the geological and tectonic structure and geological field information of the study area in order to highlight the risk of geodynamic processes. Such information can be obtained by knowing the density distribution in a given region. Thus, the object of the search in the process of solving the inverse problem of gravimetry is the density function, which is in the right-hand side of the considered equation (1). Therefore, the general gravimetry problem is finding the density distribution $\rho = \rho(x,y,z)$ in the volume V such that the solution of the homogeneous Dirichlet problem for the Poisson equation (1) in the extended set satisfies the additional condition (2).

As is known, the most natural way to solve inverse is to reduce them to optimization problems. In particular, the stated inverse problem can be reduced to the problem of minimizing the functional

$$I = I(\rho) = \int_S \left[\frac{\partial\psi\left(x,y,h(x,y)\right)}{\partial z} + g(x,y)\right]^2 dS, \quad (3)$$

where ψ is a solution of the considered direct problem corresponding to the given function ρ. Naturally, the solution of the inverse problem also turns out to be the solution of the optimization

problem, and the solution of the optimization problem under the condition of its existence will be the solution of this inverse problem. The practical solution of the obtained optimization problem is carried out using numerical optimization methods, for example, the gradient method [19–21].

Note that in reality the measurement of the gravitational acceleration is carried out not everywhere in a given area S, but only at certain points (x_i,y_i), $i = 1,2,\ldots,M$, where gravimeters are located. Thus, in fact, instead of (2), we have the condition

$$\frac{\partial\psi\left(x_i,y_i,h(x_i,y_i)\right)}{\partial z} = -g_i,\ i = 1,\ldots,M \qquad (4)$$

with known values g_i. Thus, in practice, either by interpolation, the transition to condition (2) is performed, followed by minimization of the functional (3), or we solve the minimization problem for the functional.

$$I = I(\rho) = \sum_{i=1}^{M}\left[\frac{\partial\psi\left(x_i,y_i,h(x_i,y_i)\right)}{\partial z} + g_i\right]^2. \qquad (5)$$

Results and discussion

For simplicity, we perform the analysis for the two-dimensional case, considering the horizontal coordinate x and the vertical coordinate z. For the direct problem in the simplest case, we consider a rectangular area in which the gravitational anomaly is located, i.e. an object significantly different in density from the environment. Figure 1 shows the density distribution over a given area, as well as the calculated distribution of the gravitational potential and its derivative in the upper part of the region corresponding to the earth's surface if the anomaly is located in the center of the considered set (Figure 1a) and near its boundary (Figure 1b).

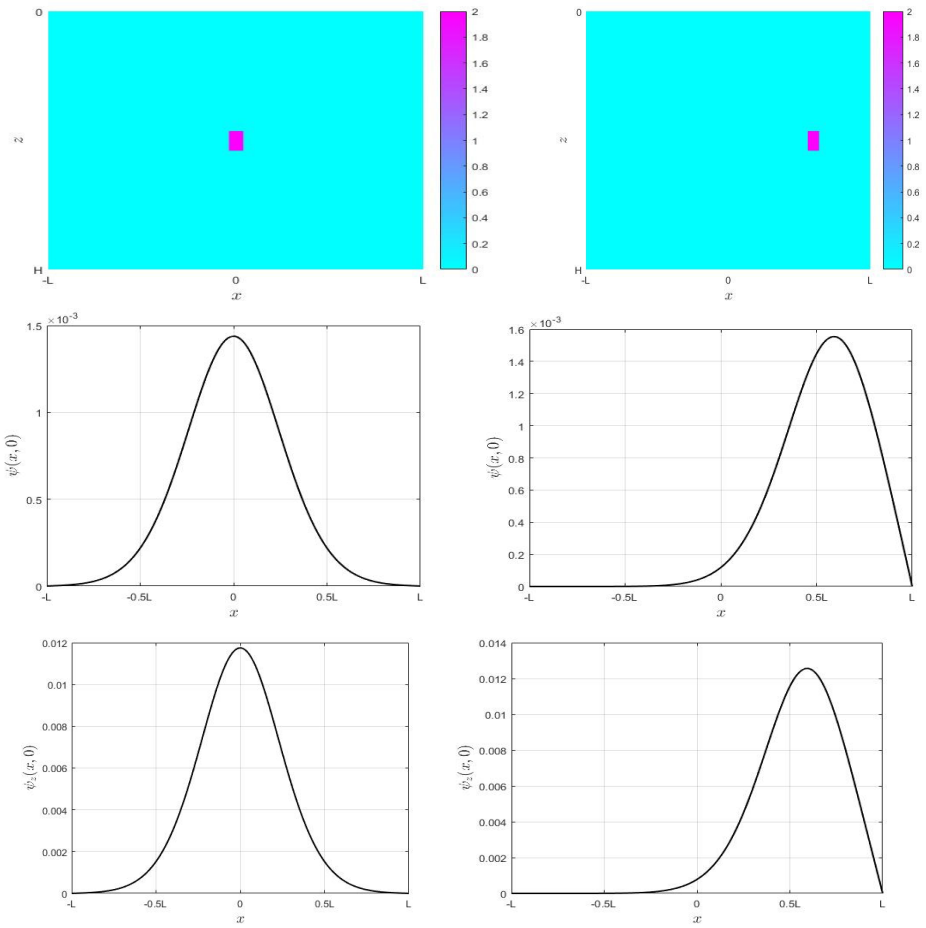

a) anomaly is in the center b) anomaly is near the boundary

Figure 1 – Density distribution, potential, and its vertical derivative for the case of rectangular anomaly

As can be seen from Figure 1a, at the location of the anomaly (point x), the potential and its vertical derivative have their maximum value. As one moves away from the anomaly, these values decreases to zero equally in both directions, which is the corollary to zero boundary conditions. However, when the anomaly is located near the boundary of the region under consideration (Figure 1b), the potential distribution and its derivative are no longer symmetrical, which is not satisfactory. The results suggest that, in order to eliminate the influence of the boundaries, the area under consideration should be significantly extended.

At the next stage of the study, we are already repelling ourselves from the geological and lithographic section of the real field. Figure 2 depicts the density distribution in the considered area, with the yellow color indicating the area filled with clay – the predominant environmental material and relatively high density, blue – the air that inside the field corresponds to the existing voids with significantly lower density, and green – oil, more lighter than clay, but heavier than air. When extending a given area, it is assumed that air is located above the surface of the earth, and clay is located outside the initial area.

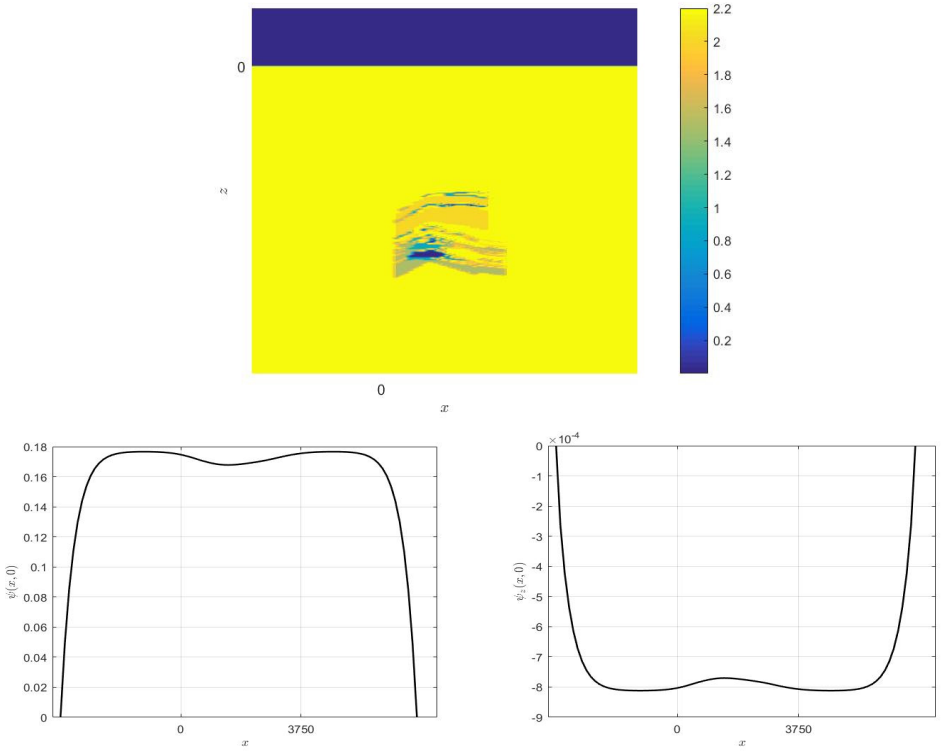

Figure 2 – Density distribution, potential, and its vertical derivative for the extended set with real parameters and usial density outside the initial set

As can be seen from the results obtained, the potential on the surface of the earth over the zone of predominance of oil and voids is lower compared to the neighboring zones where clay is predominant. This is due to the fact that the clay has a greater density. In this case, the vertical derivative of the potential is negative, since as the distance from the object increases, the potential value decreases, and the larger, the larger the potential value itself. We draw attention to the fact that outside the initial region, the potential value turns out to be rather large and decreases sharply to zero in the vicinity of the boundaries. This is explained by the fact that there is heavy clay outside the initial region, and zero potential values are rigidly set at the boundary. Besides, the potential derivative greatly increases in the neighborhood of the boundaries. Such a result cannot be considered satisfactory, and suggests that the density in the extended part of the region should be continued to zero. Indeed, we consider the gravitational field created by objects located in a given area.

At the next stage of the analysis, we carried out calculations with the extension of the set so

that the density outside the initial region is assumed to be zero. In this case, the distribution of the potential gradually decreases to zero as the boundaries approach. The value of the vertical derivative potential also tends to zero, see Figure 3.

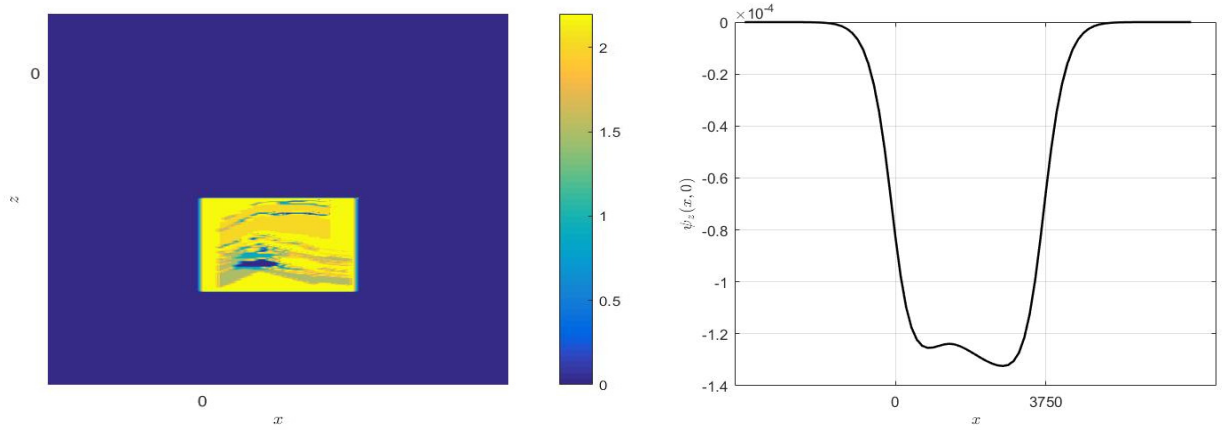

Figure 3 – Density distribution and vertical derivative of the potential for the extended set with real parameters and usial density outside the initial set

The question arises, how we can determine the size of the extended set. First, some extension is selected, and the value of the derivative potential on the earth's surface in the given region is calculated. Then the area extends again and calculations are carried out. If the newly found value of the derivative potential practically does not differ from that found earlier, then the calculations are terminated. Otherwise, a new extension is carried out.

Now consider the inverse problem. At first, we try to solve the general inverse problem for the two-dimensional case. We determine the gravitational anomaly as the square with a higher density than the density of the environment (see Figure 4a). Then we solve the Poisson equation with given boundary condition and calculate the vertical derivative of the potential at the ground surface. Now we put the result to the minimizing functional and solve the minimization problems by means of the gradient method. The iterative method converged, and the sequence of functional tends to zero. Thus, we found the solution of the optimization problem that is the solution of inverse problem too. The obtained result is shown in the Figure 4b). Unfortunately, this result is significantly different from the real. This is the corollary of the non-uniqueness of the considered inverse problem.

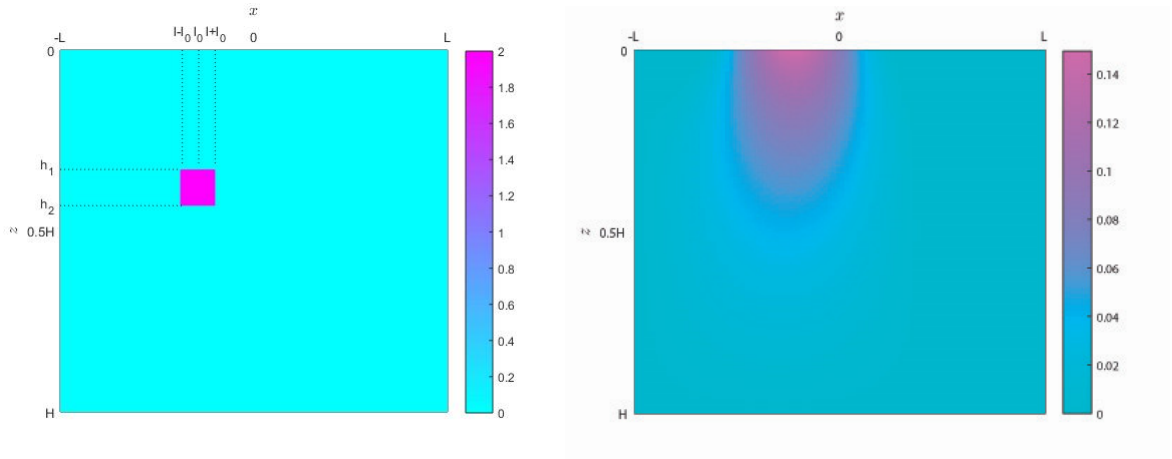

a) real position b) obtained position

Figure 4 – Position of the gravitational anomaly of the inverse problem

Its is clear that the general inverse problem of gravimetry is not very interesting because of its significantly non-uniqueness. We had a few data (boundary value of potential derivative) for finding the many information (density as a function of spatial variables). Then we consider two partial cases. For the first case, we suppose that we know the position of the homogeneous anomaly, its form and size, but its density is unknown. For the second case, we consider inverse situation. The density of the anomaly with given form and size is known, and its position is unknown. The first problem was be solved by gradient methods [19–21] with good enough exactness. The second (geometric) inverse problem has the peculiarity. The minimizing functional is not Gateaux differentiable. It is subdifferentiable only. Then we use the methods of non-smooth optimization, particularly, the subgradient method [22], the Nelder – Mead method [23], and genetic algorithms [24]. The exactness of the results was be good enough too. This is clear, because for both partial inverse problems, we determine one (constant density) or two (coordinates of the anomaly) parameters, using the knowledge of the function (vertical derivative of the potential at the ground surface).

Conclusion

Based on the obtained results, the following conclusions can be drawn:

1. The direct problem of gravimetry is based on the Poisson equation with respect to the potential of the gravitational field with a density included in the right-hand side of the equation.
2. To find the potential distribution in a given region, the given region should be extended by setting uniform Dirichlet boundary conditions on the extended set.
3. The density value outside the source region is assumed to be zero.
4. Experimentally measured the acceleration of gravity, which corresponds to the vertical derivative of the gravitational potential.
5. The method of choosing the size of the extended set is proposed.
6. The general inverse problem of gravimetry is to find the density distribution in a given area, using the measure of the potential derivative on the outer surface.
7. The general inverse problem of gravimetry has essentially not the only solution, as a result of which the value of the density distribution found using standard optimization methods may differ from its real value.
8. Some particular inverse problems of gravimetry have been solved, in particular, the restoration of constant density and coordinates of the location of the gravitational anomaly.
9. Optimization problems corresponding to inverse gravimetry can be characterized by a non-differentiable functional. In this case, non-smooth optimization methods can be used, in particular, the subgradient method, the Nelder – Mead method, and genetic algorithms.
10. The obtained results can be used in monitoring oil and gas fields.

Acknowledgment

The research was supported by the project AP05135158 “Development of geographic information system for solving the problem of gravimetric monitoring of the state of the subsoil of oil and gas regions of Kazakhstan based on high-performance computing in conditions of limited experimental data”

References

1. C. Misner, K. Thorne. Gravitation. – W.H. Freeman & Company, Princeton University Press, 1973.
2. D.D. Ivanenko, G.A. Sardanashvili Gravitation. – M .: URSS, 2008.
3. Yu.M. Nesterenko, M.Yu. Nesterenko, V.I. Dnistryanski, A.V. Glyantsev. “Influence of the development of hydrocarbon deposits on geodynamics and water systems of the Southern Urals region.” Bulletin of the Orenburg Scientific Center, Ural Branch of the Russian Academy of Sciences no. 4 (2010): 28–41.
4. Yu.O. Kuz’min “Modern geodynamics and geodynamic risk assessment for subsoil use.” AEN (1999).
5. V.A. Chernyh. “Hydro-mechanics of oil and gas production.” VNIIGAZ (2001).
6. H. Virtanen. “Studies of earth dynamics with superconducting gravimeter.” Academic Dissertation at the University of Helsinki, Geodetiska Institutet (2006): 45 p.

7. V.B. Vinogradov, L.A. Bolotnova, Gravimeters. UGGU publ. (2010).

8. S. Kabanikhin. “Inverse and Ill-posed Problems: Theory and Applications.” – Boston, Berlin: Walter de Gruyter (2012).

9. V.N. Strakhov, M.I. Lapina. “The assembly method for solving the inverse problem of gravimetry.” RAS 227, no. 2 (1976): 344–347.

10. L. Misici, F. Zirilli. “The inverse gravimetry problem: An application to the northern San Francisco craton granite.” Journal of Optimization Theory and Applications 63, no. 1 (1989): 39–49.

11. R. Barzaghi, F. “Sansó The integrated inverse gravimetric-tomographic problem: a continuous approach.” Inverse Problems 14, no. 3 (1998): 499–520.

12. V. Michel. “Regularized wavelet-based multiresolution recovery of the harmonic mass density distribution from data of the earth's gravitational field at satellite height.” Inverse Problems 21 (2005): 997–1025.

13. W. Jacoby, P. Smilde. “Gravity Interpretation: Fundamentals and Application of Gravity Inversion and Geological Interpretation.” Springer Science & Business Media (2009).

14. I. Prutkin, A. Saleh. “Gravity and magnetic data inversion for 3D topography of the Mono discontinuity in the northern Red Sea area.” Journal of Geodynamics 47, no. 5 (2009): 237–245.

15. P.I. Balk, A. Yeske “Fitting approach of V.N. Strakhov to solving inverse problems of gravity exploration: up-to-date status and real abilities.” Geophysical journal 35, no. 1 (2013): 12–26.

16. V.V. Vasin, E.N. Akimova, A.F. Miniakhmetova. “Iterative Newton Type Algorithms and Its Applications to Inverse Gravimetry Problem.” Vestnik of the South Ural State University. Series: Mathematical modelling and programming 6, no. 3 (2013): 26–33.

17. E.N. Akimova, V.V. Vasin, V.E. Misilov. “Algorithms for solving inverse gravimetry problems of finding the interface between media on multiprocessing computer systems.” Vestnik of Ufim State Aviation Technical University 18, no. 2 (2014): 208–217.

18. P. Balk, A. Dolgal, T. Balk, L. Khristenko. “Joint use of inverse gravity problem methods to increase interpretation informativity.” Geofizicheskiy Zhurnal 37, no. 4 (2017): 75–92.

19. E. Polak. Computational methods in optimization: A unified approach. – New York, Academic Press (1971).

20. R.P. Fedorenko. “Approximated solving of optimization control, problem.” Nauka (1978).

21. A. Parkinson, R. Balling, J. Hedengren. “Optimization methods for engineering design.” Provo, UT: Brigham Young University (2013).

22. N. Shor “Minimization Methods for non-differentiable functions.” –Berlin, etc. Springer-Verlag (1985).

23. M. Avriel. Nonlinear Programming: Analysis and Methods. – Dover Publishing (2003).

24. L.A. Gladkov, V.V. Kureichik, V.M. Kureichik. “Genetic Algorithms: Study Guide.” Fizmatlit (2006).

IRSTI 27.35.43

[1]S.I. Kabanikhin, [2]M.A. Bektemessov, [3]O.I. Krivorotko, [4]Zh.M. Bektemessov

[1]Institute of Computational Mathematics and Mathematical Geophysics of SB RAS, Novosibirsk, Russian, e-mail: kabanikhin@sscc.ru
[2]Abai Kazakh National Pedagogical University, Almaty, Kazakhstan, e-mail: maktagali@mail.ru
[3]Institute of Computational Mathematics and Mathematical Geophysics of SB RAS, Novosibirsk, Russian, e-mail: olga.krivorotko@sscc.ru
[4]al-Farabi Kazakh National University, Almaty, Kazakhstan, e-mail: jolaman252@gmail.com

Determination of the coefficients of nonlinear ordinary differential equations systems using additional statistical information

Abstract. The study of the clinical and epidemiological features of tuberculosis combined with HIV infection (TB + HIV) is one of the priorities in the prevention of infectious diseases and is necessary to improve the quality of medical care for patients. So this article is devoted to the mathematical model of epidemiology, its' investigation and analysis. The previous works showed what identifiability analysis is and considered methods of performing them, such as orthogonal method, eigenvalue method and etc., for more precise clarification of model parameters. However, the choice of solving the inverse problem to restore unknown parameters is playing a huge role. So here was showed the combination of two numerical algorithms, as stochastic method of simulating annealing to determine the region of the global minimum and gradient method to determine the inverse problem in a region, of solving the inverse problem that will help to create effective treatment plan for the elimination and treatment of the disease.
Key words: epidemiology, inverse problems, ODE, optimization.

Introduction

Systems of nonlinear ordinary differential equations (ODE) describe processes in biology and medicine, namely, immunology, epidemiology, pharmacokinetics, sociology, economics and etc. The equations are built on the basis of the law of mass balance and operate in a closed system. The coefficients of ODE systems characterize important parameters of the immune response, the spread rate of the disease in the region, the absorption rate of drugs, etc., which cannot be determined from statistical data and need to be clarified. Specified individual parameters will allow you to create the most effective treatment plan and action plan for the elimination and treatment of the disease. One way to identify the extent of damage to the immune system, namely the parameters of the disease, the immune response, as well as determining the optimal treatment, is mathematical modeling.

According to the characteristics of the immune response, it is already possible to numerically analyze the optimal control programs for treating a disease. Example of mathematical model of epidemiology (co-infection of HIV and tuberculosis) shows studies on the identifiability of mathematical models for ODE systems, stability of inverse problems and methods for their numerical solution and computational optimization, which are necessary to develop an algorithm for regularizing the solution of inverse problems.

In [1] the deterministic model of TB dynamics was observed, they also conducted identifiability analysis by constructing sensitivity matrix to restore the identifiable parameters. The identification of parameters was conducted by solving the linear least

squares problem using the QR factorization with column pivoting.

Model

The cause of tuberculosis (TB) is a bacterium called Mycobacterium tuberculosis, which usually affects the lungs, and TB is spread by airborne droplets (coughing, sneezing, etc.). People living with HIV (PLHIV) are at much greater risk of contracting TB than HIV-negative people. If TB is not treated properly, death is possible. Tuberculosis is one of the leading causes of death among PLHIV in the world. It can manifest itself in two ways: latently infected with TB and active way of TB.

Latently infected with TB means that not all people infected with the bacteria become ill with TB. When a person is infected with TB, but has no symptoms and does not feel sick, it is considered that he has a "latent infection of TB". Such a person is not infectious and is not able to infect other people. In about 5–10% of cases, a latent infection leads to tuberculosis. This happens if an infected person does not have sufficiently strong immunity to protect against bacteria. A person with active tuberculosis feels sick; he may have the following symptoms: cough for several weeks, chest pain, blood or sputum when coughing, weakness, fatigue, weight loss, lack of appetite, chills, fever and night sweats.

Co-infection of TB and HIV is a situation where a person lives with HIV and latent or active TB at the same time. Worldwide, TB is the leading cause of death among PLHIV, as it accounts for 25% of all deaths among PLHIV. Given the detrimental effects of HIV infection on the immune system, PLHIV with TB co-infection are 20 times more likely to develop active TB [2]. In addition, it has been proven that tuberculosis increases viral replication in PLHIV and accelerates the progression of HIV, being unhealed.

A mathematical model of the epidemiology of co-infection with tuberculosis (TB) and HIV is considered [3]:

$$\begin{cases} \dot{S} = \Lambda - \beta c S \,{}^{(I+J_3)}\!/_{N} - \lambda\sigma S \,{}^{(J^*)}\!/_{R} - \mu S, \\ \dot{L} = \beta c (S+T) \,{}^{(I+J_3)}\!/_{N} - \lambda\sigma L \,{}^{(J^*)}\!/_{R} - (\mu + k + r_1)L, \\ \dot{I} = kL - (\mu + d + r_2)I, \\ \dot{T} = r_1 L + r_2 I - \beta c T \,{}^{(I+J_3)}\!/_{N} - \lambda\sigma T \,{}^{(J^*)}\!/_{R} - \mu T, \\ \dot{J}_1 = -\beta c J_1 \,{}^{(I+J_3)}\!/_{N} + \lambda\sigma (S+T) \,{}^{(J^*)}\!/_{R} - (\alpha_1 + \mu)J_1 + r^* J_2, \\ \dot{J}_2 = \beta c J_1 \,{}^{(I+J_3)}\!/_{N} + \lambda\sigma L \,{}^{(J^*)}\!/_{R} - (\alpha_2 + \mu + k^* + r^*)J_2, \\ \dot{J}_3 = k^* J_2 - (\alpha_3 + \mu + d^*)J_3, \\ \dot{A} = \alpha_1 J_1 + \alpha_2 J_2 + \alpha_3 J_3 - (\mu + f)A, \\ S(0) = S_0, L(0) = L_0, I(0) = I_0, T(0) = T_0, \\ J_1(0) = J_{1_0}, J_2(0) = J_{2_0}, J_3(0) = J_{3_0}, A(0) = A_0. \end{cases} \quad (1)$$

Here *S(t)* – number of non-infected individuals, *L(t)* – number of individuals latently infected with TB (without HIV), *I(t)* – number of individuals with active TB (without HIV), *T(t)* – number of individuals cured of TB (without HIV), $J_1(t)$ – the number of individuals infected with HIV (without TB), $J_2(t)$ – the number of individuals infected with HIV and latently infected with TB, $J_3(t)$ – number of individuals infected with HIV and active TB, *A(t)* – number of individuals with AIDS. $N = S + L + I + T + J_1 + J_2 + J_3 + A$ _ total population, $R = S + L + T + J_1 + J_2$- active population, $J^* = J_1 + J_2 + J_3$ – people infected with HIV [4].

This model contains many parameters, 6 of which are individual in each specific case and need to be clarified $q = (\mathrm{k}, \mathrm{k}^*, \mathrm{r}_2, \alpha_1, \alpha_2, \alpha_3)^{\mathrm{T}}$. The values of the parameters q are given in Table 1.

Table 1 – Definitions of parameters used in the model (1)

Parameter	Definition	Units	Value
k	the rate of development of active TB (without HIV)	year	0,05
k^*	the rate of development of active TB (with HIV)	year	0,25
r_2	TB treatment rate (without HIV)	human/ year	1
α_1	group HIV transition rate $J_1(t)$	year	0,1
α_2	group HIV transition rate $J_2(t)$	year	0,2
α_3	group HIV transition rate $J_3(t)$	year	0,5

Let *additional information* about system (1) be known at time points t_k of only three groups of individuals:

$$I(t_k) = I_k, J_3(t_k) = J_{3k},$$

$$A(t_k) = A_k, k = 1, \dots, K$$

The mathematical model of co-infection of tuberculosis and HIV consists of 8 equations, but measurement data are known only about 3 of them once a year during the 5 years. That is, we have M = 3, K = 5. This model contains many parameters, 6 of which are individual in each specific case and need to be refined. Based on the analysis of identifiability carried out by one of the methods such as the orthogonal method [5], condition numbers, etc. [6], more precisely, in this work, by the method of eigenvalues [7-8], we will determine only 4 identifiable parameters $q = (k, r_2, \alpha_1, \alpha_3)^T$ from additional statistical information.

In the case of matrices of large dimensions or non-uniformly filled matrices, the eigenvalue method is unstable [9]. In such cases, it is recommended to use the method based on singular numbers [10], since it is known [11] that the condition number of the sensitivity matrix determines the convention (incorrectness) of system (2). The greater the condition number, the higher the incorrectness of the inverse problem (for the inversion of the sensitivity matrix, the use of regularization methods is required).

The values of the parameters, depending on the population, and the initial data are known are given in Table 2.

Table 2– Values of parameters and known initial data used in the model (1)

Parameter	Value	Unit
$S(0)$	*430*	in thousands of people
$L(0)$	*3854.5*	in thousands of people
$I(0)$	*16.875*	in thousands of people
$T(0)$	*3.412*	in thousands of people
$J_1(0)$	*3.2757*	in thousands of people
$J_2(0)$	*27.7*	in thousands of people
$J_3(0)$	*1.4*	in thousands of people
$A(0)$	*0.357*	in thousands of people
Λ	*43*	in thousands of people
N	*4315.76*	in thousands of people
μ	*0.0143*	in thousands of people
$\lambda^*\sigma$	0.529	Nondimensionalized
d^*	0.222	Nondimensionalized
f	0.997	Nondimensionalized
$\beta^* c$	0.99927	Nondimensionalized
d	0.06685	Nondimensionalized

In vector form, the inverse problem is written as follows:

$$\begin{cases} \dot{X} = F(X(t), q), X(0) = X_0, \\ X_i(t_k) = \Phi_k^i. \end{cases} \quad (2)$$

Here is the vector-function – $X = (S, L, I, T, J_1, J_2, J_3, A)$, data – $\Phi_k^i = (I_k, I_{3k}, A_k)$.

The inverse problem was reduced to the problem of minimizing the objective functional in the form:

$$J(q) = \sum_{i=1}^{3} \sum_{k=1}^{K} \left(X(t_k; q) - \Phi_k^i\right)^2 \quad (3)$$

Due to the fact that the task of minimizing the objective functional is a multiparameter, then the determination of the global minimum requires the use of combined numerical methods – method of simulated annealing and gradient method.

Methods

Simulated annealing – general algorithmic method for solving the global optimization problem, especially discrete and combinatorial optimization. Is the one examples of Monte Carlo methods. The algorithm is created by N. Metropolis and it is based on the imitation of the physical process that occurs during the crystallization of a substance, including during annealing of metals. It is assumed that atoms are already lined up in the crystal lattice, but transitions of individual atoms from one cell to another are still permissible. It is assumed that the process proceeds at a gradually decreasing temperature. The transition of an atom from one cell to another occurs with a certain probability, and the probability decreases with decreasing temperature. A stable crystal lattice corresponds to the minimum energy of the atoms, so the atom either enters a state with a lower energy level or remains in place.

By simulating such a process, one finds a point or a set of points at which the minimum of some numerical function $F(x)$ is reached, where $x = (x_1, x_2, \dots, x_m) \in X$. The solution is figured out by sequential calculation of points $x_0, x_1, \dots$, in space X; each point, starting with x_1, "pretends" to better the solution than the previous ones. Algorithm takes point x_0 as the raw data. At each step, the algorithm (which is described below) calculates a new point and lowers the value of the "temperature" value (initially positive). The algorithm stops when it reaches a point that turns out to be at a temperature of zero.

According to the algorithm the point x_{i+1} is obtained on the basis of the current point x_i as follows. The A operator that randomly modifies the point is applied to point x_i, in result we obtain new point x^*.

The point x^* becomes a point x_{i+1} with the probability $P(x^*, x_{i+1})$, which is calculated according to the Gibbs distribution:

$$P(x^* \to x_{i+1} | x_i) = \begin{cases} 1, F(x^*) - F(x_i) < 0 \\ \exp\left(-\dfrac{F(x^*) - F(x_i)}{Q_i}\right), F(x^*) - F(x_i) \geq 0 \end{cases}$$

Here $Q_i > 0$ – elements of arbitrary decreasing, converging to zero positive sequence, which sets the analogue of the falling temperature in the crystal. The rate of decrease and the law of decrease can be set at the request of the creator of the algorithm.

The simulated annealing algorithm is similar to a *gradient descent*, but due to the randomness of the choice of an intermediate point, it should fall into local minima less often than gradient descent. The simulated annealing algorithm does not guarantee finding the minimum of the function; however, with the correct policy of generating a random point in the space X, usually, the initial approximation improves.

Gradient descent – method for finding a local extremum (minimum or maximum) of a function using motion along a gradient. To minimize the function in the direction of the gradient, one-dimensional optimization methods are used, for example, the golden section method. You can also look for not the best point in the direction of the gradient, but some better than the current one.

The easiest to implement of all local optimization methods. It has rather weak convergence conditions, but at the same time the rate of convergence is rather small (linear). The gradient method step is often used as part of other optimization methods.

The description of the method is as follows: let the objective function is $F(x): X \to R$. So the optimization problem is set as:

$$F(x) \to \min_{x \in X} F(x_j)$$

In case when maximum is needed to be find, then instead of $F(x)$ we use $-F(x)$.

The basic idea of method is to go in the direction of the fastest descent, and this direction is given by anti-gradient $-\nabla F$

$$x_{j+1} = x_j - \lambda_j \nabla F(x_j)$$

where λ_j set the velocity of gradient descent and can be chosen as

- Constant (in this case method may diverge),
- Decreasing in the process of gradient descent,
- Guaranteeing the fastest descent:

To find minimum $F(x)$ we obtain

$$\lambda_j = argmin_\lambda F\left(x_{j+1}\right) = argmin_\lambda F\left(x_j - \lambda_j \nabla F(x_j)\right)$$

1. To find maximum $F(x)$ we obtain

$$\lambda_j = argmax_\lambda F\left(x_{j+1}\right) = argmax_\lambda F\left(x_j - \lambda_j \nabla F(x_j)\right)$$

And the algorithm of the gradient method is look as follows:

1. Set the initial approximation and accuracy of the calculation – x_0, ε;
2. Calculate $x_{j+1} = x_j - \lambda_j \nabla F(x_j)$, where $\lambda_j = argmin_\lambda F\left(x_j - \lambda_j \nabla F(x_j)\right)$;
3. Then check the stopping condition:
   - If $\left|x_{j+1} - x_j\right| > \varepsilon$, $\left|F\left(x_{j+1}\right) - F(x_j)\right| > \varepsilon$ or $\left\|\nabla F\left(x_{j+1}\right)\right\| > \varepsilon$ (choose one of conditions), then $j = j + 1$ and go to step 2.
   - Otherwise $x = x_{j+1}$ and end.

The stochastic *method of simulated annealing* determines the region of the global minimum, and to determine the inverse problem in this region, the *gradient method* was used, consisting in the iterative sequence of determining the solution to the inverse problem:

$$q_{n+1} = q_n - \alpha_n J'(q_n), q_0 \in Q \qquad (4)$$

Here is the descent parameter $\alpha_n = \frac{2J(q_n)}{\|J'(q_n)\|}$ characterizes the method of steepest descent, the gradient of the objective functional $J(q_n)$ has the following form [10]:

$$J'(q_n) = -\int_0^T \Psi(t)^T F_q(X(t), q)dt \qquad (5)$$

Here the vector-function $\Psi(t)$ is the solution of the conjugate problem:

$$\begin{cases} \Psi = -F_X^T(\dot{X}(t), q)\Psi(t),\ t \in \cup_{k=0}^K \left(t_k, t_{k+1}\right), t_0 = 0, t_{K+1} = T, \\ \Psi(T) = 0, \\ [\Psi]_{t=t_k} = 2\left(X(t_k; q) - \Phi_k^i\right), k = 1, \ldots., K. \end{cases} \qquad (6)$$

Jacobi matrices have the following form:

$$F_X = \left\{\frac{\partial F_i}{\partial X_j}\right\}_{i,j=\overline{1,N}}, F_q = \left\{\frac{\partial F_i}{\partial X_j}\right\}_{\substack{i=\overline{1,N}, \\ j=\overline{1,M}}} \qquad (7)$$

Results

The result of solving the inverse problem for a mathematical model of co-infection with tuberculosis and HIV using a combined method of *simulating annealing* with a *gradient method* is presented in Table 3 [13-14].

Thus, effective numerical algorithms for solving inverse problems for systems of ODE (for problems of epidemiology, pharmacokinetics and immunelogy), based on a combination of stochastic and gradient methods, have been created.

Table 3 – Solution of the inverse problem for the mathematical model of co-infection of tuberculosis and HIV

Parameter	Relative decision error q
α_1	$1.0 * 10^{-6}$
α_2	$5.7 * 10^{-5}$
α_3	$5.3 * 10^{-6}$
k	$4.1 * 10^{-10}$

Note that for each parameter, the relative error is less than 0.001%, and the parameters α_1 and k are restored better than the others, as identifiability analysis showed. The result of solving the direct problem (1) with the found parameters is shown in Figure 1a-1c for the three measured functions. Red

dots describe statistical data that were not involved in solving the inverse problem, but are presented for comparison of the forecast using methods for solving inverse problems. It is shown that the obtained solution (solid line) is in good agreement with the real data and serves as a reliable forecast [15].

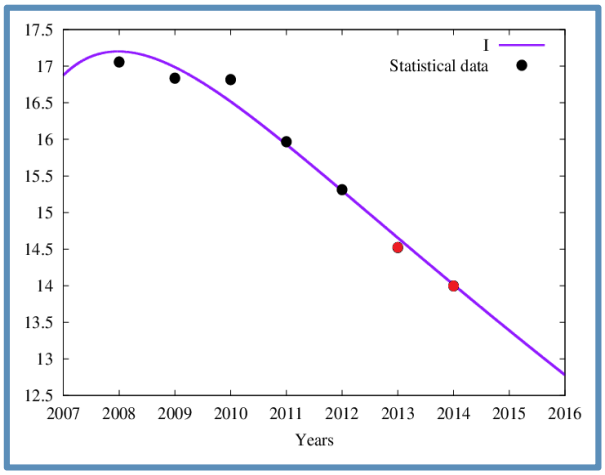

Figure 1a. – Numerical solution of the problem of the spread of co-infection of tuberculosis and HIV with specified parameters (solid line). Black dots mean data of the inverse problem, red dots – statistical data taken into account for the prediction. The number of individuals with active TB (without HIV). All values are in thousand.

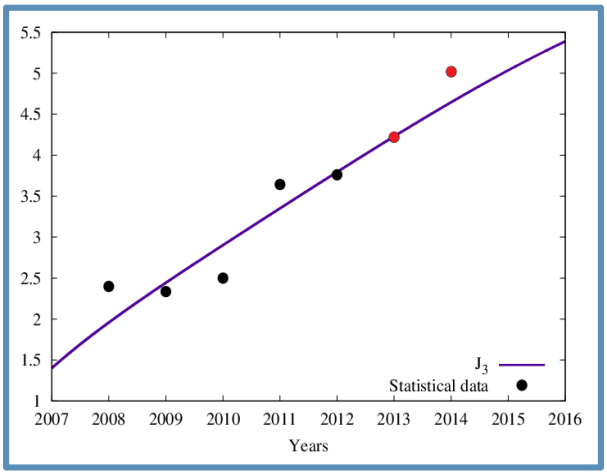

Figure 1b. – Numerical solution of the problem of the spread of co-infection of tuberculosis and HIV with specified parameters (solid line). Black dots mean data of the inverse problem, red dots – statistical data taken into account for the prediction. The number of individuals infected with HIV and the active form of TB. All values are in thousand.

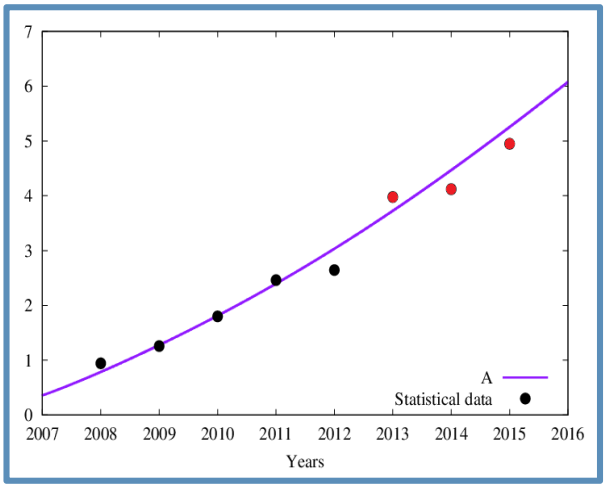

Figure 1c. – Numerical solution of the problem of the spread of co-infection of tuberculosis and HIV with specified parameters (solid line). Black dots mean data of the inverse problem, red dots – statistical data taken into account for the prediction. The number of individuals with AIDS. All values are in thousand.

Conclusion

The research and analysis of the problem arising in bio-medicine has been carried out, the theoretical aspects of this task have been built, including identifiability analysis, which is an important step in the study of the mathematical model, and is necessary for the correct solution of the inverse problem, since it shows the uniqueness, existence and / or stability of the solution .

New combined numerical algorithms for solving the direct and inverse problems of epidemiology have been built. Efficient numerical algorithms for solving inverse problems for systems of ODE (for problems of epidemiology, pharmacokinetics and immunology), based on a combination of statistical and gradient methods, have been created.

Numerical algorithms for solving the problems of determining the coefficients of nonlinear ODE systems using additional statistical information were developed and analyzed.

Thus, the conducted scientific work opens up new directions for the development of research in science and technology, namely, the refinement of mathematical models will improve the prognosis of the disease or the development of the epidemic, which would entail the need for a plan of measures for treating patients and eliminating the consequences of the disease / epidemic.

This work was supported by the grant of the Committee of Science of the Ministry of Education and Science of the Republic of Kazakhstan (AP05134121 "Numerical methods of identiability of inverse and ill-posed problems of natural science".

References

1. Moualeu-Ngangue D.P., Röblitz S., Ehrig R., Deuflhard P. “Parameter identification in a tuberculosis model for Cameroon.” PloS one. 10(4) (2015) e0120607. doi:10.1371/journal.pone.0120607.

2. Pawlowski A., Jansson M., Sköld M., Rottenberg M.E., Källenius G. “Tuberculosis and HIV Co-Infection.” PLoS Pathog. 8(2) (2012) e1002464. doi:10.1371/journal.ppat.1002464.

3. Adams B.M., Banks H.T., Davidian M., Kwon Hee-Dae, Tran H.T., Wynne S.N., Rosenberg E.S. “HIV dynamics: Modeling, data analysis, and optimal treatment protocols.” Journal of Computational and Applied Mathematics vol. 184 (2005): 10–49.

4. Perelson A.S., Nelson P.W. “Mathematical Analysis of HIV-I: Dynamics in Vivo.” SIAM Rev vol. 41, no.1 (1999): 3-44.

5. Vajda S, Rabitz H, Walter E, Lecourtier Y. “Qualitative and quantitative identifiability analysis of nonlinear chemical kinetiv-models.” Chemical Engineering Communications vol. 83 (1989): 191–219.

6. Miao H., Xia X., Perelson A.S., Wu H. “On Identifiability of nonlinear ODE models and applications in viral dynamics.” SIAM Rev. Soc. Ind. Appl. Math. vol. 53 (1) (2011): 3–39.

7. Yao K.Z., Shaw B.M., Kou B., McAuley K.B., Bacon D.W. “Modeling ethylene/butene copolymerization with multi-site catalysts: Parameter estimability and experimental design.” Polymer Reaction Engineering vol. 11 (2003): 563–588.

8. Quaiser T., Monnigmann M. “Systematic identifiability testing for unambiguous mechanistic modeling – application to JAK-STAT, MAPkinase, and NF-kB signaling pathway models.” BMC Syst Biol. no.3 (2009): 50–71.

9. Годунов С.К. Лекции по современным аспектам линейной алгебры. – Новосибирск: Научная книга (2002): 216.

10.Kabanikhin S.I., Krivorotko O.I., Ermolenko D.V., Kashtanova V.N., Latyshenko V.A. “Inverse problems of immunology and epidemiology.” Eurasian Journal of Mathematical and Computer Applications. vol.5 (2017): 14–35.

11.КабанихинС.И. Обратные и некорректные задачи. Новосибирск: Сибирское научное издательство (2009): 460.

12.Kabanikhin S.I., Krivorotko O.I. “Identification of biological models described by systems of nonlinear differential equations.” Journal of Inverse and Ill-Posed Problems vol.23(5) (2015): 519-527.

13.Kabanikhin S., Krivorotko O., Kashtanova V. “A combined numerical algorithm for reconstructing the mathematical model for tuberculosis transmission with control programs.” Journal of Inverse and Ill-Posed Problems vol. 26(1) (2018): 121-131.

14.Kabanikhin S.I., Krivorotko O.I., Yermolenko D.V., Banks H.T. “A numerical algorithm for constructing a mathematical model of intracellular dynamics for individual HIV treatment.” Journal of Inverse and Ill-Posed Problems vol. 26(6) (2018): 859–873.

15.Miao H, Dykes C, Demeter LM, Perelson AS, Wu H. “Modeling and estimation of kinetic parameters and replication fitness of HIV-1 from Flow-cytometry-based growth competition experiments.” Bull Math Biol. no.70 (2008): 1749–1771.

IRSTI 27.41.41

[1]B.T. Zhumagulov, [1,2]N.M. Temirbekov, [3]Zh.R. Zhaksylykova

[1]National Engineering Academy, Almaty, Kazakhstan
[2]Kazakhstan engineering and technological University,
Almaty, Kazakhstan email: temirbekov@rambler.ru
[3]Kazakh National Pedagogical University named after Abai,
Almaty, Kazakhstan email: zhaksylykova0507@mail.ru

Variational method for approximate solution of the Dirichlet problem

Abstract. Several numerical methods can be used to approximate the solution of the problem. In order to determine the most effective of them, it is necessary to carefully study each method. The most efficient approximation method is characterized by properties such as high accuracy of the solution, fewer iterations and parameters in the calculation, calculation speed, etc.
In this paper we consider the Dirichlet problem for the Poisson equation described by the initial-boundary value problem for the elliptic type of the second order. As an effective iterative method for its approximate solution, variational methods for constructing difference equations and variational methods for constructing iterative algorithms were used. The article presents the results of calculations developed using the variational method for the selected model problem. Examples of calculations for model problems are given. The results of the computational experiment demonstrate the high efficiency of the proposed iterative method.
Key words: Dirichlet problem, difference scheme, Ritz method, conjugate gradient method.

Introduction

Finding in an analytical form of the problems solution of mathematical physics is fraught with considerable mathematical difficulties. Known results apply only to the simplest cases. In other cases, are used different numerical methods of the approximate solution.

In this paper, is consider an elliptic differential equation. At the solution:

1) To construct difference equations was used a variance method, proposed in 1908 by German mathematician V. Ritz, which is called Ritz method. The solution found by this method $u_n(x)$, under certain conditions, tends to exact solution $u(x)$, when $n \to \infty$.

Questions of convergence of solutions obtained by the Ritz method are considered in numerous papers and monographs.

2) To construct iterative algorithms, was used the method of conjugate gradients, which stands out for its efficiency among the known iterative methods used to solve systems of linear algebraic equations.

In solving the problem, the Ritz method [1-2] was used to construct the difference equations, iterative algorithms were constructed by the method of conjugate gradients [3-4]. Comparing the results obtained by the variational method with the results obtained in the literature [4-7], it was found that the advantage of the chosen variational method is the simplicity and efficiency of memory use. Such advantages of this method will certainly be acceptable when solving large-scale problems.

Variational methods for constructing difference equations.

Consideration of the problem in general shape in the operator form

$$Lu = f,\ u \in \Phi(L) \qquad (1)$$

when $\Phi(L)$ – is an operator domain L

This task is equivalent to the corresponding variational problem.

$$J(u)=\min_{v\in\Phi(L)} J(v), \tag{2}$$

when $J(v)=(Lv,v)-2(f,v)$.

Consideration of the Ritz method use in solving an elliptic differential equation of the form

$$-\sum_{i,j=1}^{2}\frac{\partial}{\partial x_i}\left(A_{ij}(x)\frac{\partial u}{\partial x_j}\right)=f(x),\ \text{in } D \tag{3}$$

with boundary condition

$$u\big|_{\partial D}=0 \tag{4}$$

where D is a bounded domain with a piecewise linear boundary ∂D, $A_{ij}(x)=A_{ji}(x)$ bounded functions and for an arbitrary vector $\xi=(\xi_1,\xi_2)^{/}$ is done inequality

$$\mu_0\sum_{i=1}^{2}\xi_i^{\,2}\le\inf_{x\in D}\sum_{i,j=1}^{2}A_{ij}(x)\xi_i\xi_j\le\sup_{x\in D}\sum_{i,j=1}^{2}A_{ij}(x)\xi_i\xi_j\le\mu_1\sum_{i=1}^{n}\xi_i^{\,2}$$

with positive constants $\mu_0\le\mu_1$.

It can be shown that the operator of problems (3) and (4) is symmetric and positive definite, and the problem itself reduces to finding a function that minimizes in space $\overset{\circ}{W}{}_2^{1}(D)$ a quadratic functional

$$J(u)=\int_D\left(\sum_{i,j=1}^{2}A_{ij}(x)\frac{\partial u}{\partial x_i}\frac{\partial u}{\partial x_j}\right)dD-2\int_D uf\,dD \tag{5}$$

To find an approximate solution of problem (5), is applied the Ritz method with special-type F_h subspaces that satisfy condition (4).

After, we construct F_h subspaces. To simplify the presentation, it is illustrated by the example of piecewise linear approximations, when domain $D=\{(x_1,x_2):0<x_1,x_2<1\}$ is a square. This area is covered with a uniform square grid with a pitch $h=\frac{1}{N+1}$ and then divide each of the squares $D_{k,l}$ with diagonal. All the internal vertices of the triangles are numbered through $\{p_{k,l}\}_{k,l=1}^{N}$, the union of all triangles with a point of its vertex $p_{k,l}$ mark through $D_{k,l}^{h}$.

$D_{k,l}^{h}$ can be represented as a union of six triangles $\{D_{k,l,m}^{h}\}_{m=1}^{6}$, the order of numbering is indicated in fig.1

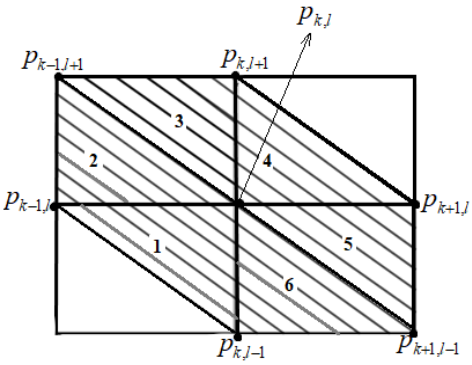

Figure 1 – $\{D_{k,l,m}^{h}\}_{m=1}^{6}$ triangle designation

To each internal node (x_k,y_l), $k,l=\overline{1,N}$ of the grids is assigned a piecewise linear basic function $\varphi_{k,l}(x,y)$. We define each of these functions $\varphi_{k,l}(x,y)$ for the entered grid.

To set $\varphi_{k,l}(x,y)$ analytical, enough for each triangle entering the carrier $\varphi_{k,l}(x,y)$, to create an equation for the plane passing through the unit in $p_{k,l}$, and in the other two of its vertices through zero. Calculating basic functions $\varphi_{k,l}(x,y)$ in each of triangles $\{D_{k,l,m}^{h}\}_{m=1}^{6}$ we build a system of basic functions

$$\varphi_{k,l}(x,y)=\begin{cases}1-\frac{1}{h}(x_k-x)-\frac{1}{h}(y_l-y),\ (x,y)\in D^h_{k,l,1},\\ 1-\frac{1}{h}(x_k-x),\ (x,y)\in D^h_{k,l,2},\\ 1+\frac{1}{h}(y_l-y),\ (x,y)\in D^h_{k,l,3},\\ 1+\frac{1}{h}(x_k-x)+\frac{1}{h}(y_l-y),\ (x,y)\in D^h_{k,l,4},\\ 1+\frac{1}{h}(x_k-x),\ (x,y)\in D^h_{k,l,5},\\ 1-\frac{1}{h}(y_l-y),\ (x,y)\in D^h_{k,l,6}.\end{cases} \tag{6}$$

To build an approximate $u^h(x)$ solution of the problem (1) and (2) we apply Ritz method using basis $\{\varphi_{k,l}(x)\}_{k,l=1}^N$

$$u^h(x)=\sum_{k,l=1}^{N}\alpha_{k,l}\varphi_{k,l}(x) \tag{7}$$

As a result, comes a system of linear equations

$$A\alpha=g \tag{8}$$

where $\alpha=(\alpha_1,\alpha_2,...,\alpha_{N^2})^T$ - vector, made up from decomposition coefficients $\{\alpha_{N(k-1)+l}=\alpha_{k,l}\}_{k,l=1}^N$, $g=(g_1,g_2,...,g_{N^2})^T$ - vector with components

$$g_{N(k-1)+l}=g_{k,l}=\int_{D_{k,l}} f\varphi_{k,l}(x)dD,\ k,l=\overline{1,N} \tag{9}$$

and the elements of matrix A are calculated by the formulas

$$a_{k,l}^{i,j}=a_{N(k-1)+l,N(i-1)+j}=$$
$$=\int_D\sum_{s,t=1}^{2}A_{st}(x)\frac{\partial\phi_{k,l}}{\partial x_s}\frac{\partial\phi_{i,j}}{\partial x_t}dD,\quad k,l,i,j=\overline{1,N} \tag{10}$$

We consider Dirichlet problem in the area D with border ∂D with variable coefficients $p(x,y)$ and $q(x,y)$

$$-\frac{\partial}{\partial x}p(x,y)\frac{\partial u}{\partial x}-\frac{\partial}{\partial y}q(x,y)\frac{\partial u}{\partial y}=f(x,y),\ \text{in}\ D \tag{11}$$

with boundary condition

$$u\big|_{\partial D}=0 \tag{12}$$

The equation (10) is multiplied by the function $u(x,y)$ and integrated by D in parts, given the boundary condition (12) we obtain

$$\int_D p(x,y)\left(\frac{\partial u}{\partial x}\right)^2dD+\int_D q(x,y)\left(\frac{\partial u}{\partial y}\right)^2dD=\int_D f(x,y)udD$$

According to (5) we construct the functional

$$J(u)=\int_D p(x,y)\left(\frac{\partial u}{\partial x}\right)^2dD+\int_D q(x,y)\left(\frac{\partial u}{\partial y}\right)^2dD-2\int_D f(x,y)udD \tag{13}$$

To apply the Ritz method in (13) the function $u(x,y)$ replacing by decomposition (7) we get

$$J\left(u^h\left(\alpha_{k,l}\right)\right)=\int_D p(x,y)\left(\frac{\partial}{\partial x}\sum_{k,l=1}^{N}\alpha_{k,l}\varphi_{k,l}(x)\right)^2 dD+\int_D q(x,y)\left(\frac{\partial}{\partial y}\sum_{k,l=1}^{N}\alpha_{k,l}\varphi_{k,l}(x)\right)^2 dD-$$
$$-2\int_D f(x,y)\sum_{k,l=1}^{N}\alpha_{k,l}\varphi_{k,l}(x)dD,\quad k,l=1,...,N$$

Next, the derivatives are found and equating to zero, we get the following equations

$$\frac{\partial J\left(u^h\left(\alpha_{k,l}\right)\right)}{\partial \alpha_{k,l}}=\int_D p(x,y)\left(\sum_{k,l=1}^{N}\alpha_{k,l}\frac{\partial \phi_{k,l}(x)}{\partial x}\right)\frac{\partial \phi_{k,l}(x)}{\partial x}dD+$$
$$+\int_D q(x,y)\left(\sum_{k,l=1}^{N}\alpha_{k,l}\frac{\partial \phi_{k,l}(x)}{\partial y}\right)\frac{\partial \phi_{k,l}(x)}{\partial y}dD-\int_D f(x,y)\phi_{k,l}(x)\,dD=0,\quad k,l=1,...,N.$$

Taking $\alpha_{k,l}$ out from bracket, it is put in the form of

$$\frac{\partial J(u^h)}{\partial \alpha_{k,l}}=\left[\int_D p(x,y)\left(\sum_{k,l=1}^{N}\frac{\partial \phi_{k,l}(x)}{\partial x}\right)\frac{\partial \phi_{k,l}(x)}{\partial x}dD+\int_D q(x,y)\left(\sum_{k,l=1}^{N}\frac{\partial \phi_{k,l}(x)}{\partial y}\right)\frac{\partial \phi_{k,l}(x)}{\partial y}dD\right]\alpha_{k,l}-$$

$$-\int_D f(x,y)\phi_{k,l}(x)\,dD=0,\quad k,l=\overline{1,N}.$$

Thus, according to (9) and (10) introducing the notation

$$a_{k,l}^{i,j}=a_{N(k-1)+l,N(i-1)+j}=\int_D p(x,y)\left(\sum_{k,l=1}^{N}\frac{\partial \phi_{k,l}(x)}{\partial x}\right)\frac{\partial \phi_{i,j}(x)}{\partial x}dD+$$
$$+\int_D q(x,y)\left(\sum_{k,l=1}^{N}\frac{\partial \phi_{k,l}(x)}{\partial y}\right)\frac{\partial \phi_{i,j}(x)}{\partial y}dD,\ k,l,i,j=\overline{1,N},\tag{14}$$

we get a system of linear algebraic equations (8).

Given the symmetry and block tridiagonal of matrix A, it is enough to define

$$a_{k,l}^{k,l},\ a_{k,l}^{k,l-1},\ a_{k,l}^{k-1,l},\ a_{k,l}^{k-1,l+1},\ k,l=\overline{1,N}.$$

I. Accroding (13), where $i,j=k,l$ we find $a_{k,l}^{k,l}$

$$a_{k,l}^{k,l}=\int_{D_{k,l}^h}\left[p(x,y)\left(\frac{\partial \phi_{k,l}}{\partial x}\right)^2+q(x,y)\left(\frac{\partial \phi_{k,l}}{\partial y}\right)^2\right]dD=$$
$$=\int_{D_1}\left[p(x,y)\left(\frac{\partial \phi_{k,l}}{\partial x}\right)^2+q(x,y)\left(\frac{\partial \phi_{k,l}}{\partial y}\right)^2\right]dxdy+\int_{D_2}\left[p(x,y)\left(\frac{\partial \phi_{k,l}}{\partial x}\right)^2+q(x,y)\left(\frac{\partial \phi_{k,l}}{\partial y}\right)^2\right]dxdy+$$
$$+\int_{D_3}\left[p(x,y)\left(\frac{\partial \phi_{k,l}}{\partial x}\right)^2+q(x,y)\left(\frac{\partial \phi_{k,l}}{\partial y}\right)^2\right]dxdy+\int_{D_4}\left[p(x,y)\left(\frac{\partial \phi_{k,l}}{\partial x}\right)^2+q(x,y)\left(\frac{\partial \phi_{k,l}}{\partial y}\right)^2\right]dxdy+$$
$$+\int_{D_5}\left[p(x,y)\left(\frac{\partial \phi_{k,l}}{\partial x}\right)^2+q(x,y)\left(\frac{\partial \phi_{k,l}}{\partial y}\right)^2\right]dxdy+\int_{D_6}\left[p(x,y)\left(\frac{\partial \phi_{k,l}}{\partial x}\right)^2+q(x,y)\left(\frac{\partial \phi_{k,l}}{\partial y}\right)^2\right]dxdy.\tag{15}$$

We calculate the integrals in each of the areas $D^h_{k,l}$, taking into consideration form of basis function $\varphi_{k,l}(x,y)$ in considered area.

Further, all found six values are substituted in (15). In this case, we combine integrals with the same values and use the notation

$$\widetilde{P}_{k\pm\frac{1}{2},l} = \frac{1}{h^2}\int\limits_{D^h_{k,l}\cap D^h_{k\pm1,l}} p(x,y)dxdy \qquad (16)$$

$$\widetilde{Q}_{k,l\pm\frac{1}{2}} = \frac{1}{h^2}\int\limits_{D^h_{k,l}\cap D^h_{k,l\pm1}} q(x,y)dxdy \qquad (17)$$

It comes,

$$a^{k,l-1}_{k,l} = \int\limits_{D_1\cup D_6}\left(p(x,y)\frac{\partial\phi_{k,l}}{\partial x}\frac{\partial\phi_{k,l-1}}{\partial x} + q(x,y)\frac{\partial\phi_{k,l}}{\partial y}\frac{\partial\phi_{k,l-1}}{\partial y}\right)dxdy =$$
$$= \int\limits_{D_1}\left(p(x,y)\frac{\partial\phi_{k,l}}{\partial x}\frac{\partial\phi_{k,l-1}}{\partial x} + q(x,y)\frac{\partial\phi_{k,l}}{\partial y}\frac{\partial\phi_{k,l-1}}{\partial y}\right)dxdy + \qquad (19)$$
$$+\int\limits_{D_6}\left(p(x,y)\frac{\partial\phi_{k,l}}{\partial x}\frac{\partial\phi_{k,l-1}}{\partial x} + q(x,y)\frac{\partial\phi_{k,l}}{\partial y}\frac{\partial\phi_{k,l-1}}{\partial y}\right)dxdy$$

The found values of the integrals, substituting in (19) and using the notation (17) we get

$$a^{k,l-1}_{k,l} = -\frac{1}{h^2}\int\limits_{D_1} q(x,y)dxdy - \frac{1}{h^2}\int\limits_{D_6} q(x,y)dxdy =$$
$$= -\frac{1}{h^2}\cdot\int\limits_{D_1\cup D_6} q(x,y)dxdy = -\tilde{Q}_{k,l-\frac{1}{2}} \qquad (20)$$

III. To find $a^{k-1,l}_{k,l}$ by formula (14), where $i,j = k-1,l$ we move vertex $p_{k,l}$ for one pitch to left and from fig.1. it is seen that $p_{k,l}$ and $p_{k-1,l}$ are the vertexes of triangles D_1 and D_2. It means, $a^{k-1,l}_{k,l}$ is defined in the triangles of D_1 and D_2.

$$a^{k-1,l}_{k,l} = \int\limits_{D_1\cup D_2}\left(p(x,y)\frac{\partial\phi_{k,l}}{\partial x}\frac{\partial\phi_{k-1,l}}{\partial x} + q(x,y)\frac{\partial\phi_{k,l}}{\partial y}\frac{\partial\phi_{k-1,l}}{\partial y}\right)dxdy =$$
$$= \int\limits_{D_1}\left(p(x,y)\frac{\partial\phi_{k,l}}{\partial x}\frac{\partial\phi_{k-1,l}}{\partial x} + q(x,y)\frac{\partial\phi_{k,l}}{\partial y}\frac{\partial\phi_{k-1,l}}{\partial y}\right)dxdy + \qquad (21)$$
$$+\int\limits_{D_2}\left(p(x,y)\frac{\partial\phi_{k,l}}{\partial x}\frac{\partial\phi_{k-1,l}}{\partial x} + q(x,y)\frac{\partial\phi_{k,l}}{\partial y}\frac{\partial\phi_{k-1,l}}{\partial y}\right)dxdy.$$

Found values $a^{k-1,l}_{k,l}$, in the triangles D_1 and D_2 substitute in (21) with (16) and get

$$a^{k-1,l}_{k,l} = -\frac{1}{h^2}\cdot\int\limits_{D_1} p(x,y)dxdy - \frac{1}{h^2}\cdot\int\limits_{D_2} p(x,y)dxdy =$$
$$= -\frac{1}{h^2}\cdot\int\limits_{D_1\cup D_2} p(x,y)dxdy = -\tilde{P}_{k-\frac{1}{2},l} \qquad (22)$$

IV. It remains only to identify the element, $a^{k-1,l+1}_{k,l}$. For that the vertex $p_{k,l}$, needs to be moved firstly for one pitch to left and then for one pitch up. According to fig.1. it is seen that $p_{k,l}$ and $p_{k-1,l+1}$ are the vertexes of the triangles D_2 and D_3. But

$$a^{k,l}_{k,l} = \widetilde{P}_{k-\frac{1}{2},l} + \widetilde{Q}_{k,l-\frac{1}{2}} + \widetilde{P}_{k+\frac{1}{2},l} + \widetilde{Q}_{k,l+\frac{1}{2}}. \qquad (18)$$

II. To find element $a^{k,l-1}_{k,l}$ as in the first case we use the formula (14), where $i,j = k,l-1$ and to define the place $p_{k,l-1}$ we down the vertex $p_{k,l}$ lower for one pitch. According to fig.1. it is seen that the vertexes $p_{k,l}$ and $p_{k,l-1}$ are in triangle D_1 and D_6. So, it means, $a^{k,l-1}_{k,l}$ are defined only in this area.

with the selected shift of $p_{k,l}$ the vertex $p_{k-1,l+1}$ would not belong to any of six triangles. Therefore

$$a_{k,l}^{k-1,l+1} = 0 \tag{23}$$

All found values (18), (20), (22), (23) substituting in (8), taking into account the symmetry of the matrix A we get

$$\left(\tilde{P}_{k-\frac{1}{2},l} + \tilde{Q}_{k,l-\frac{1}{2}} + \tilde{P}_{k+\frac{1}{2},l} + \tilde{Q}_{k,l+\frac{1}{2}}\right)\alpha_{k,l} - \tilde{Q}_{k,l-\frac{1}{2}}\alpha_{k,l-1} - \\ -\tilde{Q}_{k,l+\frac{1}{2}}\alpha_{k,l+1} - \tilde{P}_{k-\frac{1}{2},l}\alpha_{k-1,l} - \tilde{P}_{k+\frac{1}{2},l}\alpha_{k+1,l};\ k,l = \overline{1,N} \tag{24}$$

Allowing in (24)

$$\left(A_1\alpha\right)_{k,l} = -\tilde{P}_{k-\frac{1}{2},l}\alpha_{k-1,l} + \left(\tilde{P}_{k-\frac{1}{2},l} + \tilde{P}_{k+\frac{1}{2},l}\right)\alpha_{k,l} - \\ -\tilde{P}_{k+\frac{1}{2},l}\alpha_{k+1,l};\ k,l = \overline{1,N} \tag{25}$$

$$\left(A_2\alpha\right)_{k,l} = -\tilde{Q}_{k,l-\frac{1}{2}}\alpha_{k,l-1} + \left(\tilde{Q}_{k,l-\frac{1}{2}} + \tilde{Q}_{k,l+\frac{1}{2}}\right)\alpha_{k,l} - \\ -\tilde{Q}_{k,l+\frac{1}{2}}\alpha_{k,l+1};\ k,l = \overline{1,N} \tag{26}$$

Then, using $A_1 + A_2 = A$, we get system (8)

Variational methods for constructing iterative algorithms

For numerical solution of system (6), one can apply variational type methods, such as, the method of rapid descent, the method of minimal corrections, the method of conjugate gradients, etc.

The conjugate gradient method is most preferable for systems with a self-adjoint positive matrix $A = A^* > 0$. With poor conditioning of the matrix, this method does not always become computationally stable.

Operator A is self-adjoint and positive definite operator in the space of grid functions H_h^0. Into H_h^0 we insert scalar product

$$(u,v) = \sum_{i,j=1}^{N-1} u_{i,j} v_{i,j} h_1 h_2$$

and norm

$$\|u\| = \sqrt{(u,u)}.$$

To solve an equation of the form $A\alpha = g$ we use the conjugate gradient method. The iteration process is implemented in the following order:

I. Preparation before the iterative process

For given $\alpha_{i,j}^0$ the residual is calculated $s_{i,j}^0 = r_{i,j}^0 = \left(A\alpha^0\right)_{i,j} - g_{i,j}\ i = 1,...,n_1,\ j = 1,...,n_2$;

II. k – integration of the method

1) Calculate the parameter: $\gamma_k = \dfrac{\left(r_{i,j}^{k-1}, r_{i,j}^{k-1}\right)}{\left(As_{i,j}^k, s_{i,j}^{k-1}\right)}$,

2) $r_{i,j}^k = r_{i,j}^{k-1} - \gamma_k As_{i,j}^k$

3) The following approximation of the solution is calculated by the formula: $\alpha_{i,j}^k = \alpha_{i,j}^{k-1} - \gamma_k s_{i,j}^k$

4) Calculate the parameter: $\beta_k = \dfrac{\left(r_{i,j}^k, r_{i,j}^k\right)}{\left(r_{i,j}^{k-1}, r_{i,j}^{k-1}\right)}$

5) The auxiliary value is calculated by the formula: $s_{i,j}^{k+1} = r_{i,j}^k + \beta_n s_{i,j}^k$

where

$$\left(As^k\right)_{i,j} = \frac{1}{h_1^2}\left[\tilde{P}_{i+\frac{1}{2},j}\left(s_{i+1,j} - s_{i,j}\right) - \tilde{P}_{i-\frac{1}{2},j}\left(s_{i,j} - s_{i-1,j}\right)\right] + \\ + \frac{1}{h_2^2}\left[\tilde{Q}_{i+\frac{1}{2},j}\left(s_{i,j+1} - s_{i,j}\right) - \tilde{Q}_{i,j-\frac{1}{2}}\left(s_{i,j} - s_{i,j-1}\right)\right]; \\ i,j = \overline{1,N}$$

\This process continues until the criterion for stopping the iterations $\left\|\alpha^{k+1} - \alpha^k\right\| \le \varepsilon$ is satisfied.

Calculation examples

To illustrate the proposed method, we consider an example of the problem (11) – (12) in a circle.

Let in a rectangular area D is a circle Ω with R radius and center (c_1, c_2). It is required to find an approximate solution of the Dirichlet problem for the Poisson equation.

$$\frac{\partial^2 u}{\partial x_1^2} + \frac{\partial^2 u}{\partial x_2^2} = -x_1 \cdot x_2$$

In the circle, under the condition

$$u(x_1, x_2)\big|_{\partial\Omega} = 0$$

Then

$$\overline{D} = \{(x_1, x_2),\ a_1 \le x_1 \le a_2,\ b_1 \le x_2 \le b_2\},$$

$$\Omega = \left\{(x_1, x_2),\ (x_1 - c_1)^2 + (x_2 - c_2)^2 \le R^2\right\},$$

$$\partial\Omega = \left\{(x_1, x_2),\ (x_1 - c_1)^2 + (x_2 - c_2)^2 = R^2\right\}.$$

Auxiliary problem of the fictitious domains method

$$\begin{cases} \dfrac{\partial}{\partial x_1}\left(p(x_1, x_2)\dfrac{\partial u^\varepsilon}{\partial x_1}\right) + \dfrac{\partial}{\partial x_2}\left(q(x_1, x_2)\dfrac{\partial u^\varepsilon}{\partial x_2}\right) = -x_1 \cdot x_2, \\ u^\varepsilon(x_1, x_2)\big|_{\partial D} = 0 \end{cases}$$

$$p(x_1, x_2) = q(x_1, x_2) = \begin{cases} 1, & (x_1, x_2) \in \Omega, \\ 1/\varepsilon, & (x_1, x_2) \in D/\Omega. \end{cases}$$

$$f^\varepsilon(x_1, x_2) = \begin{cases} -x_1 \cdot x_2, & (x_1, x_2) \in \Omega \\ 0, & (x_1, x_2) \in D/\Omega. \end{cases}$$

Were conducted numerical experiments. Below is the table 1 for the number of iterations N and calculation errors $\|u_h - u\|_C$ at $n_1 = n_2 = 101$ and various meanings ε for Ritz method.

Table 1 – Results of numerical experiments

n_1	n_2	$1/\varepsilon$	N	$\|u_h - u\|_C$
101	101	10^2	1221	0.003888
101	101	10^3	3395	0.003820
101	101	10^4	7920	0.003819
101	101	10^5	12737	0.003818
101	101	10^6	20042	0.003817
101	101	10^7	26592	0.003816

The results show that with an increase in the number of grid nodes, the error in the solution decreases. In fig. 2 shown the result of solving the problem using an explicit difference scheme with $\varepsilon_* = \varepsilon = 10^{-4}$ on a uniform grid with a size of 101 × 101. Therefore, the original system of linear algebraic equations has 101 × 101 unknowns.

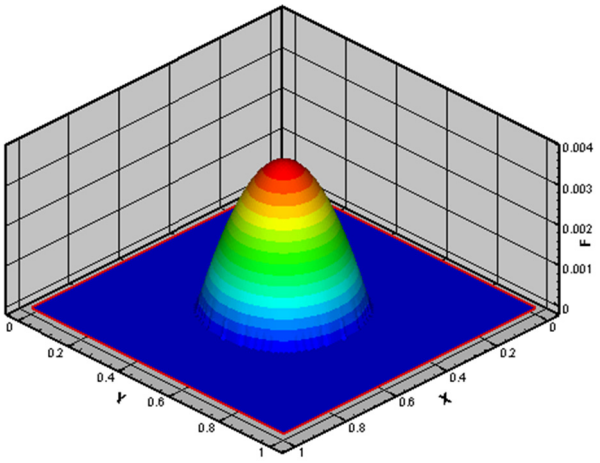

Figure 2 – Solution of the Dirichlet problem for the Poisson equation in a circle

Conclusion

Today, the task of developing and modifying numerical methods remains relevant. However, the development process of computing technology shifts the emphasis from the creation of new numerical methods to the study and classification of old ones in order to identify the best. Now for modern powerful computers, such characteristics as the amount of required memory, and the number of arithmetic operations are not necessarily in the foreground. More preferred are those methods that are distinguished by the ease of implementation on a computer, and allow to solve a wider class of problems.

The special advantages of this method are its simplicity and low memory costs, which makes it effective in solving large-scale problems.

The results of the computational experiment confirm the efficiency of the proposed method for solving the Dirichlet problem for the Poisson equation and its rather high efficiency.

References

1. Marchýk G.I. “Metody vychıslıtelnoı matematıkı.” Naýka (1989): 608.

2. Mýhambetjanov A.T., Otelbaev M.O., Smagýlov Sh.S. “Ob odnom novom prıblıjennom

metode reshenıe nelıneınyh kraevyh zadach." Vychıslıtelnye tehnologıı 3, no. 4 (1998).

3. Samarskii A.A. "Teorıia raznostnyh shem." Naýka (1983): 616.

4. Bakhvalov N.S, Zhidkov N.P, Kobelkov G.M. Chislennye metody – Izd.: Binom (2008).

5. N.M. Temırbekov, J.R. Jaksylykova. "Ob ıteratsıonnom metode fıktıvnyh oblastei dlıa reshenıia ellıptıcheskogo ýravnenıia v oblastıah so slojnoı geometrıeı." Izvestıia MKTÝ ım. H.A.Iasavı, Serıia matematıka, fızıka, ınformatıka. 1, no. 1(4) (2018): 128-132.

6. N.M.Temirbekov, Zh.R.Zhaksylykova. "AnIterative Method for Solving Non linear Navier-Stokes Equationsin Complex Domains Taking into Account Boundary Conditions with Uniform Accuracy." AIP Conference Proceedings 1997, 020036 (2018); doi: 10.1063/1.5049030.

7. Temirbekov A.N., Wójcik W. "Numerical Implementation of the Fictitious Domain Method for Elliptic Equations." International Journal of Electronics and Telecommunications 60, no. 3 (2014): 219-223.

8. Temirbekov A.N. "Numerical implementtation of the method of fictitious domains for elliptic equations." 3rd International Conference on Analysis and Applied Mathematics, ICAAM 1759 (2016): 020053-1–020053-6; doi: 10.1063/1.4959667.

9. Kireev V.I., Panteleev A.V., Chislennye metody v primerakh i zadachakh. Uchebnoe posobie. 4-e izd., ispr.-SPb.: Izdatel'stvo «Lan'» (2015): 488.

10. Samarskii A. A., Nikolaev E. S. "Metody reshenia setochnyh uravnenii." Naýka (1978): 592.

11. Bykov V.M., Nizameev Kh.R. Variatsionnye metody v mekhanike sploshnykh sred: Metodicheskie ukazaniya po spetskursu. Chelyabinsk: Chelyabinskiy gos. un-t (2001): 36.

12. Berezin I.S., Zhidkov N.P. "Metody vychisleniy." GIFML 2 (1959): 620.

IRSTI 27.31.21

[1,2]N.M. Koshkarbayev, [1,2,3]B.T. Torebek

[1]Al-Farabi Kazakh National University, Almaty, Kazakhstan
[2]Institute of Mathematics and Mathematical Modeling, Almaty, Kazakhstan
[3]Department of Mathematics, Ghent University002C Ghent, Belgium
e-mail: torebek@math.kz

Nonexistence of travelling wave solution of the Korteweg-de Vries Benjamin Bona Mahony equation

Abstract. This paper is devoted to the Korteweg-de Vries Benjamin Bona Mahony equation in an infinite domain. The paper discusses weak solutions of the Korteweg-de Vries Benjamin Bona Mahony equation without any conditions at infinity. This particular problem arises from the phenomenon of long breaking wave with small amplitude in fluid. In fluid dynamics, a breaking wave is a wave whose amplitude reaches a critical level at which some process can suddenly start to occur that causes large amounts of wave energy to be transformed into turbulent kinetic energy.
For the Korteweg-de Vries Benjamin Bona Mahony equation, we obtain the conditions of blowing-up of travelling wave solutions in finite time. Moreover, there is an explicit upper bound estimate for the wavelength of the corresponding singular traveling wave, depending on the speed of waves. The proof of the results is based on the nonlinear capacity method. In closing, we provide the numerical examples.
Key words: Breaking waves, Korteweg-de Vries-Benjamin-Bona-Mahony equation; blow-up of solution, travelling wave solution.

1. Introduction

1.1. Breaking waves

In fluid dynamics, a breaking wave is a wave whose amplitude reaches a critical level at which some process can suddenly start to occur that causes large amounts of wave energy to be transformed into turbulent kinetic energy. At this point, simple physical models that describe wave dynamics often become invalid, particularly those that assume linear behavior.

Breaking of water surface waves may occur anywhere that the amplitude is sufficient, including in mid-ocean. However, it is particularly common on beaches because wave heights are amplified in the region of shallower water (because the group velocity is lower there). There are three basic types of breaking water waves [1]. They are spilling, plunging and surging:

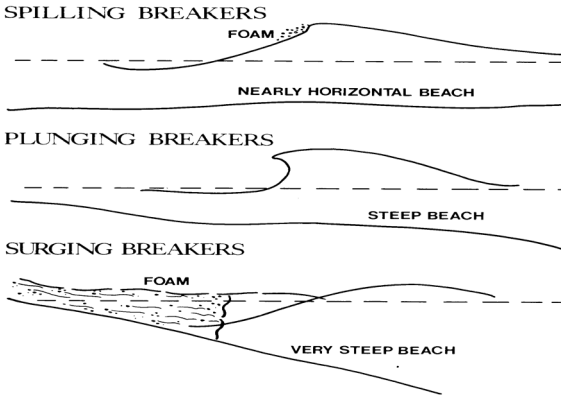

Figure 4 – Types of breaking water waves

1.2. Mathematical model

In this section we present the well-known mathematical model of the Korteweg de Vries-Benjamin-Bona-Mahony equation (see. [2]).

One of the well-known non-linear equations that embody both variance and non-linearity and is actively used in applications is the Korteweg-de Vries equation [3] which models the undirectional propagation of weakly nonlinear and weakly dispersive waves:

$$\eta_t + c\left(1 + \frac{3h}{2}\eta\right)\eta_x + \frac{ch^2}{6}\eta_{xxx} = 0, \qquad (1)$$

where η is the vertical excursion of the free surface above the still water level, $h$is the uniform undisturbed water depth and $c = \sqrt{gh}$ is the speed of linear gravity waves (g being the gravity acceleration).

The Benjamin-Bona-Mahony equation is an alternative to the Korteweg-de Vries equation [4] which is described as follows:

$$\eta_t + c\left(1 + \frac{3h}{2}\eta\right)\eta_x - \frac{ch^2}{6}\eta_{txx} = 0.$$

We consider the following scaled dependent and independent variables:

$$\eta \leftarrow \frac{\eta}{a_0}, \qquad x \leftarrow \frac{x}{l}, \qquad t \leftarrow \frac{ct}{l},$$

where a_0 is the characteristic wave amplitude and l is the characteristic wavelength. In dimensionless variables KdV equation (1) reads:

$$\eta_t + \left(1 + \frac{3\epsilon}{2}\eta\right)\eta_x + \frac{\mu^2}{6}\eta_{xxx} = 0,$$

where parameter $\epsilon = \frac{a_0}{h}$ measures the nonlinearity and $\mu = \frac{h}{l}$ is the dispersion parameter. The relative importance of these two effects is measured by the so-called Stokes-Ursell number [5]:

$$S = \frac{\epsilon}{\mu^2} \equiv \frac{a_0 l^2}{h^3}.$$

The last equation can be further simplified if we perform an additional change of variables:

$$\eta \leftarrow \frac{3\mu^2}{a_0}\eta, \qquad x \leftarrow \frac{\sqrt{6}}{\mu}(x - t), \qquad t \leftarrow \frac{\sqrt{6}}{\mu}t,$$

which yields the following simple equation including explicitly the Stokes-Ursell number S:

$$\eta_t + S\eta\eta_x + \eta_{xxx} = 0.$$

The last scaled KdV equation can be further generalized by using the low-order asymptotic relations in order to alternate higher order terms as it was proposed by Bona and Smith [6]. This step is rather standard and we do not provide here the details of the derivation [7]:

$$\eta_t + S\eta\eta_x + \eta_{xxx} - \delta\eta_{txx} = 0, \qquad (2)$$

where $\delta \in \mathbb{R}$. The equation (2) is so-called Korteweg-de Vries-Benjamin-Bona-Mahony equation.

We note that for a particular value of the Stokes-Ursell number $S = 1$ another simpler scaling is possible when all the lengths (x and η) are scaled by the mean water depth h.

1.3. Statement of the problem

We consider one of the mathematical problem of the breaking water waves, the Korteweg-de Vries-Benjamin-Bona-Mahony equation:

$$\eta_t + \eta\eta_x + \eta_{xxx} - \eta_{txx} - \eta_x = 0, t > 0, x \in \mathbb{R}. \qquad (3)$$

The Korteweg-de Vries-Benjamin-Bona-Mahony equation has important application in different physical situations such as waves on shallow water, and processes in semiconductors with differential conductivity.

In [8], traveling-wave solutions $u(x,t) = f(x - ct)$ are sought for the equation (3) which describes wave the processes in semiconductors with strong spatial dispersion. In [8-12] the authors obtained sufficient conditions for the finite time blow-up of solutions of time and space initial problems for the Korteweg-de Vries and Benjamin–Bona–Mahony type equations.

In this paper, based on the method of nonlinear capacity [13-15], the existence of singular travelling wave solutions of the equation (3) is proved.

2. Singular travelling wave solutions

We consider the traveling wave type solutions of the Korteweg-de Vries-Benjamin Bona Mahony equation (3):

$$\eta(x,t) = \eta(\xi),$$

where $\xi = x - ct$ and c is the wave velocity. Then $\eta(\xi)$ satisfies

$$(1+c)\eta''' + \eta\eta' - (1+c)\eta' = 0. \quad (4)$$

Equation (4) admits the following integrals:

$$(1+c)\eta'' + \frac{\eta^2}{2} - (1+c)\eta + C = 0, \quad (5)$$

where C is an arbitrary constant.

2.1. Nonexistence of travelling wave solution

A weak solution of (5) is a function $\eta \in L^2(I), I \subset \mathbb{R}$ that satisfies the integral identity

$$\int_I \eta^2(\xi)\varphi(\xi)d\xi = -2(1+c)\int_I \eta(\xi)\big(\varphi''(\xi) - \varphi(\xi)\big)d\xi - 2C\int_I \varphi(\xi)d\xi \quad (6)$$

for $\varphi \in C_0^2(I)$.

We multiply equation (5) by a nonnegative test function $\varphi \in C_0^2(I)$ with compact support. Then after integration we obtain (6). Hence, by the Young inequality with parameter $a > 0$, we find that

$$\int_I \eta^2(\xi)\varphi(\xi)d\xi \le \frac{(1+c)}{a}\int_I \eta^2(\xi)\varphi(\xi)d\xi + a(1+c)\int_I \frac{\big(\varphi''(\xi) - \varphi(\xi)\big)^2}{\varphi(\xi)}d\xi - 2C\int_I \varphi(\xi)d\xi. \quad (7)$$

We now take the test function:

$$\varphi(\xi) = \varphi_0(\tau), \tau = \frac{\xi}{L},$$

where $L \ge 2$ is a free parameter and the function $0 \le \varphi_0 \in C^2(I)$ such that

$$\varphi_0(\tau) = \begin{cases} 1 \ \ if \ \ |\tau| \le 1, \\ 0 \ \ if \ \ |\tau| \ge 2. \end{cases}$$

Let the function φ_0 satisfies the following properties

$$\alpha = \int_{-2}^{2} \frac{|L^2\varphi_0(\tau) - \varphi_0''(\tau)|^2}{\varphi_0(\tau)}d\tau < \infty,$$

and

$$\beta = \int_{-2}^{2} \varphi_0(\tau)d\tau < \infty.$$

Then, if $a = c + 1$ the inequality (7) implies

$$(1+c)(2+c)\frac{\alpha}{L^2} \ge 2C\beta.$$

From this it directly follows that if there exist C such that the inequality (7) holds, then there is no such bounded travelling wave solution of equation (5).

Then the following results are true

Theorem 1. The equation (4) with support $L \ge 2$, satisfying the inequality

$$C > \frac{(c+1)(c+2)\alpha}{2\beta L^2} \quad (8)$$

does not admit a solution.

Thus, a sufficient condition for the existence of an unbounded traveling wave with a wavelength L_* is the fulfillment of the inequality

$$\frac{2L^2}{(c+1)(c+2)}C > \frac{\alpha}{\beta}$$

with $L > L_*$.

2.2. Numerical examples

In this subsection we consider some numerical examples for equation (5) with different viscosities. We consider some initial data (at $x = ct$) for a traveling wave. In this case, we note that the nonexistence of a solution to equation (5) depends on the conditions (8).

First, consider an example where the wave velocity is small enough. That is, consider a fluid with a velocity between zero and one. Then, as seen from the Figure 1, the traveling wave breaks relatively quickly.

Let us now study a fluid with a velocity between 50 and 100. In this case, the time of breaking the wave slightly increases. It is easy to see from the Figure 2.

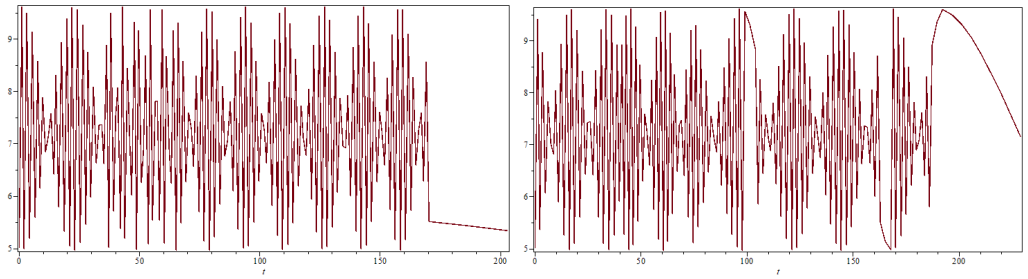

Figure 2 – Singular travelling waves

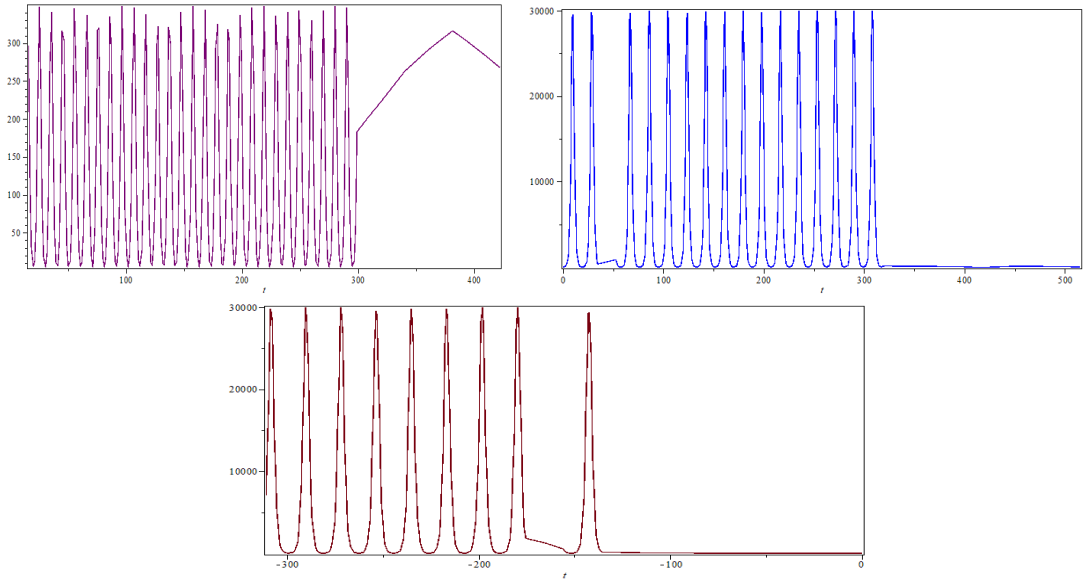

Figure 3 – Breaking travelling waves

Now let the fluid velocity be large enough. That is, consider a fluid with a velocity of about one thousand. In this case, as seen from the Figure 3 the time of breaks of traveling waves will be quite large.

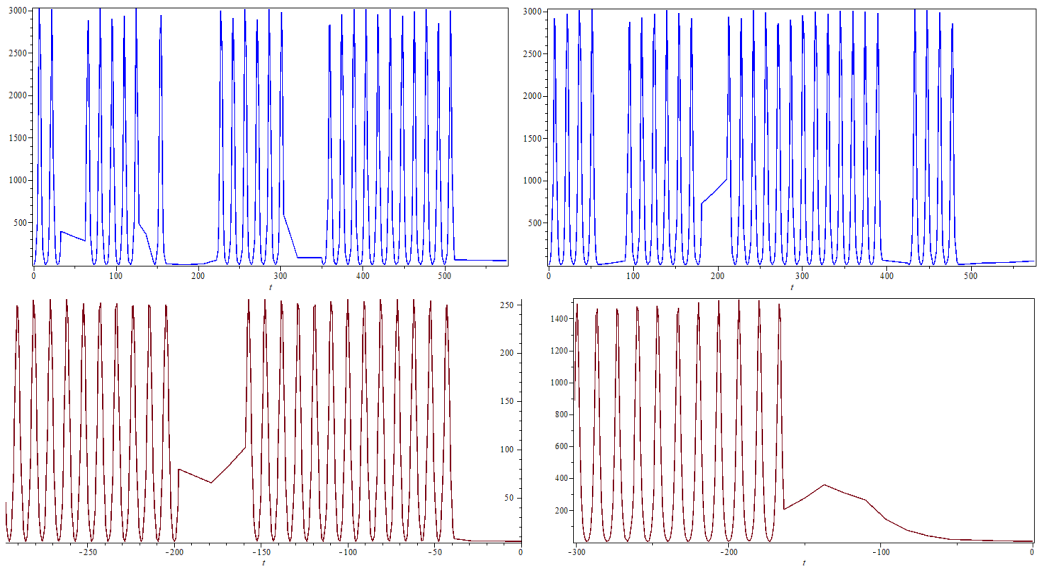

Figure 4 – Breaking travelling waves

Analyzing the above examples, we come to the conclusion that with an increase of the wave velocity, the time of wave break-up increases.

Conclusion

The present paper is devoted to the Korteweg-de Vries-Benjamin-Bona-Mahony equation in an infinite interval. This particular problem arises from the phenomenon of long breaking waves with small amplitude in fluid. For the Korteweg-de Vries-Benjamin-Bona-Mahony equation, we proved the nonexistence of the singular travelling wave solutions. Moreover, we provide some examples.

Acknowledgements

The research is financially supported by a grant from the Ministry of Science and Education of the Republic of Kazakhstan (Grants №AP05131756). No new data was collected or generated during the course of research.

References

1. T. Sarpkaya, M. Isaacson. “Mechanics of wave forces on o□shore structures. Van Nostrand Reinhold.” (1981).

2. D. Dutykh, E. Pelinovsky. “Numerical simulation of a solitonic gas in KdV and KdV-BBM equations.” Physics Letters A.V. 378, no. 42 (2014): 3102-3110.

3. D. J. Korteweg, G. de Vries, “On the change of form of long waves advancing in a rectangular canal, and on a new type of long stationary waves.” Philos. Mag. 39:5, (1895): 422-443.

4. T.B. Benjamin, J.L. Bona, J.J. Mahony. “Model equations for long waves in nonlinear dispersive systems.” Philos. Trans. R. Soc. Lond. 272, (1972): 47-78.

5. F. Ursell, “The long-wave paradox in the theory of gravity waves,” Proc. Camb. Philos. Soc. 49, (1953): 685-694.

6. J. L. Bona, R. Smith, “A model for the two-way propagation of water waves in a channel,” Math. Proc. Camb. Philos. Soc. 79, (1976): 167-182.

7. M. Francius, E. N. Pelinovsky, A. V. Slunyaev. “Wave dynamics in nonlinear media with two dispersionless limits for long and short waves.” Phys. Lett. A. 280:2, (2001): 53-57.

8. A.B. Al’shin, M. O. Korpusov, E.V. Yushkov. “Traveling-wave solution to a nonlinear equation in semiconductors with strong spatial dispersion.” Comput. Math. and Math. Phys., 48, (2008): 764-768.

9. M.O. Korpusov, E.V. Yushkov. “Local Solvability and Blow-Up for Benjamin-Bona-Mahony- Burgers, Rosenau-Burgers and Korteweg-de Vries-Benjamin-Bona-Mahony Equations.” Electronic Journal of Differential Equations 69, (2014): 1-16.

10. S.I. Pokhozhaev. “On the Singular Solutions of the Korteweg-de Vries Equation.” Mathematical Notes 88:5, (2010): 741-747.

11. S.I. Pokhozhaev. “On the Nonexistence of Global Solutions for Some Initial-Boundary Value Problems for the Korteweg-de Vries Equation.” Differential Equations 47:4, (2011): 488-493.

12. S.I. Pokhozhaev. “Blow-Up of Smooth Solutions of the Korteweg-de Vries Equation.” Nonlinear Analysis: Theory, Methods and Applications 75:12, (2012): 4688-4698.

13. S.I. Pokhozhaev. “Essentially nonlinear capacities induced by differential operators.” Dokl. Akad. Nauk 357:5, (1997): 592-594 .

14. E. Mitidieri, S.I. Pokhozhaev. “A priori estimates and blow-up of solutions of nonlinear partial di□erential equations and inequalities.” Proc. Steklov Inst. Math. 234, (2001): 1-362.

15. E. Mitidieri, S. I. Pokhozhaev. “Towards a Unified Approach to Nonexistence of Solutions for a Class of Differential Inequalities.” Milan Journal of Mathematics 72, (2004): 129-162.

IRSTI 27.35.14

[1]A. Issakhov, [2]T. Yang, [3]A. Baitureyeva

[1]Faculty of Mechanical Mathematics, Al-Farabi Kazakh National University,
Almaty, Kazakhstan, e-mail: alibek.issakhov@gmail.com
[3]Department of Design Engineering and Mathematics, Middlesex University,
London, United Kingdom, e-mail: T.Yang@mdx.ac.uk
[3]Faculty of Mechanical Mathematics, Al-Farabi Kazakh National University,
Almaty, Kazakhstan, e-mail: baitureyeva.aiymzhan@gmail.com

CFD simulation of pollution dispersion from thermal power plants in the atmosphere

Abstract. This paper presents CFD simulation of pollution dispersion from a thermal power plant. Carbon dioxide was chosen as the scattering gas, as it constitutes the main share of emissions from the energy industry. The model was tested using experimental results performed using wind tunnel data available in the literature. A comparative analysis of the results of this article with experimental and numerical data was performed. It showed that the results of this article were closer to the experimental results than the calculations of previous authors. The minimum relative error with the experiment was less by 4.11% at the pipe exit and by 2.52% at a distance x/D=3 from the source, than other results. Based on this verification, the spread of pollution from thermal power plant (TPP) in real physical dimensions was modeled. The k-epsilon turbulence model was used taking into account buoyancy. The calculations were performed using the ANSYS Fluent 18.1 software package. As a result, the distance from the source was calculated, at which pollution will reach the ground surface (~ 2 km). Obtained distance is quite big since this TPP is located in an area which is far from residential settlements and there are no natural or architectural obstacles around.
Key words: Navier-Stokes equations, mass transfer, numerical modeling, air pollution, concentration, thermal power plant.

Introduction

Air pollution every year becomes an increasingly serious large-scale problem. Plants and various energy facilities (such as thermal power plants, nuclear power plants, etc.) produce a large amount of pollutants that dispersed in the atmosphere, damage the flora, fauna, buildings and harm human health. The European Environment Agency (2018) gives the following definition of air pollution: “the presence of contaminant or pollutant substances in the air that do not disperse properly and that interfere with human health or welfare, or produce other harmful environmental effects.” [1].

According to the final emissions report for 2017, published in March 2018, global energy-related CO_2 emissions have increased and reached a historic maximum. At the same time, special attention should be paid to the energy sector, since the share of energy is more than two thirds of total greenhouse gas emissions and more than 80% of CO_2 emissions [2]. Therefore, in this paper, CO_2 was selected as the main test substance of pollution. The background annual CO_2 concentration on the Earth is equal to 400.88 ppm=0.0004 (mass fraction) [3].

To determine the extent of air pollution impact on the environment and people, it is important to take into account the physical principles affecting the movement and dispersion of pollutants [4].

Due to the rapid growth of computer capabilities, in particular, large-scale parallel computing, it becomes advisable to use computer simulation to calculate scientific and technical engineering problems. Nowadays technologies are rapidly developing, as a result of which their productivity has increased exponentially over time.

According to the data, over the past 60 years, computing power has increased in productivity by 1 trillion times. [5]

Therefore, people use computational fluid dynamics to conduct large-scale computer modeling of important scientific and engineering topics [6-7].

The study of jet behavior in crossflow is important for various applications, especially for chimneys, because the interaction between the jet and crossflow fluids affects the pollution dispersion into the atmosphere [8].

A review and description of the works devoted to the study of the nature of jet motion in a crossflow is given in [9-14]. Early studies of jets in crossflow were devoted to the derivation of empirical equations for the flight path and the principles of scaling [15-18]. To this end, the authors conducted numerous experimental studies. Recent research in this area is described in [19, 20]. Further, there have been many studies of vortex structures (vortex pairs rotating in opposite directions, horseshoe vortices); stability and destruction of the jet [21-22].

The purpose of this work was to assess the impact of emissions on the environment based on a numerical model of the spread of pollutants from sources. One of the pipes of Ekibastuz Thermal Power Plant-1 (Kazakhstan) was chosen as a real physical object of research [23]. Its height is 330 [m], the pipe diameter is 10 [m].

Mathematical model

Computational fluid dynamics has proven to be an effective tool for modeling the behavior of jets in crossflow. Modeling of such problems is based on the resolution of the Navier-Stokes equations (the equation of continuity and the equation of motion) [24-25]. It was found that Reynolds-averaged Navier-Stokes equations (RANS) modeling, can qualitatively predict the behavior of the total flow and concentration [26]. Past studies have revealed that non-stationary large eddy simulation (LES) models provide good agreement with experimental results in pollutant dispersion problems [27]. However, the computational cost of this model is about 100 times higher than the cost required for the RANS model [28]. Important observations regarding RANS k-epsilon were noted in [29].

In present work, RANS k-epsilon model was used. Also, a comparative analysis of the obtained results with the experimental [30] and numerical [31] data was carried out. The SIMPLE method was chosen for the calculation. This method has been applied in multiple numerical studies and, when compared with experimental data, has shown good agreement. [29].

Test problem

A detailed description of the test problem and experiment is given in [30, 31]. The test problem domain is a three-dimensional channel with a pipe inside it. The pipe diameter (jet width) was D=12.7 [mm], which was used as a characteristic unit of length. The dimensions of the geometry are shown in Figure 1.

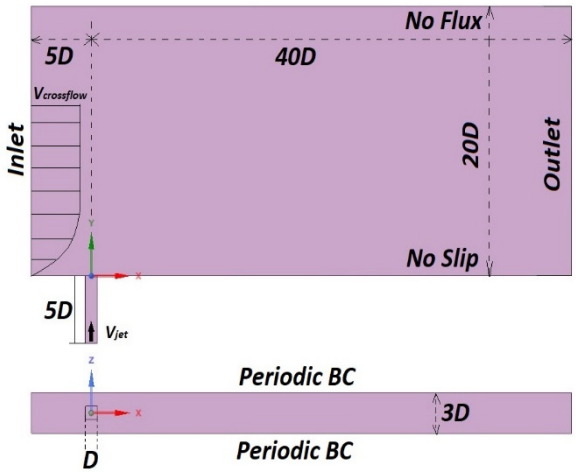

Figure 1 – Configuration of the computational domain of the test problem

An unstructured grid was constructed, the total number of nodes was 533 697 (See Table 1). The ratio of the jet velocity to the velocity of the crossflow is denoted as $R = V_{jet} / V_{crossflow}$. In the present work, R=0.5 was considered: the jet velocity was 5.5 $[ms^{-1}]$, the crossflow velocity was 11 $[ms^{-1}]$.

Table 1 – Number of grid points

NI	230
NJ	100
NK	21
Total body sizing	0.0025 [m]
Total nodes	533 697

Air was chosen as the main fluid material for the crossflow and the jet. The Reynolds number has been defined as:

$$Re_{jet} = \rho V_{jet} D/\mu = 4700. \quad (1)$$

Five types of boundary conditions were used: inlet, outlet, periodic, no slip, no flux (see Figure 1). According to experimental data, the thickness of the boundary layer is equal to 2D. The wind velocity profile was defined by a power law with exponent 1/7 within the boundary layer and was set as constant 11 $[ms^{-1}]$ above it. Since a smooth surface was used in the experiment, the roughness height was zero.

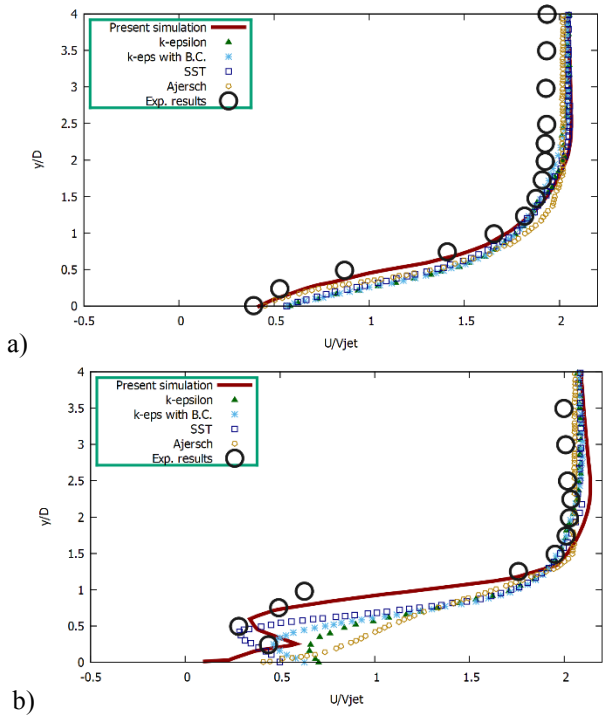

Figure 2 – Comparison of the obtained results with experiment data and calculations of other authors. (a) x/D=0.0, (b) x/D=3.0

Figure 2 shows a comparison of the numerical results of this study with experimental data and numerical solutions of other authors at various distances from the jet (R=0.5; x/D=0.0 and x/D=3.0). At the Figure 2,b the values of the red line (u/Vjet) at y/D=0 approach zero, while the plots of other authors in this interval show the values of u/Vjet~0.5 – 0.7. A zero value is more reliable from a physical point of view, as this is a near-wall field. Also, in this region (y/D~0 – 1) the relative errors of present simulation are smaller, than others (see Table 2). Based on this data, the solutions obtained in this work turned out to be more accurate than the calculations obtained by other authors [30, 31]. The reason is the quality of the grid: in this work, an unstructured grid was used (the number of nodes was 533 697), while in [31] a structured grid was used (the number of nodes was 265 000).

Table 2 – Relative errors of numerical simulations for R=0.5

	Min. relative error		Max. relative error	
x/D	0.0	3.0	0.0	3.0
k-epsilon	6.78%	7.54%	87.74%	207.23%
k-eps with BC	6.57%	6.2%	85.16%	169.66%
SST	6.57%	7.9%	72.9%	170.1%
Ajersch	9.65%	8.32%	51.37%	279.52%
Present paper	2.46%	3.68%	22.58%	89.13%

Ekibastuz thermal power plant-1: full-scale emission distribution modeling

After verification and validation of the numerical algorithm, pollution dispersion from a real power plant (TPP) in full scale dimensions was modeled. Ekibastuz Thermal Power Plant-1 (Kazakhstan) was chosen as a real physical object of research (Figure 3). The power plant consists of a main building and two pipes. The dimensions of the main building are: length — 500 m, width — 132 m, height — 64 m. The height of the chimneys is 300 meters (built in 1980) and 330 meters (built in 1982), the exit pipe diameter for each is 10 meters. The 3D computational domain has dimensions 8000×2496×3000 m and the distance between the domain inlet and tallest pipe is 2000 m. Also, the tallest pipe is located in the origin of the coordinate system (Figure 4).

Figure 3 – Ekibastuz Thermal Power Station 1 (Kazakhstan, Ekibastuz city)

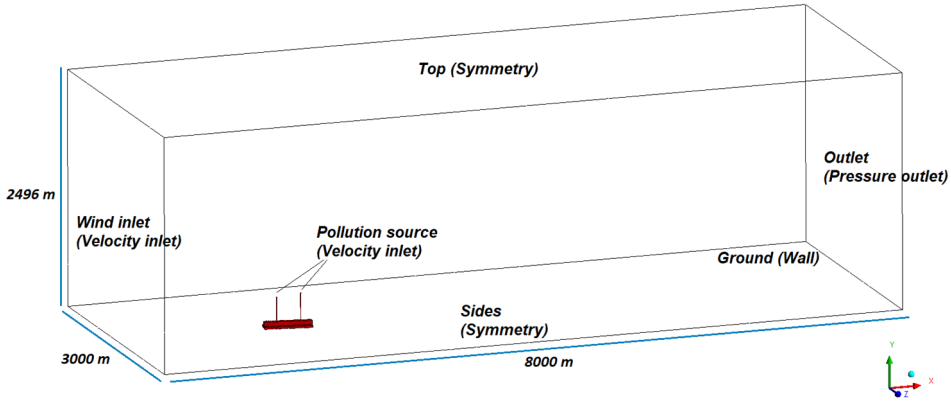

Figure 4 – Computational domain and boundary conditions for the Ekibastuz TPP simulation

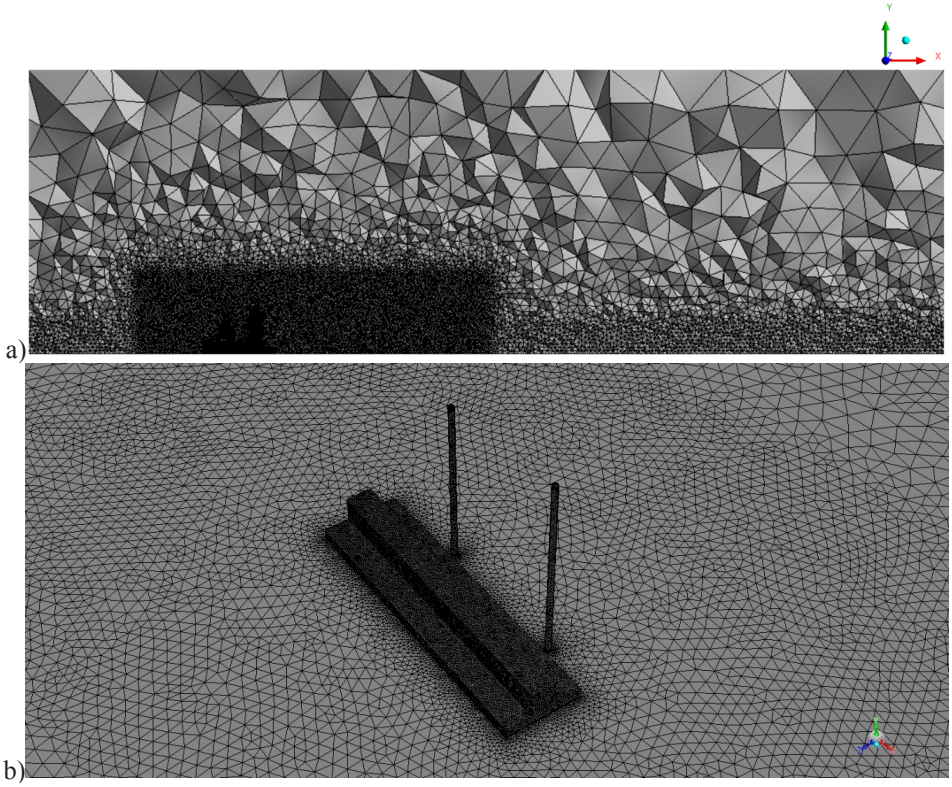

Figure 5 – Computational mesh of Ekibastuz TPP model: **(a)** cross-section view, **(b)** scaled view

The grid was built on the same principle as in the test problem, i.e. refined in the area of the pollution movement trajectory (Figure 5).

Before calculations, mesh sensitivity analysis was performed. According to the results, the grid consisting of 5,193,038 triangular elements was chosen as the main grid for further calculations.

The distance Z_P from the center point P of the wall-adjacent cells to the ground surface (bottom of domain) is 0.49 m, there was set inflation with the growth rate coefficient 1.2 since this is exactly the size of the first cell (height of first cell <1 m) that was recommended previously for an accurate simulation of the atmospheric boundary layer [29].

Since in this case it was not possible to measure experimentally the profile of velocity u, turbulence kinetic energy k or dissipation rate ε, their initial profiles were set according to the [33], which describes the profiles of these components that are most suitable for modeling wind engineering problems.

$$u = \frac{u_*}{\kappa} ln\left(\frac{y + y_0}{y_0}\right)$$

$$k = \frac{{u_*}^2}{\sqrt{C_\mu}}$$

$$\varepsilon = \frac{{u_*}^3}{\kappa(y + y_0)}$$

Where $C_\mu = 0.09$, $y_0 = 0.2, \kappa = 0.4$, u_* – friction velocity, which is calculated as:

$$u_* = \frac{\kappa\, u_{ref}}{\ln(y_{ref} + y_0)}$$

Here u_{ref} was set to 7 m/s, according to the meteorological data and the wind rose presented in Figure 6. $y_{ref} = 10\,m$ since air measurements as a rule are made at this height. According to these data, the wind most often blows from the southwest (more than 288 hours per year), therefore this direction was chosen for calculations.

The temperature of the ground was set to be equal to the maximum average temperature for the year: 28 degrees. According to the meteorological data of Ekibastuz city, this temperature is set in July (Figure 7).

The emission temperature was set to 315°C. Emission rate is 31.5 m/s. Thus, the momentum ratio is $M=W_S/U_H=4.5$, where W_S is the vertical exhaust velocity and U_H – the horizontal wind velocity at the reference height (10 m). According to the data, the following substances are released into the atmosphere from the Ekibastuz TPP per year (Table 3).

Table 3 – Emissions from Ekibastuz TPP (2016)

Type of pollutants	Unit	Amount of emissions
NO_X	tons	54,700
SO_2	tons	132,900
CO	tons	2,800
Particulate matters	tons	28,000
Persistent organic pollutants	tons	–
Volatile organic pollutants	tons	115.4
CO_2	thousand tons	24 150.7

Thus, the share of CO_2 in emissions is 99.1% and therefore the distribution of this gas was chosen for calculations.

Results

Figure 8 shows the vertical concentration profiles at various distances (x/H=5, 10, 15 and 20, where H=300 m) from the pollution sources for the default Schmidt number value of 0.7. Due to dissipation, the gas concentration decreases with increasing distance from the source. For comparison, the maximum concentration at the distance x/H=20 is almost 13 times less than the maximum concentration at the distance x/H=5 from the source. One can also notice that with increasing distance from source the height of the maximum concentration also increases. Thus, if at x/H=5 the maximum concentration point was at the height y/H=2 (600 m), then at x/H=20 the maximum concentration point is at the height y/H=3 (900 m).

Figure 9 illustrates the ground-level downstream concentration profile along the x-axis. According to the plot, the pollution reaches the earth at a distance of about x=1.5 km, which is about 1753 m from a lower stack and 1500 m from a high stack. The maximum concentration reaches about 0.04 ppm, which is a fairly optimal level of pollution for human health. Figure 10 illustrates the comparison

of ground-level lateral concentration profiles for different Sc numbers (Sc=0.7, 1.0, 1.2 and 1.4). For Sc=0.7, the concentration level is almost 2.5 times higher than with Sc=1.2 and almost 2.78 than in the other cases (Sc=1.4 and 1.0). Figure 11 illustrates the iso-surfaces of the pollution spreading. Due to dispersion, pollution dissipates with increasing distance from the source.

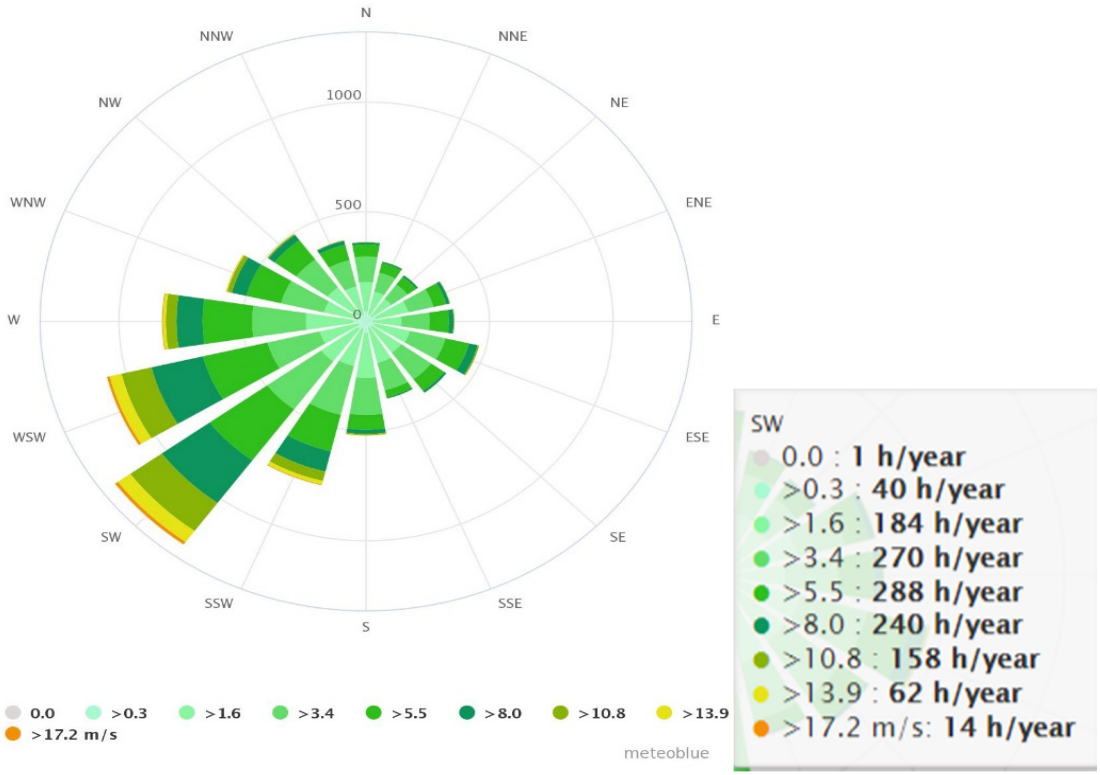

Figure 6 – Wind rose of the Ekibastuz city

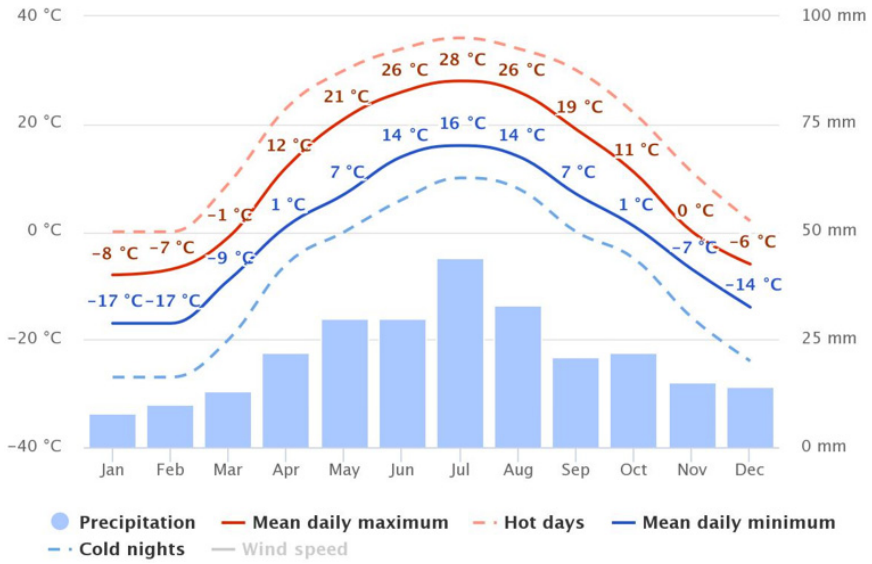

Figure 7 – Annual temperature of Ekibastuz city

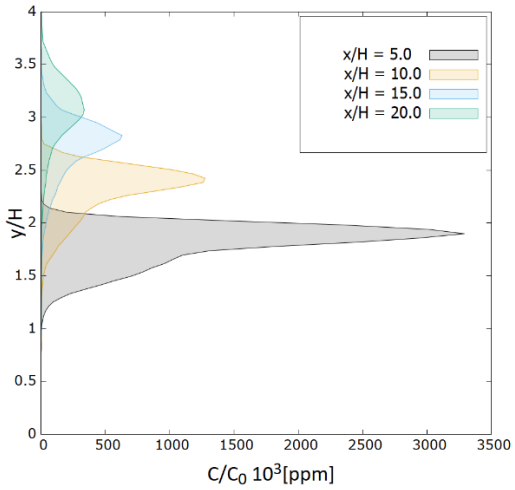

Figure 8 – Vertical concentration profiles at various distances from the pollution sources at central cross section (z/H=0).

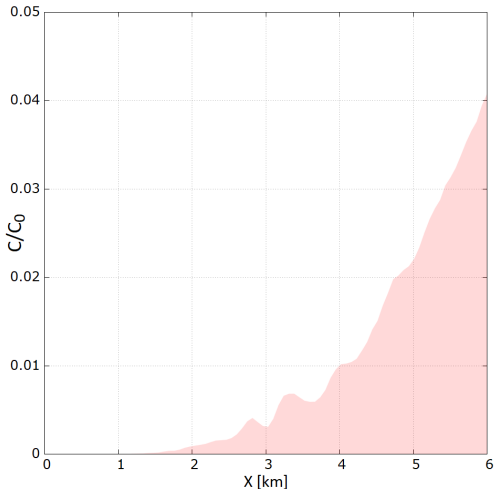

Figure 9. Ground-level (y=0) downstream concentration profile

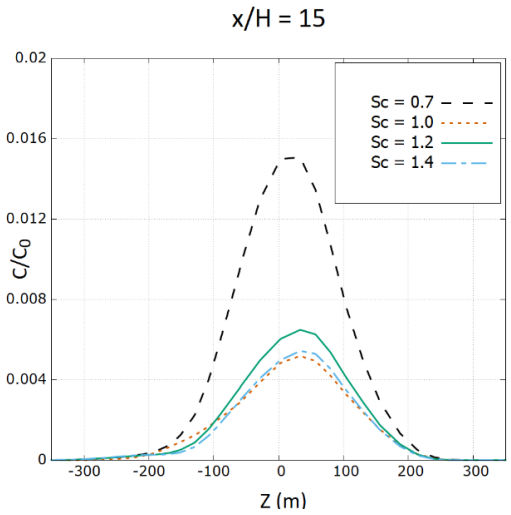

Figure 10 – Side concentration profiles at ground level (y=0) for different values of the Schmidt number (Sc)

Conclusions

The purpose of the study was to investigate the dynamics of the pollution dispersion. The mathematical model and numerical algorithm were tested using an experimental test problem. The results were closer to the experimental, compared with the data of other authors. Using the example of a real thermal power plant, CO_2 dispersion was modeled. The k-epsilon model was used without any additional dispersion models. As a result, it was determined at what distance from the source the pollution accumulates on the ground surface.

According to the obtained data, with increasing distance from the source, the concentration of pollution spreads more widely under the influence of diffusion.

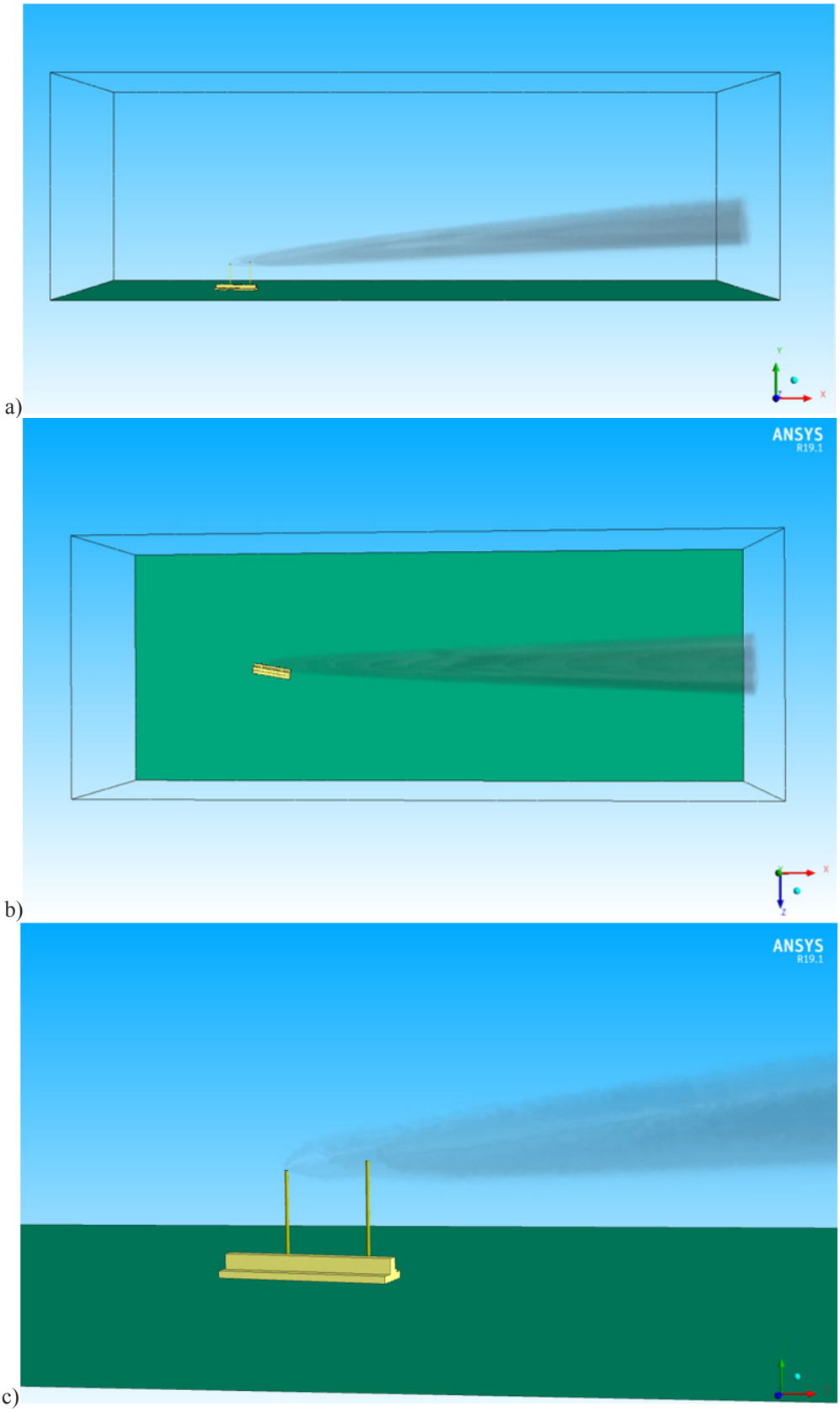

Figure 11 – Iso-surfaces of the mean concentration C/C_0=0.01 (Sc=0.7)

The farther the distance from the pipe, the lower the concentration of the substance. The various Sc numbers were tested for gas dispersion modelling, Sc=0.7 showed the highest levels of concentration.

Thus, the obtained numerical data may allow to predict the optimal distance from residential areas for the construction of thermal power plants, at which the concentration of emissions will remain at a safe level in the future.

References

1. ECSC. (2018). Glossary: Primary & Secondary pollutant. [online] Available at: http://ec.europa.eu/health/scientific_committees/opinions_layman/en/indoor-air-pollution/glossary/pqrs/primary-pollutant-secondary-pollutant.htm (Accessed 5 Jul. 2018).

2. International Energy Agency (IEA). CO2 Emissions from Fuel Combustion; 2018

3. CO2 Earth. Annual CO2 Data, [online] Available at: https://www.co2.earth/annual-co2 Accessed: (15 January 2019)

4. Zavila O. Physical Modeling of Gas Pollutant Motion in the Atmosphere, Advances in Modeling of Fluid Dynamics, Dr. Chaoqun Liu (Ed.), InTech, 2012

5. Visual Capitalist. (2017). Visualizing the Trillion-Fold Increase in Computing Power. [online] Available at: https://www.visualcapitalist.com/visualizing-trillion-fold-increase-computing-power (Accessed: 15 January 2019)

6. Jiangfei Z. "The new direction of computational fluid dynamics and its application in industry", J. Phys.: Conf. Ser. 1064 012060, 2018

7. "Computational Fluid Dynamics Past, Present and Future". [online] Available at: http://aero-comlab.stanford.edu/Papers/NASA_Presentation_20121030.pdf (Accessed: 15 January 2019)

8. Rek Z. et al. "Numerical simulation of gas jet in liquid crossflow with high mean jet tocrossflow velocity ratio ". Chemical Engineering Science 172 (2017) 667–676

9. Margason, R. J. 1993 Fifty years of jet in crossflow research. In AGARD Symp. on a Jet in Cross Flow, Winchester, UK. AGARD CP 534.

10. Broadwell, J. E. , Breidenthal, R. E. 1984 Structure and mixing of a transverse jet in incompressible flow. J. Fluid Mech. 148, 405–412.

11. Karagozian, A. R. 1986 An analytical model for the vorticity associated with a transverse jet. AIAA J. 24, 429–436.

12. Hasselbrink, E.F., Mungal, M.G. 2001 Transverse jets and jet flames. Part 1. Scaling laws for strong transverse jets. J. Fluid Mech. 443, 1–25.

13. Muppidi, S., Mahesh, K. 2005 Study of trajectories of jets in crossflow using direct numerical simulations. J. Fluid. Mech. 530, 81–100.

14. Muppidi, S., Mahesh, K. 2008 Direct numerical simulation of passive scalar transport in transverse jets. J. Fluid Mech., 598, pp. 335–360.

15. Callaghan, E.E., Ruggeri, R.S., 1948. Investigation of the penetration on an air jet directed perpendicularly to an air stream.

16. Margason, R.J., 1968. The Path of a Jet Directed at Large Angles to a Subsonic Free Stream. Langley Research Center.

17. Golbitz, W.C., 1980. Time Dependent Navier-Stokes Solution of a Turbulent Gas Jet Ejected from a Rectangular Orifice into a High-Subsonic Crossflow. Faculty of the School of Engineering of the Air Force Institute of Technology.

18. Cutler, P.R.E., 2002. On the Structure and Mixing of a Jet in Crossflow. The Universe of Adelaide.

19. Erdem E., Kontis K., Saravanan S. Penetration characteristics of air, carbon dioxide and helium transverse sonic jets in mach 5 cross flow Sensors (Switzerland), 14 (2014), pp. 23462-23489.

20. Cambonie T., Gautier N., Aider J.L. Experimental study of counter-rotating vortex pair trajectories induced by a round jet in cross-flow at low velocity ratios Exp. Fluids, 54 (2013), pp. 1-13.

21. Karagozian, A.R., 2014. The jet in crossflow. Phys. Fluids 26.http://dx.doi.org/10.1063/1.4895900

22. Fric T.F., Roshko A. Vortical structure in the wake of a transverse jet J. Fluid Mech., 279 (1994), pp. 1-47,

23. Wikipedia, "Ekibastuz_GRES-1". [online] Available at: https://en.wikipedia.org/wiki/Ekibastuz_GRES-1 (Accessed: 15 January 2019)

24. Ferziger J. H., Peric M. Computational Methods for Fluid Dynamics. Springer; 3rd edition, 2013, -p. 426

25. Chung T. J. Computational Fluid Dynamics. Cambridge University Press, 2002 – p. 1012.

26. Tominaga, Y., Stathopoulos, T., 2009. Numerical simulation of dispersion around an isolated cubic building: comparison of various types of k–e models. Atmospheric Environment 43, 3200–3210.

27. M. Chavez et al., "Near-field pollutant dispersion in the built environment by CFD and

wind tunnel simulations". J. Wind Eng. Ind. Aerodyn. 99 (2011) 330–339

28. Cheng, Y., Lien, F.S., Yee, E., Sinclair, R., 2003. A comparison of large eddy simulations with a standard k-e RANS model for the prediction of a fully developed turbulent flow over a matrix of cubes. Journal of Wind Engineering and Industrial Aerodynamics 91, 1301–1328.

29. Blocken B. et al., "Numerical evaluation of pollutant dispersion in the built environment: Comparisons between models and experiments". J. Wind Eng. Ind. Aerodyn. 96 (2008) 1817–1831

30. Ajersch, P., Zhou, J. M., Ketler, S., Salcudean, M., and Gartshore, I. S., "Multiple Jets in a Crossflow: Detailed Measurements and Numerical Simulations," International Gas Turbine and Aeroengine Congress and Exposition, ASME Paper 95-GT-9, Houston, TX, June 1995, pp. 1–16.

31. Keimasi M.R., Taeibi-Rahni M., "Numerical Simulation of Jets in a Crossflow Using Different Turbulence Models", AIAA journal, Vol. 39, No. 12, December 2001

32. ANSYS Fluent Theory Guide 15, ANSYS Ltd., 2013.

33. Richards, P.J., Hoxey, R.P., 1993. Appropriate boundary conditions for computational wind engineering models using the k-ε turbulence model. J. wind Eng. ind. aerodyn. 46, 145-153.

IRSTI 28.23.15

[1]M.N. Kalimoldayev, [1]O.Zh. Mamyrbayev,
[2]A.S. Kydyrbekova, [2]N.O. Mekebayev

[1]Institute of Information and Computational Technology, Almaty, Kazakhstan
[2]al-Farabi Kazakh National University, Almaty, Kazakhstan
e-mail: kas.aizat@mail.ru

Voice verification and identification using i-vector representation

Abstract. In the area of voice recognition, many methods have been proposed over time. Automatic speaker recognition technology has reached a good level of performance, but still needs to be improved. Signature verification (SV) is one of the most common methods of identity verification in the banking sector, where for security reasons, it is very important to have an accurate method for automatic signature verification (ASV). ASV is usually solved by comparing a test signature with a registration signature(-s) signed by the person whose identity is declared in two ways: online and offline. In this study, a new i-vector based method is proposed for SV online. In the proposed method, a fixed-length vector, called an i-vector, is extracted from each signature, and then this vector is used to create a template. Several methods, such as the nuisance attribute projection and the within-class covariance normalization, are also being investigated to reduce the intra-class variation in the i-vector space. At the stage of evaluation and decision-making, they also propose to apply the support vector machine with two classes.
In this article, a new low-dimensional space, depending on the dynamics and the channel, is determined using a simple factor analysis, also known as i-vector. I-vectors have proven to be the most efficient functions for text independent speaker verification in recent studies.
Key words: i-vectors, dimensionality reduction, UBM size, speaker identification

Introduction

As time goes, voice processing technology is becoming more and more mature. Using advances in signal processing and machine learning, ASV is implemented in two ways: online and offline. With offline verification, also called static verification, we have access only to the signature image [1-3]. In such methods, we usually normalize the image size after some preprocessing, and then extract the elements from the image using a sliding window. These functions are then used to compare two signatures. On the other hand, there are online methods, also called dynamic methods, where information related to signature dynamics is provided, as well as signature image [4-6]. Dynamic information includes pressure, velocity, azimuth, etc. In these methods, changes in vertical and horizontal directions are commonly used as shape-related elements. These methods have better performance than autonomous methods and are more reliable because they use more information extracted from the signature. In addition to these advantages, signature forgery is more difficult in these methods because they use dynamic characteristics, such as speed and azimuth, which are very difficult to simulate. Our focus is on online methods. There have been a lot of SV online studies that can be grouped into two main categories:

Methods based on global signature features. These methods attempt to extract a fixed-length vector from the entire signature so that the signatures can be easily compared in vector form. These methods can be further divided into two subcategories: in the first, we try to extract global functions from the entire set of signatures. For example, in [7] Jane uses the number of strokes as a global feature. The authors use other functions such as average speed, average pressure, and the number of times the pen is lifted during signature in [8]. As a good example of Fierrez-Aguilar, [4] introduced 100 global attributes sorted by their individual discriminatory power. A subset of these functions is also used in other studies [5, 9-12]. In the second subcategory, a transformation is applied to the signature to obtain a fixed-length vector. For

example, the wavelet transform is used in [13] to extract the feature vector from the entire signature. In another study, the discrete cosine transformation (DCT) is used to obtain a fixed length feature vector [6]. The proposed method in this paper belongs to this group.

Functional methods. Methods in this category are more focused on comparing signatures and calculating the distance between two signatures. In these methods, each signature is represented using a sequence of local features extracted from it. This category can also be divided into two subcategories: the methods in the first do not perform any modeling. In fact, in these methods, a set of references is stored for each individual, and during the test, the input signature is compared to the set of references for decision-making. The most common method in this subcategory is Dynamic Time-Warping (DTW), which is used in many studies [14–17].

The second category includes methods that train a probabilistic model for each person, using signatures in his/her control set. These methods typically use probabilities for evaluation and decision making. The most common methods in this subcategory are the hidden Markov model (HMM) [18–22] and the Gaussian mixture model (GMM) [23–25].

In the area of voice recognition, the use of Gaussian mixture models (GMM) to create universal background models (UMM) and collaborative factor analysis (JFA), by far the most popular i-vector, has increased its accuracy in creating a specific dynamics model. However, sometimes we do not need to know what language the speaker speaks, because in some situations only one of them is the most important, while others are relatively less critical. Speaker verification is becoming increasingly important as a solution to secure biometric keys for industrial, forensic and government purposes, such as data encryption on mobile devices or user verification at contact centers. It seems that users are annoyed with the persistence of multiple PINs and passwords, that is, biometric data that cannot be lost or forgotten, provide significant advantages in terms of usability.

i-vector

The i-vector was first proposed for speaker recognition application, and then was applied in other applications, such as language identification, accent identification, gender recognition, age assessment, emotion recognition, sound scene classification, etc. In the main application of this method (i.e. speaker recognition), a vector of fixed length, called an i-vector, is extracted from a speech signal of arbitrary duration. In this article, we give a description of the i-vector problem and a brief overview of the initial results. We begin with a very brief description of the key components of the i-vector based on the speaker recognition system. In the following steps, this vector is used for scoring and recognition. Although i-vector is used mainly in many speech applications, it is less well known in other areas. In this article, we use the i-vector, which is usually used to recognize the speaker in the SV. Despite their different areas, speech biometrics and signature biometrics are similar in nature, as both must extract subject-specific patterns from a captured signal contaminated by changes from various irrelevant sources. Since the analysis of total variability factors is an embedded i-vector learning step that helps eliminate distractions in biometric analysis and extracts a unique identity representation vector, we expect the i-vector to be able to provide a promising solution for the signature extraction problem.

There are two reasons for using this method for SV. First, online signatures have a variable length, similar to speech signals. Using this method, we can get a fixed-length vector that facilitates the following steps in making a decision. Therefore, after extracting the temporal features from each signature, we extract the i-vector. Since we get a fixed-length vector for each signature, we can put this method in the first category above. The second reason is that a person's signatures usually differ slightly each time. These differences lead to changes within the class, which in turn increase the false rejection rate (FRR). In various applications of the i-vector in speech processing, various ways have been proposed to reduce intraclass variations, which can also be accepted in this application. Similar to the case of speaker verification, we also suggest using two different methods to reduce the undesirable effects of intra-class changes. Since there are several signature samples for each person as a reference set at the registration stage, we suggested adding them to the data used to train variation compensation methods within the class. In addition, we proposed to apply the 2nd class support vector machine (SVM) method to distinguish between i-vectors extracted from genuine and fake signatures. The experimental results showed the effectiveness of these ideas on two different databases.

Extract statistics

At this stage, for each sequence of attributes, the Baum-Welch statistic of zero and first order is calculated using UBM [26,27].

Given that Xi is a complete set of feature vectors for learning the i-th signature, the zero and first order statistics for the c-th UBM component is calculated as follows:

$$N_c\,(X_i) = \sum_t r_{i,t}^c \qquad (1)$$

The variability of the speaker or session is the variability manifested by a given speaker from one recording session to another. This type of variability is usually associated with channel effects, although this is not strictly accurate, since there are also changes within the dynamics and phonetic change. In this approach, the speech segment is represented by a low-dimensional "identity vector" (ivector – for short) extracted by factor analysis. The i-vector approach has become state-of-the-art in speaker verification, and in this paper we show that it can be successfully applied to speaker identification as well. The approach provides an elegant way to reduce multidimensional sequential input data to a low-dimensional vector of features of a fixed length, while retaining most of the relevant information [28]. The basic idea is that the session-and channel-dependent supervectors of the Gaussian mixture model cascade model (GMM) can be modeled as

$$s = m + Tw \qquad (2)$$

where m is the session-and channel-independent component of the average supervector obtained from UBM, T is the basis matrix covering the subspace encompassing the important (both for the dynamics and the session) in the supervector space, and w is the standard, normally distributed hidden variable. For each observation sequence representing the statement, our i-vector is the point estimate of the maximum a posteriori (MAP) for the hidden variable w. Our i-vector extractor learning procedure is based on the efficient implementation proposed in [29].

The contribution of this study is to evaluate the result of factors affecting the i-vector, based on the speaker's sound identification. We study this in terms of parameters, where we evaluate and analyze how the various parameters of the i-vector extractor, such as the size of the Universal Background Model (UBM) and the dimension of the i-vector, affect the accuracy of speaker detection. The UBM size refers to the Gaussian component, which is the corresponding adapted component in the dynamics model. The I-vector dimension is equal to the "rank" of its own matrix. Based on Huang, a greater i-vector dimension would not give a large performance improvement of the classification, but significantly increased the computational costs. In [30] the literature discussed by reducing computations will allow efficient use of the i-vector in more applications. In this study, the recorded computation time is to investigate whether both factors affect the computation or not, and and the next direction for the next study is determined.

To record the voice in the present work, a complex of technical devices was used, the block diagram of which is shown in Fig.1. The block diagram of the system includes: microphone 1, low-frequency amplifier 2, analog-to-digital converter 3, software 4, and a computer unit 5, which records the amplitude-time and calculation of the frequency dependences of the signal.

To identify an unknown voice recording, a database of speakers was compiled and registered. Using the above equipment, voice signals were recorded, which formed the database.

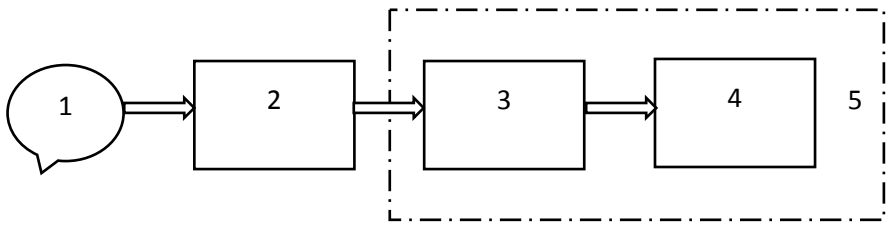

Figure1 – A block diagram of the hardware of the voice identification system

When scaling, or weighing, all experimental data are reduced to the same scale. This procedure is necessary to reduce the impact on the analysis of strongly pronounced variables. There are various ways of scaling [28], in this work standardization has been applied, since it is the most studied and tested. Standardization uses standard deviation – S_{dev}, which is one of the most commonly used weighting factors. In addition, each element of the matrix X is multiplied by the value $1/S_{dev}$:

$$X_{ik}^{scaled} = X_{ik} \frac{1}{S_{dev}}, \quad (3)$$

where X_{ik} is the i-th variable of the k -th sample, X_{ik}^{scaled} – is the i-th scaled variable of the k -th sample, S_{dev} – is the standard deviation of the sample.

Figure 2 shows the block diagram of the method used in this paper. The i-vector system consists of two main parts: the front part and the rear part. The first consists of the extraction of cepstral features and UBM learning, while the latter includes sufficient statistical calculation, T-matrix training, i-vector extraction, dimension reduction and evaluation.

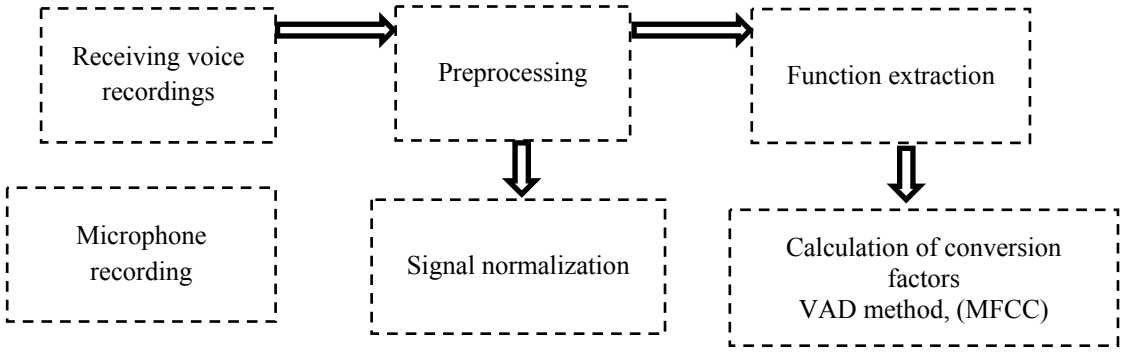

Figure 2 – Block diagram of the experiment with the speaker's identification system

Function extraction

First, simple energy speech activity detection (VAD) is performed to discard unnecessary part of the voices. Energy-based VAD is used when energy values are first calculated at the frame level, followed by data normalization and, finally, voice activity detection. A class with a higher average is considered to be the speaker's sound, and therefore the corresponding segments of the sound are preserved until smooth. Second, the characteristics of MFCC and log energy, together with their first and second order derivatives, are computed in 20 ms of Hamming window frames every 10 ms. Then the determination of the activity of the speaker's sound is applied, and the speaker's sound is normalized in accordance with the standard normal distribution.

To solve the problem of identification of the individual, the analysis of the individual frequency spectrum of voice signals is the main one. In this setting, the first two factors (the amplitude and duration of the signal) are random and need to get rid of them. To do this, all signals were reduced to one amplitude, that is, the amplitude normalization was performed:

$$a_i^{norm} = \frac{a_i}{a_{max}} \quad (4)$$

where a_i is the measured amplitude, a_i^{norm} is the maximum amplitude, normalized amplitude, i = 0,1, ..., k.

In order to remove the second factor (speech rate), time normalization was performed. The second factor was taken into account programmatically by using the same number of samples. The amplitude-frequency characteristics in the form of the recorded audio signal spectrum were analyzed directly. The frequency spectra had the form of the dependence of the amplitude A from the frequency f.

When recording voice signals in real conditions, it is possible to impose random factors, including both external mechanical noise and hardware noise. Median filtering [31] was used for their suppression, which consisted in exclusion from the initial emission signal.

The current lack of a clear systematization of voice features, as well as the existence of a large number of voice characteristics of various levels, such as the basic tone [32], formant frequencies

[33,34] and others [35,36], is a certain difficulty in choosing most informative features and characteristics for a specific identification method and requires a separate study. This section provides qualitative and quantitative estimates for the selection of informative voice characteristics. The difference in voice timbres is described by different frequency spectra of voice signals. Fourier decomposition is a natural mathematical apparatus for frequency spectrum analysis. Processing of data representing numerical amplitude-time dependences can be carried out using discrete Fourier transform:

$$A(k) = \sum_{n=0}^{N-1} a(n) e^{-j2\pi \frac{k}{N} n},$$

$$k = 0,1,2,\dots,N-1 \quad (5)$$

$$a(n) = \frac{1}{N} \sum_{k=0}^{N-1} A(k) e^{-j2\pi \frac{k}{N} n},$$

$$k = 0,1,2,\dots,N-1 \quad (6)$$

where A(k), a(n) are direct and inverse discrete Fourier transforms, respectively, k and n are sample numbers, and N is the number of samples. Coefficients A (k) can be used precisely as the elements of the matrix X, forming rows in this matrix.

I-vector extraction

I-Vector based systems. As explained earlier, at present, the i-vector in the space of complete variability has become a modern approach to voice recognition.

This method, which was introduced after its predecessor, the joint factor analysis, can be considered as a method of extracting a compact representation with a fixed length in the presence of an arbitrary length signal. The extracted compact unit vector can then be used either to measure similarity based on vector distance or as input for any further feature transformation or modeling. There are certain steps to extract the i-vector from the signal. First the features should be extracted from the input signal, then the Baum – Welch statistics should be extracted from the features, and finally the i-vector is calculated using these statistics. We will explain these steps in detail below.

For each statement, the corresponding feature sequence is eventually transformed into an i-vector using a GMM-based i-vector extractor with three different UBM-sized components trained from the combined features from all the samples included in our training data (Fig.3). Three UBM sizes that make up 32, 64 and 128 components.

Assuming that we have calculated the zero and first order statistics using (7) and (8), we can calculate the a posteriori covariance matrix [i.e. (w_i, w_j)], average (i.e. $E[w_i]$ and second moment (i.e. $[w_i w_i^t]$ for wi, using the following relations:

$$Cov(w_i, w_j) = (I + \sum_c N_c(X_i) T_c^t \sum_c^{-1} T_c)^{-1} \quad (7)$$

$$E[w_i] = \left(Cov(w_i, w_j) \sum_c T_c^t \sum_c^{-1} F_c(X_i)\right)^{-1} \quad (8)$$

$$E(w_i, w_i^t) = Cov(w_i, w_j) + E[w_i] E[wi]^t \quad (9)$$

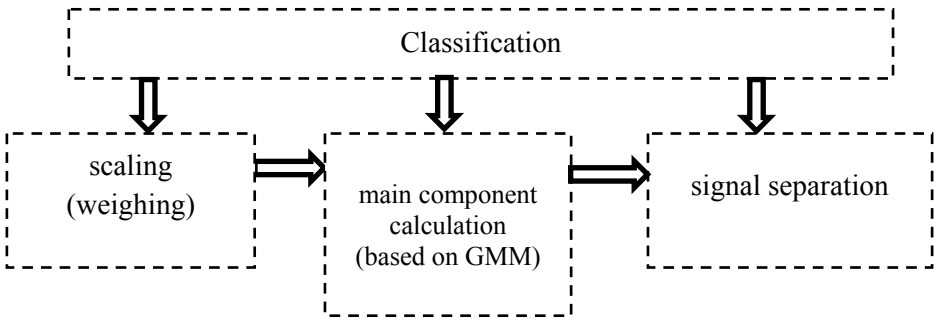

Figure 3 – Using projection methods

Post processing

Since the simulation of i-vectors contains information about the dynamics and channel variability in the same space at the same time, the channel compensation technique in the common factor space is required to eliminate undesirable effects. Channel-compensated approaches play a major role in I-vector speaker recognition systems. Therefore, channel compensation is necessary to ensure that test data obtained from different channels can be properly evaluated by loudspeaker models. For channel compensation to be possible, channel variability should be modeled explicitly.

Before calculating the verification estimates, channel bleaching, linear discriminant analysis (LDA) and within-class covariance normalization (WCCN) were performed to compensate for the channel.

We used the same dataset to train the total variability matrix to evaluate the LDA and WCCN matrices. Since the extracted i-vectors contain variations both within and between accents, the goal of dimension reduction is to project the i-vectors into a space where the variability between accents is maximal and the variability within the accent is minimized. In this study, three different measurements were experimented with: 100, 200, and 400. Thus, we optimized the parameters of the i-vector to experiment and evaluate the result.

Scoring

Finally, the identification result from the system is given by calculating the similarity score. The simplest and fastest counting function, that is, the cosine distance, is calculated between the i-vectors from the dynamics model and the i-vector from the test segment. The decision-making and evaluation process is then computed, and the system performance is then represented using accuracy 91,11%, CMC curves, and detection error tradeoff (DET).

t-SNE for individual signatures using raw i-vectors (i.e., without applying any transformations) (Figure 4)

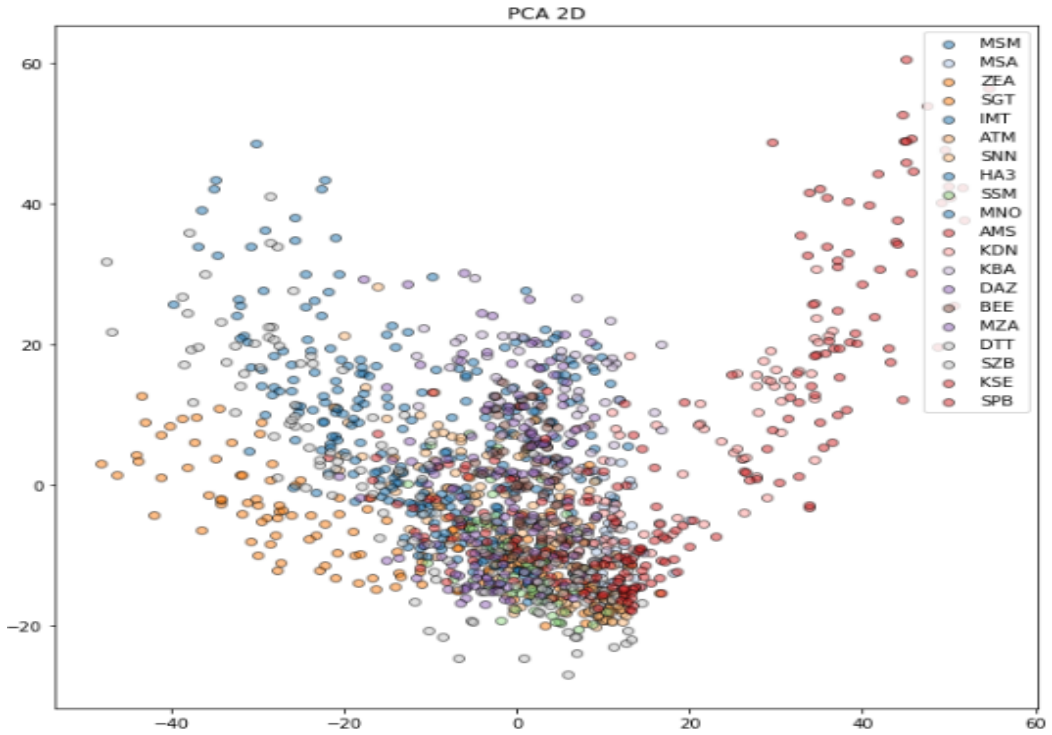

Figure 4 – Two-dimensional data representation

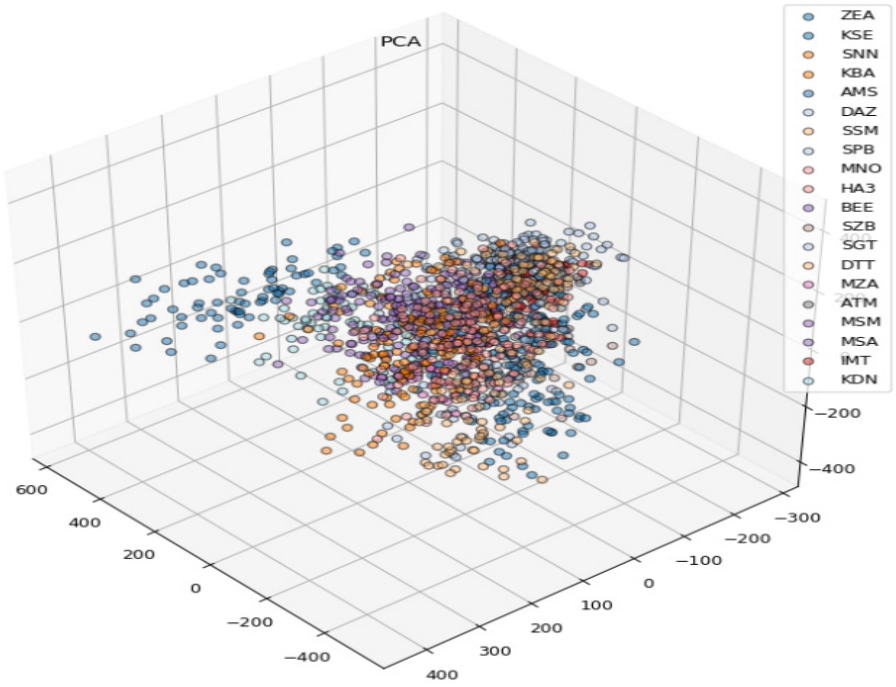

Figure 5 – Three-dimensional data representation

As shown in Fig. 5, for both projection methods, all points are combined into compact areas not intersecting with each other, each area corresponds to the records of one speaker. This indicates that both methods have provided a reliable separation of speakers by voice data.

Note that the direct comparison of the above graphs of accounts for the methods of main components (Fig. 4) and projections on latent structures (Fig. 5) does not allow to quantify these calculation options. The advantage of one method over another can be estimated from the residual dispersion graph.

Result and discussion

A series of experiments was conducted to study the effect of the number of UBM components, vector dimension, and post-processing techniques. These experiments were conducted using a set of voices – a set of open source toolkit and extensible tools for recognition of the modern level. 50 votes taken from the database were used for the evaluation.

The adaptation of projection methods of the main components and projections on latent structures in relation to the analysis of acoustic signals in technologies of personal identification by voice has been carried out.

The speech database of voice data intended for tasks of voice identification and differing in considerable number of repetitions of phrases by the same speakers is created. The use of this database by increasing the number of repetitions provides a more accurate assessment of the identification result.

Comparison of various informative parameters of voice signals used as a feature vector in projection analysis methods has been carried out. The residual dispersions were calculated that showed the preference for the use of voice identification of the Mel-cepstral decomposition coefficients, which improve the separation of the source signals according to their features and reduce the contribution of random distortions.

We found that the accuracy increases as the dimension of the i-vector increases. In addition, our results showed that the UBM with smaller size outperforms larger UBM. In addition, the result of the time calculation shows that the processing takes longer when the dimension of the i-vector increases and the size of UBM is larger.

Conclusion

In this article, we studied how the i-vector extractor parameter, such as the UBM size and i-vector dimension, affects the accuracy of voice

identification. As for the parameters, the highest accuracy was achieved when using UBM with Gaussians and an i-vector dimension. They are similar to those reported in the general voice recognition literature. As for the data, we found that the selection of UBM training data is the most important part, followed by the dimension of the i-vector. This is understandable because the earlier components of the system affect the quality of the remaining steps.

For further research, we propose to study the effect for a larger i-vector dimension and a larger UBM size. For this study, we do not do this because of the long computation time, because we use the small size of the speaker's database. In the following studies, we can reduce the computation time by exploring other factors that influence this, and add additional data to further study this effect of the experiment.

This work carried out in the framework of the project "Development of technologies for multilingual automatic speech recognition using deep neural networks".

References

1. Kalera, M.K., Srihari, S., Xu, A . "Verifying and Identifying Signatures Offline Using Distance Statistics" Int. J. Pattern Recognit. Artif. Intel. 18, (07) (2004): 1339–1360.
2. Singh, J., Sharma, M . "Verifying signatures offline using neural networks." J. Inf. I-manager. Technol.1, (4) (2012): 35.
3. Daramola, S.A., Ibiyemi, TS.S . "Autonomous signature recognition using the hidden Markov model (HMM)." Int. J. Comput. Appl. 10, (2) (2010): 17–22.
4. Firres-Aguilar, J., Nanni, L., Lopez, Penalba, J., et al . "An online signature verification system based on a combination of local and global information." Audio and video biometric authentication of identity (2005): 523–532.
5. Nanni, L . "Advanced Improved multi-match method for online signature verification with global functions and tokenized random numbers." Neurocomputing, 69, (16) (2006): 2402-2406.
6. Liu Y., Yang, Z., Yang, L . "Online Signature Verification Based on DCT and Sparse Representation," IEEE Trans. Cybern. 45, (11), (2015): 2498-2511.
7. Jane AK, Griss FD, Connell S.D . "Online Signature Verification." Pattern Recognit. 35, (12) (2002): 2963-2972.
8. Lee.L.L., Berger.T., Aviczer.E. "Reliable Online Human Signature Verification Systems." IEEE Trans. Pattern Anal. Max Intell. 18, (6) (1996): 643–647.
9. Nanni, L., Lumini, A. "Parsen window classifier ensemble for online signature verification." Neurocomputing 68 (2005): 217–224.
10. Lei, H., Govindaraju, W . "Comparative study of the consistency of functions in verifying signatures online." Pattern Recognit. Lett. 26, (15) (2005): 2483-2489.
11. Richiardi, J., Ketabdar, H., Drygajlo, A . "Selecting local and global functions for online signature verification." 2005 Proc. Eighth int. Conf. Analysis and recognition of documents (2005): 625–629.
12. Nanni, L. "Experimental comparison of single-class classifiers for online signature verification," Neurocomputing 69, (7) (2006): 869–873.
13. Leytman DZ, George S.E. "Verification of a handwritten signature online using wavelets and neural back distribution networks". 2001 Proc. Sixth Int. Conf. Analysis and recognition of documents (2001): 992–996.
14. Kholmatov A., Yanikoglu B. "Identity Authentication Using the Improved Signature Verification Method on the Internet", Pattern Recognit. Lett. 26, (15) (2005): 2400–2408.
15. Vivaracho-Pascual, C., Faundez-Zanuy, M., Pascual, JM "An effective low-cost approach for recognizing signatures online based on the normalization of length and fractional distances." Pattern Recognit. 42, (1) (2009): 183–193.
16. Sato, Y., Kogure, K. "Online signature verification based on the form, movement, and pressure of the letter." Proc. Sixth Int. Conf. Pattern Recognition.(1982): 823–826.
17. R. Martens, Klezen L. "Optimization of dynamic programming for online signature verification". 1997 Proc. Fourth Int. Conf. Document Analysis and Recognition 2 (1997): 53–656.
18. Firres J., Ortega-Garcia J., Ramos D. "Online Signature Verification Based on HMM: Character Extraction and Signature Modeling." Pattern Recognit. Lett., 28, (16) (2007): 2325–2334.
19. Dolfing, J., Aarts, E., Van Oosterhout, J. "Online Signature Verification Using Hidden Markov Models." 1998 Proc. Fourteenth Int. Conf. Pattern Recognition 2 (1998): 1309–1312.
20. Van BL, Garcia-Salichetti S., Dorizzi B. B. "On the use of the Viterbi path along with

information about the probability of MMOs for online signature verification", IEEE Trans. Syst. Cybern Man B, Cybern. 37, (5) (2007): 1237–1247.

21. Rua, EA, Castro, JLA. "Online Signature Verification Based on Generative Models", IEEE Trans. Syst. Cybern Man B, Cybern. 42, (4) (2012): 1231–1242.

22. Jan L., Vijazha B., Prasad R . "Using Hidden Markov Models for Verifying Signatures", Pattern Recognit. 28, (2) (1995): 161-170.

23. Richiardi, J., Drygajlo, A. "Gaussian Mixture Models for Online Signature Verification." Proc. 2003 ACM SIGMM Workshop on Biometric Methods and Applications (2003): 115–122.

24. Miguel-Hurtado, O., Mengibar-Pozo, L., Lorenz, MG et al . "Signature verification online using models with dynamic time distortion and Gaussian mixture". 2007 41st Annual IEEE Int. Carnahan Conf. Security Technology (2007): 23–29.

25. Kenny P., Owel P., Dehak N., et al "Investigation of the variability of interspecific systems in speaker verification." IEEE Trans. Audio Speech Lang. Process. 16, (5), (2008): 980-988.

26. Kenny P., Bulian G., Dumushel P. "Modeling Your Own Voices with Rare Learning Data", IEEE Trans. Speech Audio Process., 13, (3), (2005): 345–354.

27. Hamm A., Hennebert J., Ingold R. "Models of a Gaussian mixture for verifying the signature of an abyss". Machine learning for multimodal interaction (2006): 102–113

28. Zhen Huang, Yu-Chei Cheng, Kehuang Li, Ville Hautamaki, Chin-Hui Li. "Blind segmentation method for detecting acoustic events based on I-vector". Proc. Annu. Conf. Int. Speech Comm. Assoc. INTERSPESH August: (2013): 2282–2286.

29. Ondrey Glembeck, Lukas Burghet, Pavel Mateyka, Martin Carafiat and Patrick Kenny "Simplification and optimization of i-vector extraction". ICASSP, IEEE Int. Conf. Acoust. The process of the speech signal (2011): 4516–4519.

30. Ayvazyan, S.A. "Applied statistics: Classification and reduction of dimension." Finance and Statistics (1989): 607

31. Grigoryan, R.L. "Comparison of various ways to assess the similarity of the distributions of the pitch frequency in the problem of speaker identification by his speech." Speech technology no. 3 (2010): 35–38.

32. Golubinsky, A.N. "Method of estimating formant frequencies based on the polyharmonic mathematical model of the speech signal." Speech technology no. 3 (2010): 29–34.

33. Konev, A.A. "On one algorithm for estimating formant frequencies in the interval of closed vocal folds." Speech technology no. 3 (2010): 50–53.

34. Golubinsky, A.N. "The model of a speech signal in the form of a pulse AM-oscillations with several carriers to verify the personality by voice." Control Systems and Information Technologies no.4 (2007): 86–91.

35. Roldugin, S.V. "Models of speech signals for voice identification." Radiotekhnika no. 11 (2002): 79–81.

36. Azarov, I.S. "Calculation of instantaneous harmonic parameters of a speech signal." Speech technology no. 1 (2008): 67–77.

IRSTI 27.35.14

[1,2*]A.S. Zhumali, [1]B.A. Satenova, [1,2]O.L. Karuna

[1]Al-Farabi Kazakh National University, Almaty, Kazakhstan
[2]National Engineering Academy, Almaty, Kazakhstan
[*]e-mail: ainura.z89@gmail.com

Lattice Boltzmann method simulation of thermal flow dynamics in a channel

Abstract. The objective of this paper is the simulation of thermal flow dynamics in a channel. The mathematical model in a two-dimensional formulation is described by Navier-Stokes equations, continuity and temperature equations. For the numerical simulation of the problem the Lattice Boltzmann method applying the D2Q9 model is used. The validity of this method is tested by comparing the numerical solution to the analytical solution of the planar channel flow and error rates are calculated for various sizes of the computational grid. The test problem of thermal Poiseuille flow in the channel was solved to deactivate the correctness of the developed algorithm. Very good agreement between the exact and numerical solution of this problem is shown.
Key words: The lattice Boltzmann method, thermal flow dynamics, Poiseuille flow.

Introduction

Thermal flows play an important role in the flow dynamics. Recently, there has been an effort to increase the capability of the lattice Boltzmann method in order to solve for fluid flows including heat transfer [1, 2]. A detailed analysis can be found in [3].

Generally, the thermal lattice Boltzmann model (TLBE) can be divided into several categories [4]. The first is the multispeed scheme, the second is the double distribution function (DDF) scheme and the last is the hybrid thermal lattice Boltzmann equation (HTLBE) scheme [3]. The multi-speed scheme is a plain extension of the Boltzmann isothermal models with a lattice, in which only the velocity distribution function is affected. In double distribution function scheme, different distribution functions are used, one for the velocity field and the other for the temperature field or internal energy. The main advantage of the DDF scheme compared to the multi-speed scheme is to increase the numerical stability, and therefore it is widely used. The hybrid computational scheme combines the LBE and Finite difference (FD) or Finite volume (FV) methods [5]. In this paper we use DDF scheme.

The goal of this paper is the numerical implementation of thermal flow dynamics in a channel in a two-dimensional case. With the help of LBE method the profiles of velocities and temperature at different values of parameters in the system of differential equations and at different time instants are investigated.

Statement of the problem

In this paper we considered 2-D thermal flow in planar channel. The flow driven by a body force. We set cold temperature at the bottom wall and hot temperature at the top wall of the channel (Figure 1).

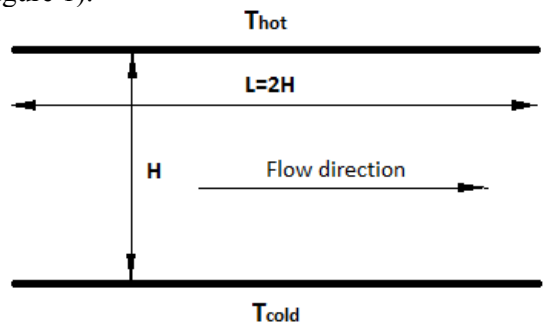

Figure 1 – The considered area

The governing equations can be written as [6]:

$$\frac{\partial u_i}{\partial t} + \frac{\partial}{\partial x_j}\left(u_i u_j\right) = -\frac{1}{\rho}\frac{\partial p}{\partial x_i} + \nu\frac{\partial^2 u_i}{\partial x_j \partial x_j} + F_x,$$

$$\frac{\partial u_i}{\partial x_i} = 0,$$

$$\frac{\partial T}{\partial t} + \frac{\partial}{\partial x_j}\left(u_j T\right) = k\frac{\partial^2 T}{\partial x_j \partial x_j}.$$

Here, ρ is the linear function of the temperature T and F_x is the body force

$$\rho = \rho_0 - \rho_0\beta(T - T_0),$$

$$F_x = 8\rho_0\nu u_{\max}/H^2,$$

where ρ_0 is the average density, T_0 is the average temperature, β is the coefficient of thermal expansion.

We assume that at the initial time, the velocity and temperature in the channel are zero. Periodic boundary conditions are used at the channel inlet and outlet for u_1, u_2, T, p. And the following boundary conditions are applied on channel walls

$$u_1(x_1, x_2 = 0, t) = u_1(x_1, x_2 = H, t) =$$
$$= u_2(x_1, x_2 = 0, t) = u_2(x_1, x_2 = H, t) = 0,$$

$$T(x_1, x_2 = 0, t) = T_{cold},$$
$$T(x_1, x_2 = H, t) = T_{hot}.$$

Numerical method

The lattice Boltzmann equation (LBE) method is a discrete model of a continuous medium. Currently, the LBE method may well compete with traditional methods of computational hydrodynamics, and in some areas (flows in a porous medium, multiphase and multicomponent flows) it has significant advantages [7-9]. By this method an intermediate scale model is used to simulate fluid flow. It applies simulation of the motion of fluid particles in order to capture the macroscopic parameters of the fluid. The area is discretized by uniform cartesian cells. Each cell contains a fixed number of distribution functions, which represent the number of fluid particles moving in these discrete directions. Depending on the dimension and the number of directions of velocity, there are various models that can be used. In the present study, a two-dimensional flow and a two-dimensional square lattice with nine discrete velocities (D2Q9 model) are examined. For each velocity vector, the value of the distribution function is stored. In the D2Q9 model (Figure 2), the velocities are calculated using the formulas

$$e_0 = (0,0),\ e_1 = (1,0),\ e_2 = (0,1),$$
$$e_3 = (-1,0),\ e_4 = (0,-1),$$
$$e_5 = (1,1),\ e_6 = (-1,1),$$
$$e_7 = (-1,-1),\ e_8 = (1,-1),$$

where $c = \Delta x/\Delta t$ and k – lattice velocity direction.

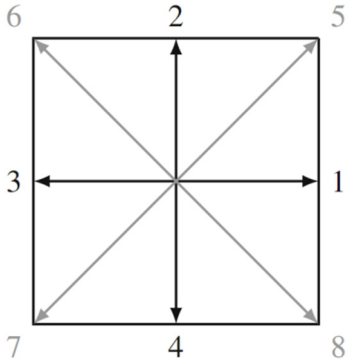

Figure 2 – D2Q9-model

Distribution functions are calculated by solving the lattice Boltzmann equation, which is a special discretization of the Boltzmann kinetic equation. After introducing the Bhatnagar – Gross – Crook approximation, we can formulate the Boltzmann equation in the form [10]

$$f_i(x + e_i\Delta t, t + \Delta t) = f_i(x,t) + \frac{\Delta t}{\tau}\left[f_i^{eq}(x,t) - f_i(x,t)\right],$$

where Δt denotes the lattice time step, e_i is the discrete lattice velocity in the direction i, τ denotes the lattice relaxation time, f_i^{eq} is the equilibrium distribution function. The equilibrium distribution functions are calculated by the formula

$$f_i^{eq} = \omega_i \rho \left[1 + \frac{e_i \cdot \vec{u}}{c_s^2} + \frac{1}{2} \frac{\left(e_i \cdot \vec{u}\right)^2}{c_s^4} - \frac{1}{2} \frac{\vec{u}^2}{c_s^2} \right]$$

where the values of the weight coefficients ω_i are as follows:

$$\omega_i = \begin{cases} 4/9, & i = 0, \\ 1/9, & i = 1,2,3,4, \\ 1/36, & i = 5,6,7,8, \end{cases}$$

and $c_s = c/\sqrt{3}$ is the lattice speed of sound.

The macroscopic variables for the density and velocity of a fluid are calculated as the first two moments of the distribution functions for each cell:

$$\rho = \sum_{i=0}^{8} f_i, \qquad \vec{u} = \frac{1}{\rho} \sum_{i=1}^{8} f_i e_i.$$

For the temperature field, the distribution g is

$$g_i(x + e_i \Delta t, t + \Delta t) = \\ = g_i(x,t) + \frac{\Delta t}{\tau_g} \left[g_i^{eq}(x,t) - g_i(x,t) \right].$$

The equilibrium distribution functions for the temperature field are determined by the formulas:

$$g_i^{eq} = \omega_i T \left[1 + \frac{e_i \cdot \vec{u}}{c_s^2} + \frac{1}{2} \frac{\left(e_i \cdot \vec{u}\right)^2}{c_s^4} - \frac{1}{2} \frac{\vec{u}^2}{c_s^2} \right]$$

The temperature field is calculated by the formula

$$T = \sum_{i=0}^{8} g_i.$$

As the no-slip boundary condition in fixed walls of channel the mid-link bounce back scheme is used [6,11]. According to the scheme, the wall boundary is located half lattice away from the boundaries of the fluid nodes. At the boundary node, the outward post-streaming distribution is equal to the inward pre-streaming distribution:

$$f_{\bar{i}}(x_B, t + \Delta t) = f_i(x_B, t),$$

where x_B is the coordinates of the boundary node, f_i is the pre-streaming distribution function with discrete velocity e_i, which points into the boundary. $f_{\bar{i}}$ is the post-streaming distribution function in the direction opposite to e_i. For the constant temperature boundary, the distribution function can be obtained as

$$g_{\bar{i}}(x_B, t + \Delta t) = -g_i(x_B, t) + 2\omega_i T_B,$$

where T_B is the temperature of the top or bottom wall and ω_i is the weight coefficients.

Algorithm for applying the lattice Boltzmann method:

1. Discretization of the physical domain and nondimensionalization of the related parameters;
2. Choice of simulation parameters;
3. Domain initialization;
4. Collision step;
5. Application of the boundary conditions;
6. Streaming step;
7. Calculation of the macroscopic parameters;
8. Verification of convergence criteria. If criterion is met, then end of routine, else go to 4.

Analytical solution and numerical results

In order to check the developed algorithm for solving the problem of thermal flow, the problem of two-dimensional Poiseuille flow in channel is solved.

Table 1 sets the parameters for calculating the test problem. The simulation was performed with different sizes of the computational domain: $N_x \times N_y = 100 \times 50,\ 200 \times 100$. The maximum velocity $u_{\max}$ in the channel and the sound speed c_s are 0.1 and 0.5773, respectively. Kinematic viscosity $\nu = 9.021 \cdot 10^{-3}$. The height of the channel $H = 1$. The Reynolds number $\mathrm{Re} = u_{\max} \cdot H/\nu \approx 10$. In the present study the Prandtl number $\mathrm{Pr} = \frac{\nu}{k} = 0.7$. Relaxation parameters are defined as [12] $\tau = \frac{\nu}{c_s^2 \cdot \Delta t} + 0.5$ and $\tau_g = \frac{k}{2c_s^2 \Delta t} + 0.5$.

Along the X axis the constant pressure difference is maintained:

$$\frac{\Delta p}{x_{out}-x_{in}}=\frac{8\eta u_{\max}}{(y_{top}-y_{bot})^2},$$

where Δp is the pressure difference, $\Delta p = p_{out} - p_{in}$, p_{out} and p_{in} are the pressure at the outlet and at the inlet of the channel, respectively, η is the dynamic viscosity, x_{out} and x_{in} are the outlet and the inlet boundaries, respectively, y_{top} and y_{bot} are the top and the bottom walls boundaries, respectively.

Table 1 – Simulation parameters

Parameters	
scaling factor, *scale*	$scale = 1:2$
number of points along the x axis N_x	$N_x = 100 \cdot scale$
number of points along the y axis, N_y	$N_y = 50 \cdot scale$
relaxation parameter, τ	$\tau = \sqrt{3/16} + 0.5$
maximum velocity in a channel, $u_{\max}$	$u_{\max} = 0.1 / scale$
kinematic viscosity, v	$\nu = (2\tau - 1)/6$
Reynolds number, Re	$\mathrm{Re} = 10$
Prandtl number, Pr	$\mathrm{Pr} = 0.7$
channel outlet pressure, p_{out}	$p_{out} = 1$

The analytical solutions for the velocity and the temperature fields are calculated as [12,13]:

$$u_{exact}(y)=u_{\max}\left(1-\frac{y^2}{L^2}\right),$$

$$T_{exact}(y)=T_{bot}+\frac{(T_{top}-T_{bot})}{H}y+ +\frac{1}{3}\mathrm{Pr}\,u_{\max}^2\left[1-\left(\frac{2y}{H}-1\right)^4\right].$$

The comparison of the exact solution with the results of the numerical solution is observed in Figures 3 – 5.

L_1 and L_2 norms of error were calculated by the following formulas:

$$\varepsilon_{L_1}(t)=\frac{\sum_{x_1,x_2}|q_n(x_1,x_2,t)-q_b(x_1,x_2,t)|}{\sum_{x_1,x_2}|q_b(x_1,x_2,t)|},$$

$$\varepsilon_{L_2}(t)=\frac{\sqrt{\sum_{x_1,x_2}|q_n(x_1,x_2,t)-q_b(x_1,x_2,t)|^2}}{\sum_{x_1,x_2}|q_b(x_1,x_2,t)|^2}.$$

where the index *n* means numerical solution and the index *b* means analytical solution.

Increasing the grid resolution helps to reduce the error norms. If we assume that the error norm is known for different grid sizes and their ratio of the sizes of each grid to the initial one is m, then we can determine the order of accuracy using the following formula:

$$n(t)=\log_m\left(\frac{\varepsilon_0(t)}{\varepsilon_m(t)}\right).$$

In the test problem, the error norms were calculated at time $t \cdot \nu / L^2 = 1$. The accuracy orders of the numerical algorithm depending on the grid size are presented in table 2.

Figure 3 shows the predicted cross-sectional profile in the force-driven channel flow for velocity and comparison between LBM simulation and analytical solution. Solid line is the analytical solution and the symbol is the numerical result.

Table 2 – The accuracy orders of L_1 and L_2 of the velocity, depending on the grid size at $t \cdot \nu / L^2 = 1$

Grid size	$u(L_1)$	Order of accuracy, *n*	$u(L_2)$	Order of accuracy, *n*
100×50	4.6600×10^{-4}	3.8978	6.8264×10^{-2}	1.9489
200×100	1.6972×10^{-4}	3.8175	4.1198×10^{-3}	1.9087

Also, Figure 4 shows the temperature cross-sectional variation at different time instants in comparison with the analytic solution. Solid lines are the numerical results and the symbol is the analytical solution. And Figure 5 demonstrates the temperature cross-sectional profiles in comparison with the analytic solution for different Prandtl numbers. Here, solid lines are the analytical solutions and the symbols are the numerical results. As can be seen from the figures, the numerical results agree well with the analytical solutions. The general results in terms of streamwise temperature and velocity for time instants $t = 0.1$ and $t = 1$ are shown in Figures 6 and 7, respectively.

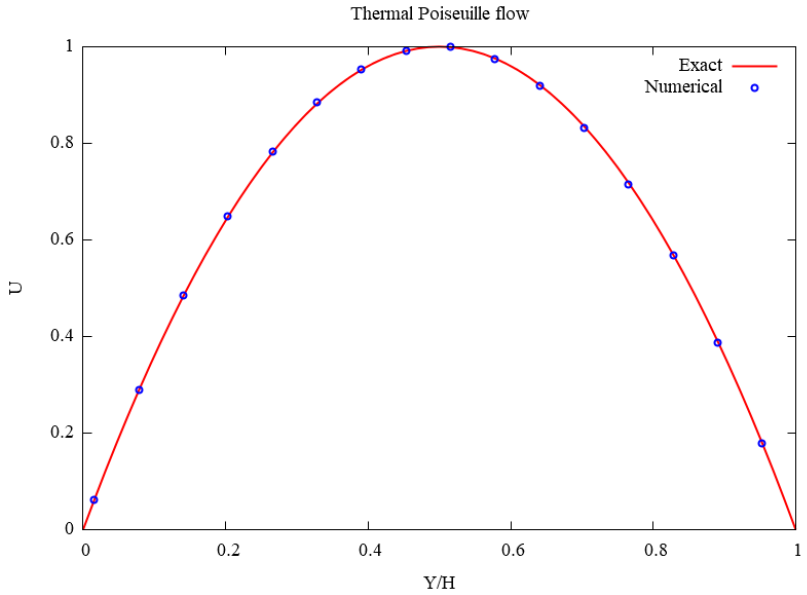

Figure 3 – Velocity profile of a 2D Poiseuille flow.
Comparison of the exact solution with the result of the numerical solution at
$T_{top} = 1,\ T_{bot} = 0,\ \ \mathrm{Pr} = 0.7,\ \ u_{\max} = 0.1$.

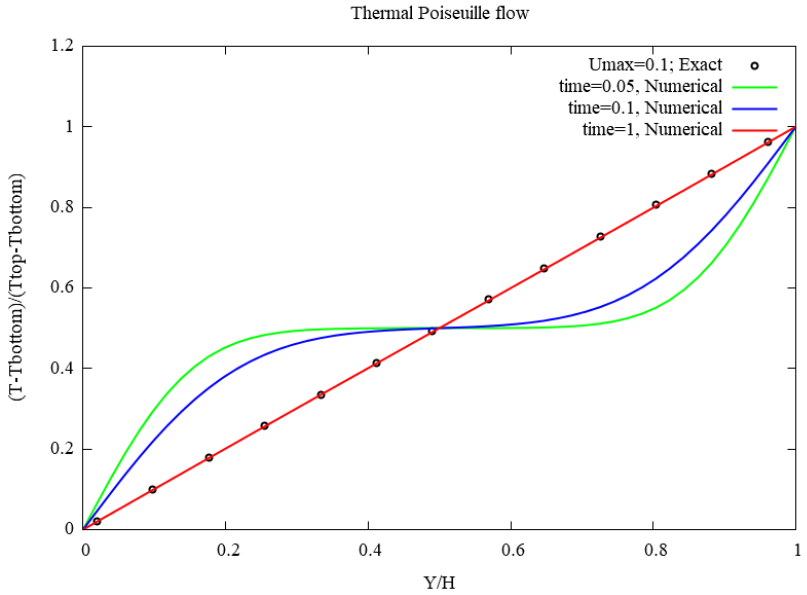

Figure 4 – Temperature variation of a 2D Poiseuille flow.
Comparison of the exact solution with the result of the numerical solution
at $T_{top} = 1,\ T_{bot} = 0,\ \ \mathrm{Pr} = 0.7,\ \ u_{\max} = 0.1$

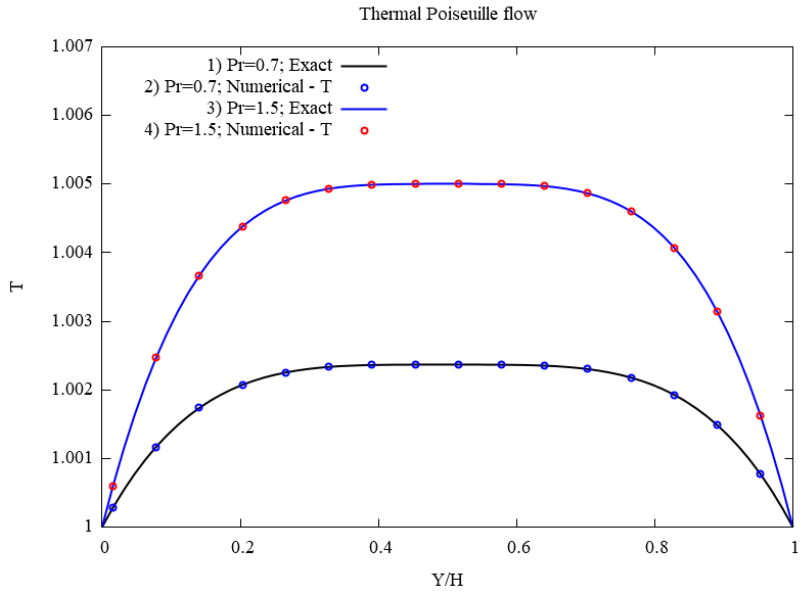

Figure 5 – Temperature profiles of a 2D Poiseuille flow.
Comparison of the exact solution with the result of the numerical solution at
$T_{top} = 1,\ T_{bot} = 1,\ \Pr = 0.7\ and\ \Pr = 1.5,\ u_{\max} = 0.1$

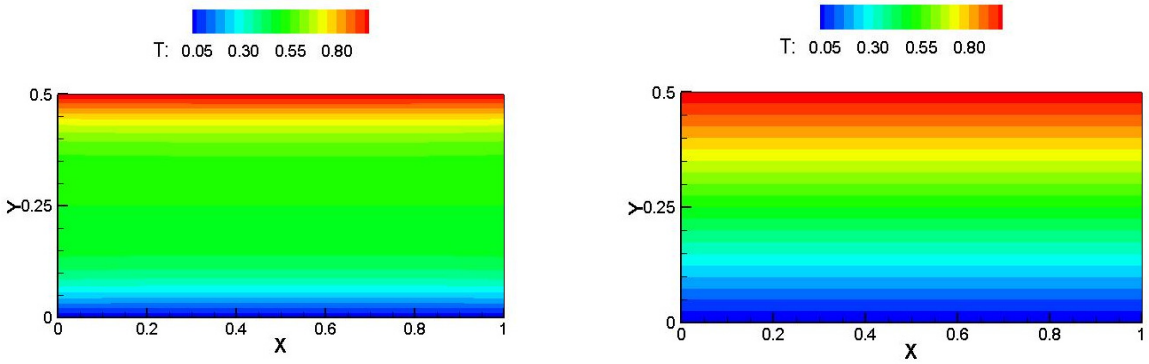

Figure 6 – Streamwise temperature at $\Pr = 0.7$, $\mathrm{Re} = 10$ and
computational time $t = 0.1$ (a) and $t = 1$ (b)

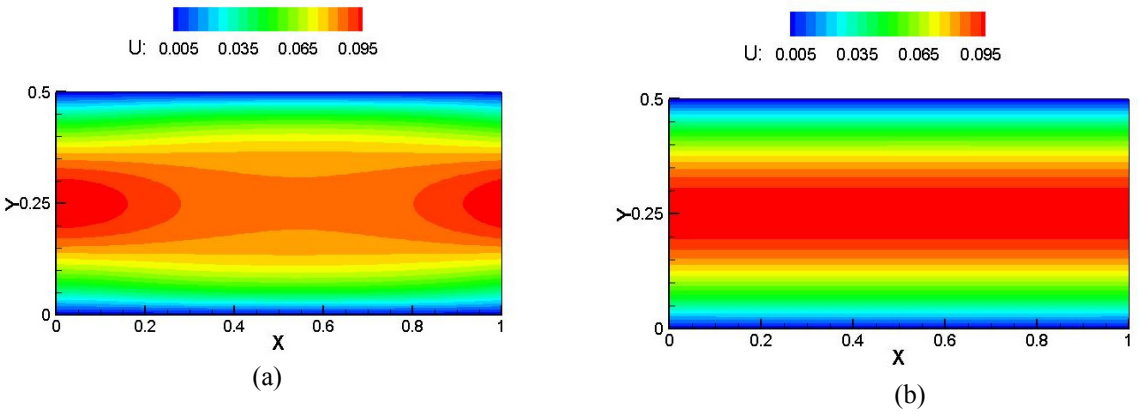

Figure 7 – Streamwise velocity at $\Pr = 0.7$, $\mathrm{Re} = 10$ and
computational time $t = 0.1$ (a) and $t = 1$ (b)

Conclusion

The basic aim of this paper is the development of mathematical model for thermal flow in a channel and the implementation of numerical simulation of the problem by the Lattice Boltzmann method applying the D2Q9 model. The validity of this method is tested by comparing the numerical solution to the analytical solution of the planar channel flow. The comparison of the exact solution with the numerical solution for test problem of thermal Poiseuille flow given in Figures 3–5 shows a very good agreement and relationship. It is determined that the numerical method has a second order of accuracy in time. This means that the developed algorithm may well be applied to solving the problem of the dynamic thermal flow in a three-dimensional region. This result will be obtained and shown in a future research.

References

1. Y. Peng, C. Shu, Y.T. Chew, “Simplified thermal lattice Boltzmann model for incompressible thermal flows”, Phys. Rev. E 68 (2) (2003) 026701.1–026701.8.

2. A.D’Orazio, M. Corcione, G.P. Celata, “Application to natural convection enclosed flows of a lattice Boltzmann BGK model coupled with a general
purpose thermal boundary condition”, Int. J. Therm. Sci. 43 (6) (2004): 575–586.

3. P. Lallemand, L.-S. Luo, “Theory of the lattice Boltzmann method: Acoustic and thermal properties in two and three dimensions”, Phys. Rev. E 68 (3) (2003) 036706.1–036706.25.

4. Zhaoli G., Chaguang Z., Baochang S. "Thermal lattice Boltzmann equation for low Mach number flow," Physical Review E 75 (2007): 036704

5. J. Wang, L.-P. Wang, Z. Xiao, Y. Shi, and S. Chen, “A hybrid numerical simulation of isotropic compressible turbulence,” J. Comput. Phys. 229, 5257 (2010).

6. Chao Li, Lian-Ping Wang. “An immersed boundary-discrete unified gas kinetic scheme for simulating natural convection involving curved surfaces” Int. J. of Heat and Mass Transfer. – (2018): 1059-1070.

7. McNamara G.R., Zanetti G. “Use of the Boltzmann equation to simulate lattice-gas automata” Phys. Rev. Lett. vol. 61, no. 20 (1988): 2332–2335.

8. Chen S., Doolen G.D. “Lattice Boltzmann method for fluid flow” Annu. Rev. Fluid Mech. –. V. 30. P. 329–364.

9. Nourgaliev R.R., Dinh T.N., Theofanous T.G., Joseph D. “The lattice Boltzmann equation method: theoretical interpretation, numerics and implications” Int. J. of Multiphase Flow vol. 29, no. 1 (2003): 117–169.

10. Kruger, T., Kusumaatmaja, H., Kuzmin, A., Shardt, O., Silva, G., Viggen, E. M. “The Lattice Boltzmann Method.” Springer (2017): 694.

11. Portinari M. “2D and 3D verification and validation of the lattice boltzmann method” Diss École Polytechnique de Montréal (2015): 129.

12. C.-H. Liu et al. “Thermal boundary conditions for thermal lattice Boltzmann simulations”, Computers and Mathematics with Applications 59 (2010): 2178–2193.

13. F.M. White, “Viscous Fluid Flow,” 3rd ed., McGraw-Hill, New York (2006).

IRSTI 44.39.29

[1]R.K. Manatbayev, N.Kalasov[1,*], B. Bektibai[1], Ye.Nurymov[1],
K.Baktybekov[2], A. Syzdykov[2], E.M. Zulbukharova[1]

[1] al-Farabi Kazakh national university, Faculty of physics and technology,
Dept. of Thermal physics and Technical Physics, Almaty, Kazakhstan
[2] Kazakhstan Gharysh Sapary, Astana, Kazakhstan
[*]e-mail: kalasov.nurdaulet@gmail.com

Definition of the basic geometric parameters of a carousel type turbine its technological solution

Abstract. In the last 10-15 years, the use of wind energy has been developing rapidly. To date, more than 20,000 wind power units have been installed in the world, the total capacity of which exceeds several MW. Kazakhstan has significant resources of wind energy. The most known in this respect are the resources of the Dzungar Gate and Shelek Complex, located in the Almaty region (Kazakhstan). Their possibilities for use in the generation of electric power of air flows are unique.

In this paper, the main calculations for determining the influence of the design characteristics of the Darrieus wind turbine on its energy efficiency are presented. The dependence of the maximum coefficient of wind energy use of vertical axle wind wheels on the number of blades at a constant filling factor σ, on the number of blades at their constant width, on the lengthening of the blade λ is studied. Based on these results, design characteristics for a rotor with a power of 1 kW are determined, and a diagram of the wind turbine which can provide thermal protection of the wind turbine by using natural ventilation of warm air inside the rotating elements of the windmill arising from centrifugal forces is also given.

And another way of solving the technological problem is proposed. Renounce a long rotating shaft and replace it with a short axis, on which two bearings will rotate with a wind wheel attached to them. Application of the proposed design of the wind farm will simplify the manufacturing technology.

Key words: wind turbine, Darrieus, aero dynamical characteristics, natural ventilation, geometrical parameters

Introduction

The development of a reliable method of protecting a working wind turbine from adverse weather conditions is relevant. In this connection, in this paper, we propose the development of a wind turbine with an anti-icing system. This uses natural ventilation of the flow elements of the wind turbine with warm air, which does not allow the sticking of wet snowflakes on the surface of the apparatus and the formation of icing. [1] The present work is devoted to the study of the effect of geometric parameters of a turbine on its performance and some technological solution.

It is known that when designing a wind turbine, the designer needs to know the effect of the main parameters such as blade lengthening, the number of blades, blade thickness and filling factor on rotor productivity.

Currently, the main source of information for designing wind turbines with the Darrieus rotor is an experiment. The most complete and comprehensive results of experimental studies were published in [2-4].

In order to develop a semi-industrial version of the wind turbine, studies were conducted to determine the geometric parameters of the turbine. Thus, the calculations of the influence of design parameters on the energy characteristics of the turbine being

developed with an anti-icing system have been performed.

Determination of geometric parameters of the rotor influencing its energy characteristics

1) Effect of lengthening the blade. The lengthening of the blade is one of the main parameters of the design of the Darrieus rotor, which determines its aerodynamic characteristics. The levels of aerodynamic loads, including the torque are depending from the magnitude of elongation. For a single blade, the nature of this dependence is almost the same as for the wing. For elongations $\lambda<1$, the magnitude of aerodynamic loads varies linearly from λ. With increasing elongation, these loads approach their asymptotic values for $\lambda> 5$.

It follows from Fig. 1 that it is necessary to use blades with an elongation greater than 6 to provide an acceptable coefficient of wind energy utilization.

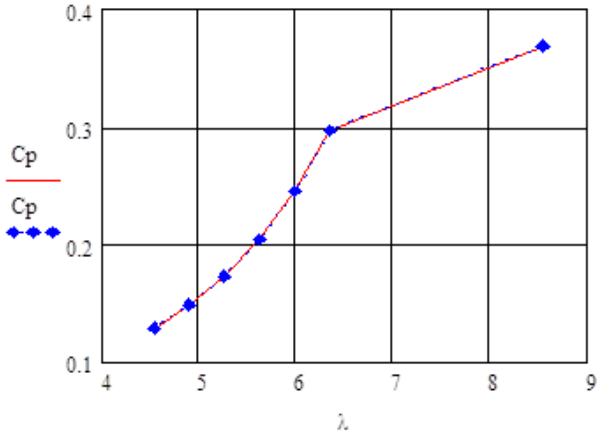

Figure 1 – Dependence of C_p on the elongation of blades *n=2, b/D=0.167, R=1.65 m, l= variable*

2) The influence of the number of blades. Another important parameter of the design is the number of blades of the Darrieus rotor. To assess the influence of the number of blades on the energy characteristics of the rotor, special studies are carried out on rotor models with different number of blades.

The study shows that the single-blade rotor has the highest energy characteristics. But in this case, the torque is experiencing large pulsations in time, which gives rise to a bunch of dynamic problems. To smoother torque of the rotor we may increase the number of blades, but energy efficiency will decrease. This is especially pronounced when the number of blades is increased, their chord is reduced to maintain the constancy of the filling factor σ. It is more effective with increasing the number of blades to maintain the length of the chord.

Fig. 2 shows the results of calculations for the study of the influence of the number of blades at a constant filling factor. It can be seen that as the number of blades increases, the wind energy utilization factor decreases.

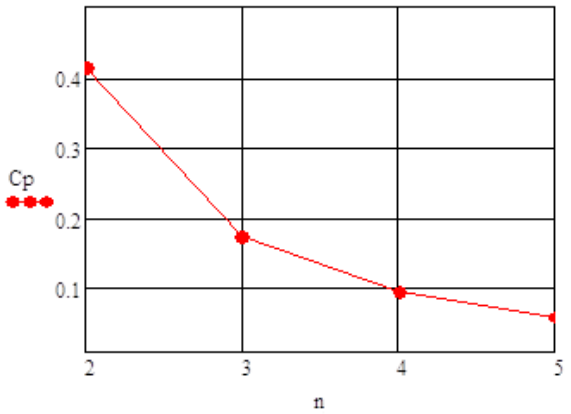

Figure 2 – Dependence of C_p on the number of blades at a constant filling factor σ=const, l=3.3 m

Fig. 3 shows that with the blade width unchanged, the efficiency of C_p falls less significantly than with constant filling with increasing number of blades.

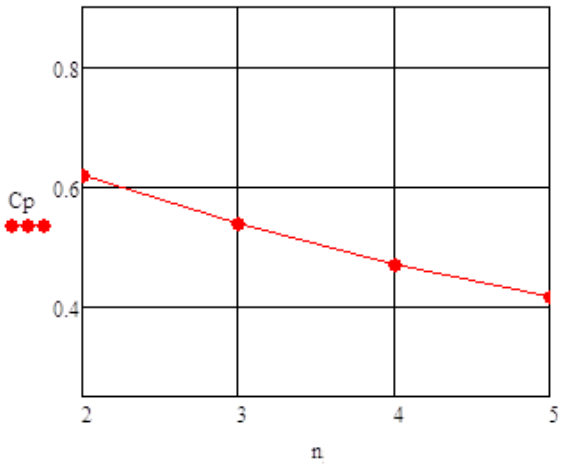

Figure 3 – Dependence of Cp on the number of blades with a constant width *b=const, D=3.3m, l=3.3m*

3) Effect of blade thickness. The effect of the relative thickness of the blade profile on the value of the maximum value of the coefficient C_p for different Reynolds numbers Re is shown in [5].

The greatest effect is achieved for blades with a relative thickness of 0.15<c<0.20. The main feature of this influence is associated with a sharp drop in C_p for thin blades. It should be noted that the same character of the dependence on the relative thickness of the profile is observed for the traction force created by the flapping wing [2].

4) Influence factor effect. The filling factor is associated with two parameters of the rotor design: the number of blades n_b and the ratio of the chord of the blade to the diameter of the rotor b/D. It should be noted that with an increase in the filling factor σ, the value of the rapidity of z decreases, at which C_p reaches its maximum.

In order to have 1 kW Darrieus rotor with direct blades with thermal protection, with an average wind speed U of 7 m / s, we find the streamlined surface of the rotor according to the formula:

$$S = \frac{2\,N_b}{C_p \rho U^3} \qquad (1)$$

where N_b – power, W; C_p – wind utilization coefficient is equal to 0.4; ρ – 1.29 kg/m^3 – air density.

The streamlined area of the rotor with a power of 1 kW should be 11.3 m2. If we assume that the rotor diameter D and the blade height l are equal, then D = l≈3.36 m. With an experimentally valid lengthening of the blade λ = l / b = 6-8, the length of the chord of the blade can be b =3.36/(6-8)=0.56-0.42 m, and the chord, on average, will be b = 0.55 m.

Since the maximum value of the coefficient C_p for different Re values is achieved for blades with a relative thickness of 0.15<c<0.20, we take the relative thickness equal to 0.18. Proceeding from this, the maximum thickness of the blade, as a fraction of the length of the chord, should be 0.09m. And the fill factor in turn will be equal to:

$$\sigma = \frac{n_b b}{D} = 0.33 \qquad (2)$$

It is important to note that the filling factor σ satisfies the conditions under which C_p reaches its maximum.

Using application packages for mathematical calculations, we can obtain the area and perimeter of the cross section. For our rotor, the perimeter of the wing was Φ = 1.04 m and the ratio to the chord b is approximately 2.1. The cross-sectional area f_1=0.0154 m^2.

Thus, geometric parameters influencing the energy characteristics of a turbine with thermal protection were determined, and internal hydraulics and warm air motions along internal channels are described in detail in [1,6,7].

The limitation of carousel type wind turbine and its technical solution

The main disadvantage in the vertical position: the vertical axis of rotation and its vertical mounting in the bearing supports. The manufacture of supports is also a complex technological task; it is required to ensure the alignment of the supports and their rigidity. Also, a disadvantage of the design is the large mass of the shaft, which presses on the lower rotational support, creates a large friction torque, which reduces the efficiency of the installation [8].

It is clear that the task of making such a shaft and its installation in a hull is a complex task. As a solution to this problem, a modular system is used. It is made from several parts-modules, and then assembled in place in one unit.

In this paper, we propose another method for solving this complex technological problem. Renounce a long rotating shaft and replace it with a short axis, on which two bearings will rotate with a wind wheel attached to them. Application of the proposed design of the wind farm will simplify the manufacturing technology. In the old design, it was necessary to have a long rotating vertical shaft, which must be fixed in two places below and above. For a 1 kW wind turbine, a shaft of about 8 m in length is required. The length of the shaft is almost equal to the length of the rotor. From above, the shaft could not be shorter than the rotor, since it is necessary to secure the upper shaft support, usually it was taut cables. It is clear that the production of such a shaft, with the achievement of coaxially and rigidity, the most complicated technological task, a special lathe capable of processing such long blanks with the required accuracy is necessary. Such a shaft is difficult to mount and provide support at the top and also affects the cost of the wind farm. The advantage of the proposed scheme is that a fixed rigid support is placed on the base (see Fig.4.), in which it is necessary to ensure alignment in the installation sites. The distance between the bearings can be 2-3 times the height of the support. In the new design, the shaft rotates inside a rigid rela-

tively short body 1.0 m long. Bearing misalignment can also have a sufficiently large value of 1-2 mm. This error will be compensated by the elasticity and flexibility of the blade design itself.

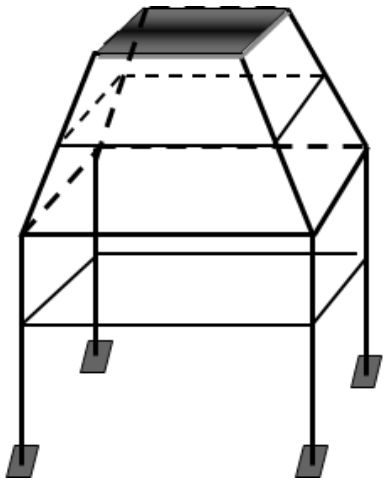

Figure 4 – Fixed rigid support

The shaft does not require high structural requirements, since the shaft does not have original surfaces.

All these factors greatly simplify the technology of manufacturing a wind power plant, by about 25-30%. It should be noted that it is the problem of a long vertical shaft that is the main one, which constrains the wide application of rotor wind turbines in practice. Also, the mass of the shortened structure with the hollow internal shaft is much smaller than the mass of the long shaft; therefore, the force of their weight will create a much smaller friction torque in the lower rotational support, which undoubtedly will increase the efficiency of the installation. This solution can be used in any scheme of a wind farm with a vertical axis of rotation of the rotor, for example, the scheme of Savonius, Darrieus, Evans, Musgrove, carousel, etc. [8, 9].

Wind installation with a shortened construction from the point of evaluation for manufacturability has a number of advantages, since the design is oriented to manufacturing in small shops, which gives a reduction in the technological cost. This design also has the advantage of being transported to remote areas for the use of farms and in small businesses.

The assembly structure consists of 12 parts (see Fig.5.). A rigid shortened body is assembled on the mounting housing 7. The rotor assembly is assembled on the mounting housing assembly on the keyway and fixed with a special nut to the rotating shaft 1. All assemblies can be mounted on supports of various designs and heights.

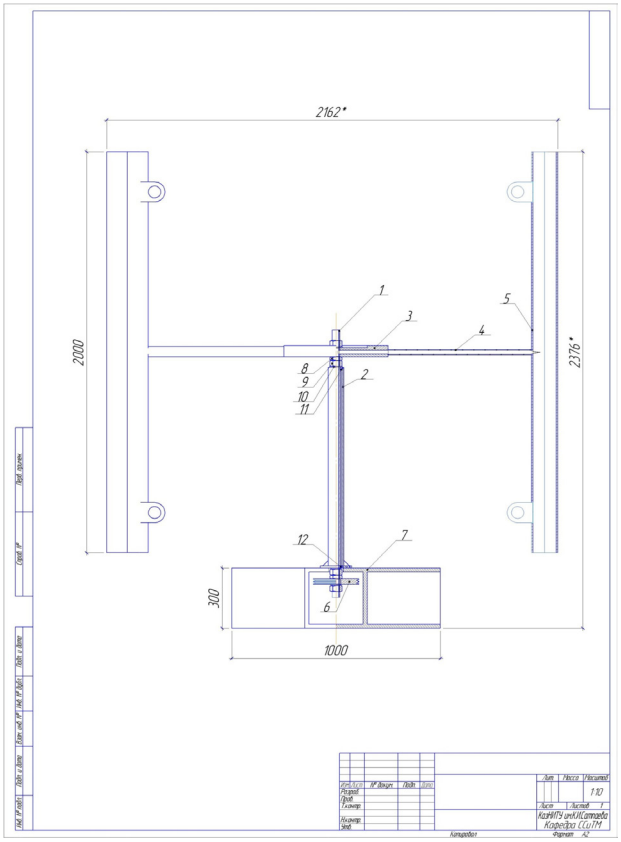

1 – rotation shaft; 2 – rigid case; 3 – hubs'
4 – wind turbine mounting unit; 5 – wind turbine blade;
6 – generator; 7 – electric drive of the vertical movement of the working body; 8.9 – special nut; 10 – washer;
11 , 12 – bearings.

Figure 5 – Assembly design wind turbine

Blades 5 windmill is made of aluminium and welded to the guiding body 4 by argon welding.

The guide body assembly is welded to the hub 3 according to the working drawing of the rotor assembly. The shortened rigid body 2 is made of a standard thick-walled tube of steel CT 3. Two standard bearings 11 and 12 are used in this design. For its intended purpose, the thrust bearing 11 is thrust, since it is affected by the weight of the rotor assembly. The lower radial single row bearing 12 operates on the rotational movement of the torque transmission from the pulley 6 to the generators generated electrical energy.

A 2 m long chord and a 0.5 m chord will be made of aluminium AD0 according to GOST 4784-97 or aluminium grade 1050 according to EN 573-3 with a thickness of 2 mm. Using tabular data with x values, the distance from the profile's bottom (in relative units, from 0 to 1, or percentages), y_t is the coordinate of the top point and y_b is the coordinate of the bottom point of the profile (also in relative units or percentages). For the symmetrical wing profile NASA-0021, the volume of the blade of the installation was determined. The density of aluminium is $\rho = 2712$ kg / m^3. Thus, the mass of one blade of the symmetrical wing profile NASA-0021 is m = 11.366 kg. Since we have 2 blades, the total mass of the blades will be m = 22.732 kg.

Swing length of 1 m and chord 0.5 m, as well as the blade, will be made of aluminum AD0 according to GOST 4784-97 or aluminum grade 1050 according to EN 573-3 with a thickness of 2 mm. Using the previous method, the mass of the fly was also determined, which is equal to m=11.366kg.

The shaft of rotation of the installation with a length of 1.334 m and an inner diameter dв=24mm will be made of structural alloy steel grade 30ХГСА, density of which is equal to ρ=7850kg/m^3. With the help of the drawing, the volume of the rotation shaft was calculated. Multiplying the volume of the shaft by the density of the material, we determined the mass of the shaft m = 1.688 kg.

Using the drawings, the mass of the outer casing was determined, which will also be made of structural alloy steel grade 30ХГСА, density of which is equal to ρ = 7850 kg/m^3. The mass of the outer tube is m = 17.34 kg.

As a result, having combined the masses of all the parts of the installation, the mass of the actual installation was determined to be m = 53.126 kg [10].

Conclusions

The dependence of the maximum coefficient of wind energy use of vertical axle wind wheels on the number of blades at a constant filling factor σ, on the number of blades at their constant width, on the lengthening of the blade λ is studied. The geometric characteristics of the blade and fly are obtained, which are the main parts of the rotor, which affect its energy efficiency.

Technological design of the components of the wind power plant has a direct relationship with labor productivity, time spent on technological preparation of production, manufacturing, maintenance and repair of the product. Therefore, the design of the technological process for the manufacture of parts must be preceded by an analysis of the technological nature of its design and, if necessary, processing for manufacturability. Technological design of the details of the wind power plant is estimated at two levels – qualitative and quantitative. A qualitative assessment and quantitative demonstration of the conformity of the design of parts during the analysing the designs of a wind power plant should met the following requirements:

– the design of the wind turbine shall be standard or consist of standard and unified structural elements;

– standard and unified blanks are used for the manufacturing of details of the wind turbines;

– dimensional accuracy and surface roughness of wind turbine components are optimal, reasonably structurally and economically;

– in determining the rigidity, shape and size, as well as the mechanical and physicochemical properties of its material, the components of the windmill were taken into account the capabilities of the manufacturing technology, storage and transportation conditions;

– accuracy and roughness of the surfaces of the components of the windmill ensure the required accuracy of installation, processing and control;

– the procurement of the components of the wind turbine must be obtained in a rational way (taking into account the volume of output and the type of production);

– in all designs of wind turbine parts, access to the surfaces to be treated and the possibility of simultaneous processing of several blanks;

Based on the analysis of the initial information of the wind turbine (the assembly drawing of the unit, the drawing of the part, the program and the annual volume of output, the type of production, the service purpose of the unit and the part), one can draw a conclusion on the expediency of a fundamental change in the method of obtaining the initial billet.

The correspondence of the surface, which will be used as technological bases, is revealed, and compliance with their requirements to the technological bases of the billet is checked. The total mass of a real installation is determined using the drawings. Also, for each part, a selection of materials was made from which the plant will be manufactured.

Nomenclature

λ – Elongation;
C_p – wind energy utilization coefficient;
n – Number of blades;
b – Chord of the blade, m;
D – Diameter, m;
R – Radius, m;
l – Blade's height, m;
σ – Filling factor;
c – Relative thickness;
Re – Reynolds number;
U – average wind speed, m/s
Φ – perimeter of the wing, m;
f_1 – cross sectional area, m^2.

References

1. R.K. Manatbayev, A. Georgiev, R. Popov, D. Dzhonova-Atanasova, A.A. Kuikabayeva, E.M. Zulbukharova. The effect of design parameters on energy characteristics of Darrieus rotor. International journal of mathematics and physics, **74**, 94-98 (2016).

2. D.N.Gorelov. The analogy between the flapping wing and the wind wheel with the vertical axis of rotation. Applied mechanics and technical physics, **50**, 152-155 (2009).

3. D.N.Gorelov, I.N.Kuzmenko, Experimental evaluation of the limiting power of a wind wheel with a vertical axis of rotation, Thermal physics and aero mechanics, **8**, 329-334 (2001)

4. A.K.Ershina, R.K.Manatbaev, Organization of natural ventilation inside the working Darrieus turbine, Small energetics, **1-2**, 63-66 (2013)

5. A.K.Ershina, R.K.Manatbaev, Determination of the hydraulic resistance of the symmetrical wing profile NASA-0021, KazNU bulletin: mathematics, mechanics and informatics section, **51**, 56-58 (2006)

6. K.J.Thuryan, D.Strickland, D.E.Berg, Power of wind turbines with a vertical axis of rotation, Aero cosmic technics, 1988

7. D.N.Gorelov, Aerodynamics of vertical axed wind turbines, KAN Polygraph center, 2012

8. D.DeRenzo, I.I.Shefter, Wind energy, Energoatomizdat, 1982

9. Manatbayev R.K., Yershina Sh. A., Yershina A.K.Method for Thermally Protecting Operating Revolving Type Wind-Power Installation, Involves Causing Internal Natural Ventilation in Wind Unit by Centrifugal Force to Heat All Elements of Wind-Power Installation by Warm Air. Patent Number(s):RU2008137251-A; RU2447318-C2International Patent Classification:F03D-003/00 Derwent Class Code(s): Q54 (Starting, ignition); X15 (Non-Fossil Fuel Power Generating Systems) Derwent Manual Code(s): X15-B01A6

10. Askarov E.S. Wind power plant with vertical axis of rotation of the wind wheel, KZ Patent№2219

IRSTI 29.03.77

[1]F.F. Komarov, [2*]T.A. Shmygaleva, [2]N. Akanbay, [2]S.A. Shafii, [3]A.A. Kuatbayeva

[1]Belarusian state university, Minsk, Belarus
[2]al-Farabi Kazakh National university, Almaty, Kazakhstan
[3] Sh.Ualikhanov Kokshetau State university, Kokshetau, Kazakhstan
[*]e-mail: shmyg1953@mail.ru

Optimization calculation algorithms on cascade and probabilistic functions and radiation defects concentration at the ionic radiation

Abstract. Work is performed within a cascade and probabilistic method which essence consists in receiving and further usage of the cascade and probabilistic functions (CPF) for various particles. CPF make sense to probability that the particle generated at some depth of h' will reach a certain depth of h after n number of impacts. In work optimization calculation algorithms of the cascade and probabilistic functions (CPF) depending on interactions number and particles penetration depth is offered, concentration of radiation defects at ionic radiation for the purpose of reduction calculation time and quality. For calculation CPF and concentration radiation defects there is an area of result, border of this area and a calculation step. Borders and a calculation step selection automation is executed.
Key words: Optimization, algorithm, calculation, cascade and probabilistic, ion, defect formation, binary search, ternary search, function.

Introduction

In recent years much attention is paid to questions of various processes mathematical modeling. Mathematical models development, calculation algorithms, research objects allows to describe many phenomena [1-3]. Modeling on the computer radiation defect formation processes in solid bodies at radiation is considered by us their various charged particles and computer modeling features on cascade and probabilistic functions and radiation defects for ions. Such works necessity is connected with a solid body defects generation and evolution management problem, for receiving, eventually, materials with the set properties [4]. For metals radiation by ions is in an efficient manner changes of such properties as the metal durability, corrosion resistance, fatigue, depreciation etc. In this direction the solid body radiation physics would be left rather academic occupation which isn't interest to practical applications without researches. It is necessary to notice that a large number of works is devoted to radiation defect formation at interaction of ions with substance problems, for example [5-8]. Losses of energy on ionization and electron shells excitement of the environment atoms weren't considered, therefore the elementary CPF was used. At charged particles to substance interaction on their movement way there are continuous energy losses. These losses result in strong dependence for both power the flying particles spectrum, and the primary beaten-out atoms (PBOA) from penetration depth. The interaction run on PBOA formation significantly depends on energy in this connection there was a need of receiving the physical and mathematical models considering real dependences of the elementary act various parameters on energy, depth.

Earlier in most cases at concrete calculations the elementary cascade and probabilistic function (CPF) was generally used, it isn't always justified as the run of interaction depends on energy [9,10]. It is necessary to investigate the received CPF behavior taking into account energy losses for ions, prove properties which they have to possess both with physical, and with mathematical points of view,

develop calculations algorithms and make CPF calculations depending on interactions number and particles penetration depth, spectrums of primary beaten-out atoms and radiation defects concentration.

Nowadays well-known methods are next: the Monte Carlo method, the Boltzmann kinetic equation, Fokker-Planck's equation, Lindhard's methods, Vineyard's methods, etc. The choice of this or that method applicability is very complex challenge as, on the one hand, because of similar tasks complexity often it is necessary to apply too many approximations which significantly worsen the calculations accuracy to obtaining final result, and on the other hand – for obtaining qualitative result it is necessary to overcome very great computing difficulties. Eventually, everything is defined by a problem specifics and the researcher ability to apply this or that method to the specific objective solution. The cascade and probabilistic method is one of options in theoretical methods numerous calculation for the spatial and power distributions of the falling and secondary particles in the environment [9–11]. From this point of view it's usage in scientific research is necessary.

Main results

The following physical model is given. Charged particle on the movement way continuously loses the energy on ionization and excitement (energy losses for each particles grade depending on energy are known and described by analytical expressions, in particular, by the Bethe-Bloch formula) [10]. Impacts happen to atoms, cores discretely. After crashes primary particles keep the movement direction. At the movement charged particles through substance their run depends on energy through the interaction section which is calculated for ions by Rutherford's formula [10]. Observations depths are according to the tables of the ion-implanted impurity spatial distribution parameters [12]. The calculated interaction section is approximated by the following expression:

$$\lambda(h) = \frac{1}{\lambda_0}\left(\frac{1}{a(E_0 - kh)} - 1\right), \qquad (1)$$

λ_0, a, E_0, k – approximation parameters, $\sigma_0 = 1/\lambda_0$.

From a recurrence relation for transition probabilities

$$\psi_n(h', h, E_0) = \int_{h'}^{h} \psi_{n-1}(h', h'', E_0)\psi_0(h'', h, E_0)\frac{1}{\lambda_0}\left(\frac{1}{a(E_0 - kh'')} - 1\right)dh'', \qquad (2)$$

we receive expression for CPF taking into account energy losses for ions in the following look:

$$\psi_n(h', h, E_0) = \frac{1}{n!\lambda_0^{\,n}}\left(\frac{E_0 - kh'}{E_0 - kh}\right)^{-l} \exp\left(\frac{h - h'}{\lambda_0}\right) * \left[\frac{\ln\left(\frac{E_0 - kh'}{E_0 - kh}\right)}{ak} - (h - h')\right]^n, \qquad (3)$$

where n – interactions number, h', h –ion generation and registration depths, $l = 1/(\lambda_0 . ak)$.

Calculations of cascade and probabilistic functions taking into account energy losses for ions depending on interactions number and particles penetration depth were carried out on a formula:

$$\psi_n(h', h.E_0) = \prod_{i=1}^{n}\left(\frac{\ln\frac{(E_0 - kh')}{(E_0 - kh)}}{\frac{ak}{\lambda_0 i}} - (h - h')\right) * \exp\left(\left(\frac{h - h'}{\lambda_0}\right) - \frac{1}{\lambda_0 ak}\ln\left(\frac{E_0 - kh'}{E_0 - kh}\right)\right). \qquad (4)$$

For optimization CPF calculation algorithms depending on interactions number and particles penetration depth, vacancy clusters concentration are used Stirling formulas [13]:

$$n! \approx n^n e^{-n} \sqrt{2\pi n} \,. \tag{5}$$

$$\ln n! \approx (n+\frac{1}{2}) \ln n - n + \frac{1}{2} \ln(2\pi) \,. \tag{6}$$

Ions spend the main energy part for ionization and excitement the environment atoms (to 99%) and only 1% goes for atomic structure defects formation. At charged particles with material interaction dot defects, Frenkel's couples, big congestions the vacancy and interstitial atoms can be formed.

Radiation defects at ionic radiation concentration calculation is carried out on a formula [11]:

$$C_k(E_0,h) = \int_{E_c}^{E_{2\max}} W(E_0,E_2,h)dE_2 \,, \tag{7}$$

$$E_{2\max} = \frac{4m_1c^2 m_2c^2}{(m_1c^2 + m_2c^2)^2} E_1 \,;$$

E_{2max} – the greatest possible energy acquired by atom, m_1c^2 – an ion rest energy. $C_k(E_0,h)$ is defined taking into account that a particle energy at h depth is $E_1(h)$. As $E_1(h)=E_0-\Delta E(h)$, that setting energy losses on ionization and excitement $\Delta E(h)$, we receive the corresponding observations h depths from a Bethe-Bloch formula. The primary beaten-out atoms spectrum is defined by the following ratio:

$$W(E_0,E_2,h) = \sum_{n=n_0}^{n_1} \int_{h-k\lambda_2}^{h} \psi_n(h') \exp\left(-\frac{h-h'}{\lambda_2}\right) \frac{w(E_1,E_2,h')dh'}{\lambda_1(h')\lambda_2} \,, \tag{8}$$

where n_0, n_1 – initial and final value of interactions number from a cascade and probabilistic function definition range. CPF $\psi_n(h')$, entering expression (8), has next appearance:

$$\psi_n(h') = \frac{1}{n!\lambda_0^n} \left(\frac{E_0}{E_0 - kh'}\right)^{\frac{1}{\lambda_0 ak}} \exp\left(\frac{h'}{\lambda_0}\right) \left(\frac{\ln\left(\frac{E_0}{E_0 - kh'}\right)}{ak} - h'\right)^n \,, \tag{9}$$

$$\lambda_1(h') = \frac{1}{\sigma_0 n_0 \left(\frac{1}{a(E_0 - kh')} - 1\right)} * 10^{24} \text{ (cm)}, \quad \lambda_2 = \frac{1}{\sigma_2 n_0} * 10^{24} \text{ (cm)}.$$

Section σ_2 is calculated by Rutherford's formula, λ_1, λ_2 – run on an ion - atomic and atom - atomic impact respectively; k– integer bigger units; $w(E_1,E_2,h')$ – PBOA spectrum in the elementary act, E_2 – primary beaten-out atom energy.

The PBOA spectrum in the elementary act is calculated on a formula:

$$\omega(E_1,E_2) = \frac{d\sigma(E_1,E_2)/dE_2}{\sigma(E_1)} \,. \tag{10}$$

Substituting expression (10) in formulas (7), (8) we receive:

$$C_k(E_0,h) = \frac{E_d E_{2\max}}{E_{2\max} - E_d} \int_{E_c}^{E_{2\max}} \frac{dE_2}{E_2^2} \sum_{n=n_0}^{n_1} \int_{h-k\lambda_2}^{h} \psi_n(h') \exp\left(-\frac{h-h'}{\lambda_2}\right) \frac{dh'}{\lambda_1(h')\lambda_2}$$

Carrying out transformations, we come to the following expression:

$$C_k(E_0,h)=\frac{E_d}{E_c}\frac{(E_{2\max}-E_c)}{(E_{2\max}-E_d)}\sum_{n=n_0}^{n_1}\int_{h-k\lambda_2}^{h}\psi_n(h')\exp\left(-\frac{h-h'}{\lambda_2}\right)\frac{dh'}{\lambda_1(h')\lambda_2}, \quad (11)$$

where E_d – average energy of shift, E_0 – initial energy of a particle, E_c – threshold energy.

To calculate radiation defects concentration on a formula (11) with usage (9) it is impossible as in each member of CPF there is an overflow. Expression for $\psi_n(h')$ it is presented in the form:

$$\Psi_n(h',h,E_0)=\exp\left(-\ln n!-n\ln\lambda_0-\frac{1}{\lambda_0 ak}\ln\left(\frac{E_0}{E_0-kh'}\right)+\frac{h'}{\lambda_0}+n\ln\left(\frac{\ln\left(\frac{E_0}{E_0-kh'}\right)}{ak}-h'\right)\right). \quad (12)$$

When calculating CPF for ions there are difficulties consisting in approximating coefficients selection and in finding real area of result both depending on interactions number and from penetration depth. The area of result is influenced by the flying particle and target atomic number, initial energy of primary particle and penetration depth. All CPF calculations for a formula (4) have been made on a C#, as the DBMS for dataful operation MS SQL Server 2014 environment was used. CPF calculations results for ions depending on interactions number and particles penetration depth are given in figures 1,2.

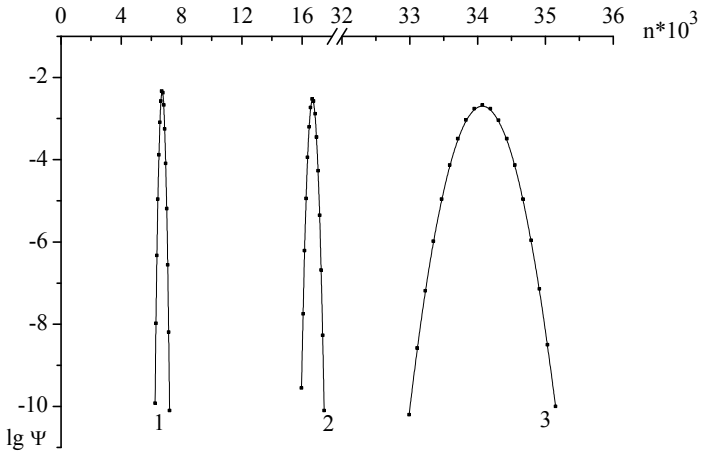

Figure 1 – CPF dependence on interactions number for the titan in iron at h=0,0001; 0,0002; 0,0003 (cm); E=1000 keV (1-3)

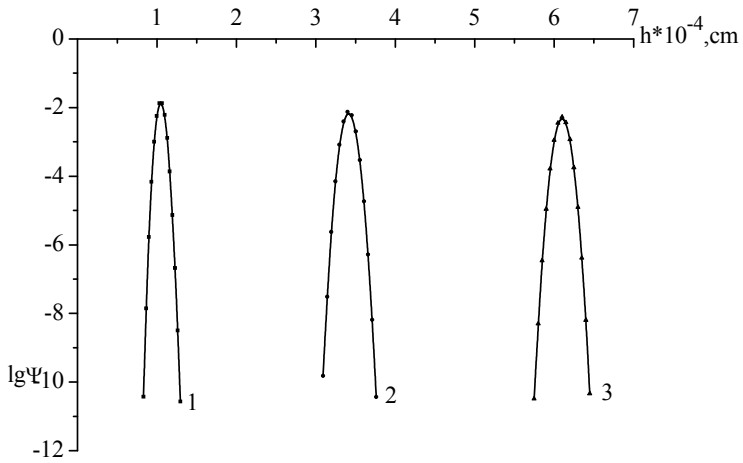

Figure 2 – Dependency $\psi_n(h', h, E_0)$, from h for aluminum in the titan at E_0 =800 keV for n= 732; 2702; 5697 (1-3)

Due carrying out CPF calculations depending on impacts number and particles penetration depth of result area behavior and a calculation step regularities are revealed. Let's note some of them. Result area behavior regularities for CPF calculated depending on interactions number consist in the following:

1. With initial energy (the flying particle and a target same) reduction with the same depth the area of result is narrowed and displaced to the left.

2. With the flying particle increase in atomic weight the area of result finding is displaced to the left relatively h/λ and is narrowed.

3. With the flying particle big atomic weight the CPF maximum value is displaced to the left relatively h/λ already with small depths, and with big depths the result is in narrow area.

4. The narrowest area of result turns out with the flying particle big atomic weight and small target on the end of a run.

At the step choice following regularities take place:

1. For the flying particle small atomic weight and small depths the step is small (about 10-20), with increase in observation depth it begins to increase.

2. With the flying particle atomic weight gain in the step respectively increases, reaching several hundred and even thousands.

3. With the flying particle big atomic weight and small targets the step considerably increases.

Let's give the regularities arising due finding a real range defined for CPF calculated depending on penetration depth:

1. Calculations shows that a small atomic weight of the flying particle and small depths area of result CPF depending on h is close to h, which corresponds h/λ. With increase in observation depth the area of result is displaced to the right and narrowed.

2. With initial energy of a particle (the flying particle and a target same) reduction with the same observation depth the area of result is displaced to the right and narrowed.

3. With increase observation in depth for any flying particle and any target the area of result is displaced to the right.

4. Depending on the flying particle atomic number at the same value of depth h the area of result is displaced to the right.

5. At the flying particle atomic number great value the area of result is displaced to the right relatively h, corresponding h/λ already with small depths and the area of result is considerably narrowed.

Step behavior regularities due CPF calculating depending on particles penetration depth are revealed.

1. For the flying particle small atomic weight the step is small, with increase in observation depth it increases, and on the end of a run very strongly.

2. With initial energy of a particle with the same observation depth (the flying particle and a target same) reduction the step also increases.

3. With the flying particle atomic weight increase for the same observation depth the step increases at first gradually, then is very sharp.

4. Step on atomic number dependence tends increase.

For automation and optimization finding CPF area of result depending on interactions number, penetration depths have been realized algorithms Ternary [14] and Binary [15] searches. The Ternary search algorithm has been modified taking into account CPF specifics: it exists in limited area. In the existing algorithms the division coefficient equal to 3 is used (ternary search). In the developed program complex the coefficient can vary. Binary (binary) search (it is also known as a halving and a dichotomy method) - the classical element search algorithm in the sorted array (vector) uses array crushing on half. It is used in computer science, calculus mathematics and mathematical programming. Ternary search is a method in computer science for finding the minimum or maximum of function, which at first strictly increases, then strictly decreases, or on the contrary. Ternary search defines that the minimum or a maximum can't lie either in the first, or in the last third of area, and then repeats search on the remained two thirds.

The concentration values calculated by a formula (11) have the following behavior: for the easy flying particles curves increase, reaching a maximum, then decreases to zero. With initial energy of a particle increase curves are displaced to the right. With increase in threshold energy E_c concentration values decreases and curves pass much below, transition through a maximum is carried out more smoothly. While energy E_0 =100 keV the curve decreases. Due the flying particle increase in atomic weight the value of function in a maximum point increases and, therefore, curves pass above while values of depths decrease. Calculation algorithms optimization with formulas (5), (6) usage is performed. After carrying out optimization in formulas (4), (11) it is visible what a counting duration was considerably reduced, for example, for germanium in aluminum at E_0 = 1000 keV, E_1 = 120 keV calculation time was 1 hour 44 minutes. After optimization calculation time has less than 1 minute. Calculations comparison results before optimization and after it is given in the table 1.

Table 1 – Definition range borders of radiation defects concentration for germanium in silicon at E_c=50 keV и E_0=1000 keV

h*10^4, cm	$C_к$, cm	E_0,keV	n_0	n_1	τ_1	τ_2
0,1	10476	1000	219	560	5'	1"
5,3	17598	800	25146	27958	10'	2"
10,6	29380	600	69624	74258	25'	3"
15,8	51189	400	147578	154312	1h	7"
18,9	77629	300	227841	236220	3h29'	15"
19,9	90354	260	264188	273220	4h12'	20"
20,9	107041	220	308961	318741	5h30'	25"
21,8	124137	180	359803	368257	7h06'	35"
22,3	123290	140	394307	403204	10h01'	1'
23,2	118373	100	474116	486299	12h41'	2'
23,9	50357	70	563193	575375	15h26'	7'
24,1	-20064	60	596160	608342	17h19'	10'

Here τ_1, τ_2 – calculation time before carrying out optimization and after it.

Calculations results of are given in figures 3-5 and in tables 2-5 [16-21].

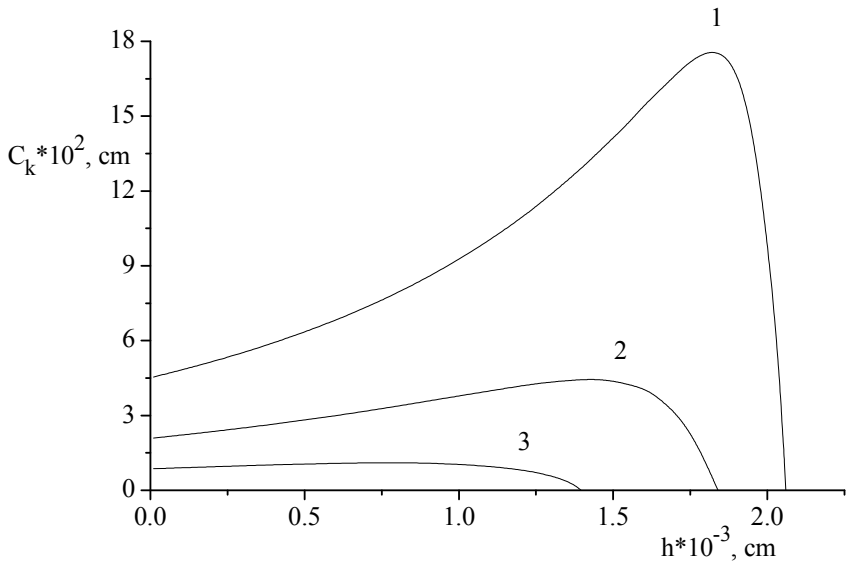

Figure 3 – Radiation defects concentration dependence on depth for the titan nitrogen ions radiation at E_0=1000 keV, E_c=50 keV(1), 100 keV (2), 200 keV (3)

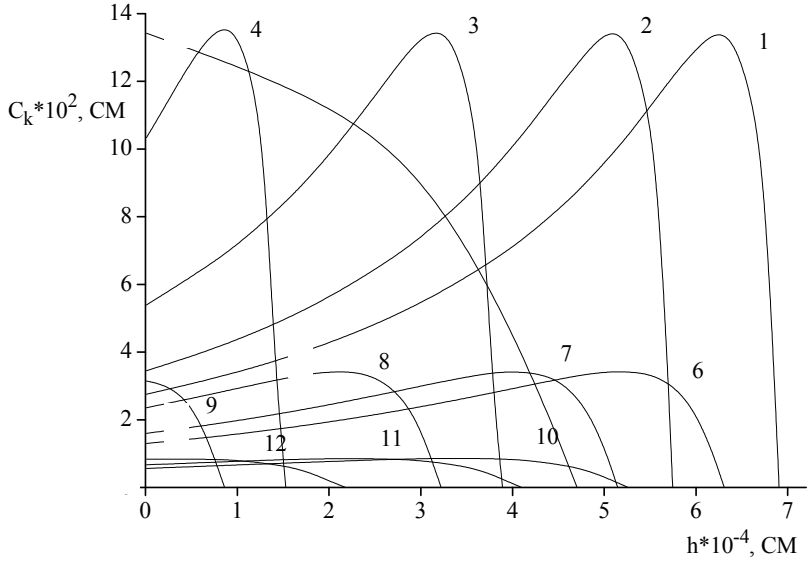

Figure 4 – Radiation defects concentration dependence on depth in the ionic radiation for nitrogen in silicon at E_c=50 keV; E_0= 1000, 800, 500, 200, 100 keV (1-5); E_c=100 keV; E_0= 1000, 800, 500, 200 keV (6-9); E_c=200 keV; E_0= 1000, 800, 500 keV (10-12)

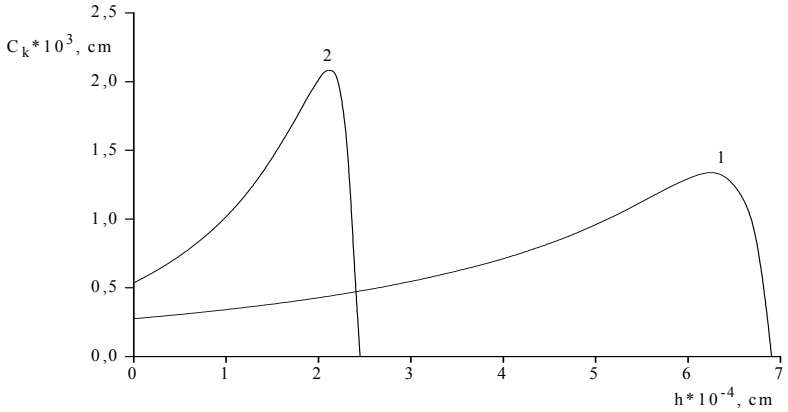

Figure 5 – Radiation defects concentration dependence on depth in the ionic radiation for nitrogen in silicon (1) and nitrogen in germanium (2) at E_0= 1000 keV; E_c=50 keV

Finding the radiation defects concentration area of result at ionic radiation has allowed to find this area's behavior regularities. Let's note some of them.

1. With increase in threshold energy with the same penetration depth value of radiation defects concentration considerably decreases, area of result borders don't change.

2. Depending on penetration depth the radiation defects concentration value increases.

3. With increase in primary particle initial energy at the same value of threshold energy and penetration depth, value of radiation defects concentration decreases.

4. The radiation defects concentration area of result borders depending on penetration depth increases, the borders change range fluctuates from 0 to 5000.

5. Depending on threshold energy at the same energy and the same penetration depth the border don't change.

Table 2 – Radiation defects concentration definition range borders for nitrogen in the titan at E_c=50 keV, E_0= 1000 keV

$h*10^4$, cm	$C_к$, cm	E_0, keV	n_0	n_1	τ
0,1	453,93	1000	0	27	1″
1,7	504,21	900	61	224	3″
3,5	569,57	800	196	439	4″60
5,4	650,76	700	376	681	6″
7,3	747,10	600	596	970	7″90
9,4	878,12	500	894	1341	9″
11,6	1050,64	400	1286	1840	13″
12,8	1165,35	350	1545	2142	14″
14	1294,26	300	1846	2474	15″70
14,5	1352,72	280	1987	2648	17″
15	1412,73	260	2138	2820	18″
15,5	1473,16	240	2301	2995	19″
16,1	1556,9	220	2514	3247	21″
16,6	1612,65	200	2709	3461	22″
17,2	1688,03	180	2967	3795	24″50
17,8	1746,76	160	3258	4105	26″
18,4	1765,86	140	3588	4455	29″
19	1695,9	120	3971	4885	31″45
19,6	1422,67	100	4422	5397	35″
20,3	677,95	80	5071	6110	41″
20,6	0	70	5406	6452	42″

Table 3 – Radiation defects concentration definition range borders for nitrogen in the aluminum at E_c=50 keV и E_0=1000 keV

h*10^4, cm	$C_к$, cm	E_0, keV	n_0	n_1
0,1	296	1000	0	32
3,5	335	900	84	310
7,1	381,5	800	250	583
10,9	439	700	469	899
14,9	511	600	751	1277
19,1	605	500	1116	1742
23,6	734	400	1607	2344
26	817	350	1923	2723
28,5	919	300	2304	3175
29,6	970	280	2493	3396
30,6	1017,6	260	2677	3611
31,7	1074	240	2895	3864
32,9	1142	220	3154	4163
34	1205	200	3414	4463
35,2	1278	180	3728	4821
36,5	1361	160	4108	5253
37,7	1422	140	4505	5703
39,1	1487,2	120	5041	6300
40,4	1460	100	5630	6965
41,9	1270	80	6465	7894
42,6	976	70	6934	8414
43,4	413	60	7558	9102
44,1	-745	50	8207	9816

Table 4 – Radiation defects concentration definition range borders for nitrogen in the silicon at E_c=200 keV и E_0= 800 keV

h*10 ^{4}, cm	$C_к$, cm	E_0, keV	n_0	n_1	τ
0,1	66,71	800	0	32	01″15
6,1	73,10	700	598	972	02″30
12,5	79,67	600	1499	2060	05″42
19,3	85,05	500	2688	3428	10″49
26,5	84,91	400	4271	5228	46″56
30,3	79,16	350	5282	6307	1′ 01″10
34,2	64,25	300	6483	7634	1′ 17″50
35,9	54,08	280	7070	8249	1′ 24″09
37,6	39,79	260	7701	8926	1′ 31″41
39,3	19,77	240	8384	9700	1′ 44″40
41,0	0	220	9124	10461	1′ 52″80

Table 5 – Radiation defects concentration definition range borders for carbon in the titan at E_c=100 keV, E_0= 500 keV

h*10 ^{4}, cm	$C_к$, cm	E_0, keV	n_0	n_1	τ
0,1	213,66	500	0	30	1″
2,1	238,34	400	132	337	4″
3,3	251,38	350	269	541	7″
4,5	255,62	300	439	769	9″
5	253,24	280	520	881	13″
5,5	246,35	260	610	994	17″
6	232,94	240	705	1110	24″
6,5	210,03	220	811	1252	26″

7,1	176,16	200	951	1423	33″
7,7	119,25	180	1109	1610	36″
8,2	24,45	160	1256	1789	11″
8,8	0	140	1456	2044	12″

Conclusions

In work, analytical expressions of cascade and probabilistic functions taking into account energy losses for ions from recurrence relations for transition probabilities are received. The approximating expression entering a recurrence relation is picked up and approximation coefficients are found, so that the theoretical correlation relation was rather high [22-24]. Algorithms are developed and optimization of calculation cascade and probabilistic functions taking into account energy losses depending on interactions number and particles penetration depth, radiation defects concentration is made at ionic radiation, calculations are carried out. Behavior regularities on CPF area of result and calculation step depending on interactions number and particles penetration depth are revealed. It is shown that the area of result is influenced significantly by the primary particle initial energy, penetration depth, the flying particle atomic number and target. Automation and optimization area of result borders selection and calculation step with ternary and binary search algorithms usage is executed. Algorithms optimization on calculation the cascade and probable functions taking into account energy losses, depending on interactions number and particles penetration depth, concentration the vacancy clusters is performed in the ionic radiation case with Stirling formula usage. Results comparison of calculation for time before carrying out optimization and after it is executed. The program complex is developed in the Microsoft Visual Studio 2015 environment in the C# programming language. The database is created in the Microsoft Server 2014 environment.

References

1. E.G. Boos, A.A. Kupchishin, A.I. Kupchishin, E.V. Shmygalev, T.A. Shmygaleva. Cascade and probabilistic method, solution of radiation and physical tasks, Boltzmann's equations. Communication with Markov's chains. -Monograph. Almaty: KazNPU after Abay, Scientific Research Institute for New Chemical Technologies and Materials under al-Farabi KazNU, 2015. – 388 p.

2. Czarnacka, K., Komarov, F.F., Romanov, I.A., Zukowski, P., Parkhomenko, I.N. AC measurements and dielectric properties of nitrogen-rich silicon nitride thin films. // Proceedings of the 2017 IEEE 7th International Conference on Nanomaterials: Applications and Properties, NAP 2017. - No. 5. P. 657-669.

3. Komarov, F.F., Milchanin, O.V., Parfimovich, I.D., Tkachev, A.G., Bychanok, D.S. Absorption and Reflectance Spectra of Microwave Radiation by an Epoxy Resin Composite with Multi-Walled Carbon Nanotubes. //Journal of Applied Spectroscopy.-2017. – Vol. 84. – No. 4. –P. 570-577.

4. Komarov F.F. Nano- and microstructuring of solids by swift heavy ions//Physics-Uspekhi. - 2017. – Vol. 187. – No. 5. –P. 465-504.

5. Komarov, F.F., Romanov, I.A., Vlasukova, L.A., Mudryi, A.V., Wendler, E. Optical and Structural Properties of Silicon with Ion-Beam Synthesized InSb Nanocrystals.// Spectroscopy.-2017. – Vol. 120. – No. 1. –P. 204-207.

6. Komarov, F.F., Konstantinov, S.V., Strel'nitskij, V.E., Pilko, V.V. Effect of Helium ion irradiation on the structure, the phase stability, and the microhardness of TiN, TiAlN, and TiAlYN nanostructured coatings. //Technical Physics.-2016. – Vol. 61. – No. 5. –P. 696-702.

7. Al'zhanova, A., Dauletbekova, A., Komarov, F., Akilbekov, A., Zdorovets, M. Peculiarities of latent track etching in SiO2/Si structures irradiated with Ar, Kr and Xe ions.-2016. – Vol. 374. – No. 1. –P. 121-124.// Nuclear Instruments and Methods in Physics Research, Section B: Beam Interactions with Materials and Atoms.-2016. – Vol. 426. – No. 1. –P. 1-56.

8. Komarov, F.F., Zayats, G.M., Komarov, A.F.,Michailov, V.V., Komsta, H.Simulation of radiation effects in SiO2/Si Structures.// Acta Physica Polonica A.-2015. . – Vol. 3. – No. 1. –P. 854-860.

9. Komarov, F., Uglov, V., Vlasukova, L., Zlotski, S., Yuvchenko, V.Drastic structure changes in pre-damaged GaAs crystals irradiated with swift heavy ions.// Nuclear Instruments and Methods in Physics Research, Section B: Beam Interactions with Materials and Atoms.-2015. – Vol. 360. – No. 4. –P. 150-155.

10. Kodanova, S.K., Ramazanov, T.S., Issanova, M.K., Golyatina, R.I., Maiorov, S.A Calculation of ion stopping in dense plasma by the Monte-Carlo method.// Journal of Physics: Conference Series.-2018. – Vol. 946. – No. 1. – P. 148-154.

11. Smyrnova, K.V., Pogrebnjak, A.D., Beresnev, V.M., Kravchenko, Y.O., Bondar, O.V. Microstructure and Physical–Mechanical Properties of (TiAlSiY)N Nanostructured Coatings Under Different Energy Conditions.// Metals and Materials International.-2018. – Vol. 24. – No. 2. –P. 241-439.

12. Kozhamkulov, B.A., Kupchishin, A.I., Bitibaeva, Z.M., Tamuzs, V.P. Radiation-Induced Defect Formation in Composite Materials and Their Destruction Under Electron Irradiation // Mechanics of Composite Materials. -2017. – Vol. 53. – No. 1. – P. 59-64.

13. Kupchishin, A.I. On positrons irradiation in the defects of vacancy type.// IOP Conference Series: Materials Science and Engineering.-2017. – Vol. 184. – No. 1. –P. 234-248.

14. Kupchishin, A.I., Niyazov, M.N., Voronova, N.A., Kirdiashkin, V.I., Abdukhairova, A.T.The effect of temperature, static load and electron beam irradiation on the deformation of linear polymers.// IOP Conference Series: Materials Science and Engineering.-2017. – Vol. 168. – No. 1. –P. 229-274.

15. Kupchishin, A.I., Kupchishin, A.A., Voronova, N.A. Cascade-probabilistic methods and solution of Boltzman type of equations for particle flow// IOP Conference Series: Materials Science and Engineering. – 2016. Vol. 110. – No. 1. – P. 123-129.

16. Kupchishin, A.I., Kupchishin, A.A., Voronova, N.A., Kirdyashkin, V.I.Positron sensing of distribution of defects in depth materials. // IOP Conference Series: Materials Science and Engineering. -2016. - Vol. 110. – No. 4. – P. 248-258.

17. Nowak, S.H., Bjeoumikhov, A., von Borany, J., Wedell, R., Ziegenrücker, R. Examples of XRF and PIXE imaging with few microns resolution using SLcam® a color X-ray camera //X-Ray Spectrometry. – 2015. – Vol. 44. – No. 3. – P. 135-140.

18. Bjeoumikhov, A., Buzanich, G., Langhoff, N., Soltau, H., (...), Wedell, R. The SLcam: A full-field energy dispersive X-ray camera.// Journal of Instrumentation.-2012. - Vol. 7. – No. 5. – P. 248-252.

19. Bock, M., Skibina, J., Fischer, D., (...), Beloglazov, V., Steinmeyer, G.Nanostructured fibers for sub-10 fs optical pulse delivery.// Laser and Photonics Reviews.- 2013. - Vol. 7. – No. 3. – P. 566-570.

20. Dubovichenko, S., Burtebayev, N., Dzhazairov-Kakhramanov, A., (...), Kliczewski, S., Sadykov, T. New measurements and phase shift analysis of p16O elastic scattering at astrophysical energies.// Chinese Physics C.-2017. - Vol. 41. – No. 1. –P. 485-495.

21. Kupchishin, A.I., Shmygalev, E.V., Shmygaleva, T.A., Jorabayev, A.B.Relationship between markov chains and radiation defect formation processes by ion irradiation.// Modern Applied Science.- 2015. – Vol. 9. – No. 3. – P. 59-70.

22. Kupchishin, A.I., Kupchishin, A.A., Shmygalev, E.V., Shmygaleva, T.A., Tlebaev, K.B. Calculation of the spatial distribution of defects and cascade- Probability functions in the materials.// Journal of Physics: Conference Series. – 2014. – Vol. 552. – No. 2. – P. 89-96.

23. Voronova N. A., Kupchishin, A.I., Kupchishin, A.A., Kuatbayeva A.A., Shmygaleva, T.A., "Computer Modeling of Depth Distribution of Vacancy Nanoclusters in Ion-Irradiated Materials".// Key Engineering Materials. – 2018. – Vol. 769. – P. 358-363.

IRSTI 44.31.31

[1,*]Z.Kh. Gabitova, [2]M. Gorokhovski, [1]A. Septemirova,
[1]A. Kalybekov, [1]G. Bulysheva

[1] Al-Farabi Kazakh National University, Almaty, Kazakhstan
[2] Ecole Centrale de Lyon, Lyon, France
*e-mail: zarina.gabitova@kaznu.kz

Numerical simulation of heat and mass transfer processes in combustion chamber of pk-39 boiler

Abstract. Over the past decades, the consumption rates of fossil energy resources has not declined, despite fundamental changes in the political, economic and social structures of society. According to experts, the share of coal in the global fuel and energy balance is more than 27%, thanks to which almost 45% of the world's electricity is generated. For each country in the world, the structure of the national energy balance is determined by the availability of its own sources of fuel and energy resources. In the Republic of Kazakhstan, coal reserves are estimated at 30 billion tons, which is 3.4% of the world's coal reserves. However, Kazakhstan's coal is characterized by low calorific value and high ash content, its combustion leads to the formation and delivery of large quantities of pollutants in air, soil and water. Pollution of the atmosphere is one of the global problems of mankind, whose solution is to optimize the combustion process and realization stringent environmental requirements for specific emissions of harmful substances with waste gases. To solve this difficult task, there is a need to improve equipment, introduce new technologies and use alternative methods for organizing a combustion process, the basis of which is to study the processes of heat and mass transfer in the presence of combustion. Irreplaceable powerful method of theoretical research of currents at availability of burning is numerical modelling. The results of a three-dimensional numerical simulation of aerodynamics, temperature flow and carbon oxides are presented. Studies have been carried out for a pulverized-angle flame of various dispersity. A comparative analysis of the obtained results with the results of the field experiment is carried out. The obtained results will allow choosing the optimal variant of the combustion process organization in order to increase its efficiency and reduce the negative impact on the environment.
Key words: simulation, coal combustion, aerodynamics, monodisperse flame, polydisperse flame, concentration fields.

Introduction

Numerical modeling is sufficiently accurate and inexpensive way to analyze complex processes that occur during combustion of the fuel in the combustion chambers of real power plants, and it allows to simultaneously consider the complex of processes that are almost impossible to do, conducting in situ experiments. Only the numerical modeling and carrying out computational experiments optimally solve scientific and project engineering tasks in this area (improvement, design of new boilers; burners upgrade; development of multistage fuel combustion systems, optimization of combustion processes and other) [1,2].

At the present stage of development of the energy industry, immediate consideration and resolution of environmental issues are required. Due to the fact, that for most countries the main sources of pollutant emissions into the atmosphere are companies operating in the burning of low-quality raw materials as well as with poorly equipped with flue gas cleaning systems, the problem of pollution of the Earth's atmosphere is an urgent. Environmentally hazardous emissions, which are products of coal combustion [3-5] reactions cause enormous damage to the earth's

ecosystem. It is therefore necessary to carry out a detailed study of physical and chemical processes that occur during combustion of energy fuels and to solve the problem of environmentally "pure" making use of coal [6,7].

Methodology of investigation

For carrying out computational experiment the combustion chamber of the real power boiler BKZ-160 Almaty TPP-3 (Kazakhstan) was selected. The boiler BKZ-160 of drum-type furnace with dry slag removal has a calculated steam generating capacity 160 t/h at a pressure of 9,8 MPa and a temperature of the superheated steam 540 0C. The boiler has a U-shaped profile with a rectangular prism furnace. Combustion chamber volume is 790 m3. On the sides of the combustion chamber located four blocks direct flow slot burners (two burners in the block) which directed at a tangent to the circle with a diameter of one meter. Each burner has a fuel mixture channel and two secondary air channel, they are located from above and from below the channel of air-fuel mixture, and divided lined piers. The top and bottom burners are also divided by a pier. In the center of burners is located oil-fired nozzle for lighting and lighting of the flame. The performance of each of the eight coal-fired burner fuels is 4 t/h.

Computational experiments on research heat and mass transfer processes have been carried out by the starting FLOREAN [8] software package, the geometry of the combustion chamber was created by a computer program «PREPROZ» (Fig. 1b). The software package FLOREAN was created to solve problems in the field of burning solid fuel and was repeatedly tested in many modern studies [1-12]. During the numerical simulation of heat and mass transfer process, the control volume method has been applied. Combustion chamber of a power boiler BKZ-160 has been divided into control volumes; it is possible to obtain 217 536 computational areas.

Numerical simulation was carried out on the basis of solutions of the Navier-Stokes equations, equations of heat diffusion and diffusion of components of the reacting mixture and the reaction products based on thermal radiation and multiphase media, equations of state, and chemical kinetics equations defining the intensity of nonlinear energy and matter [8, 13-15].

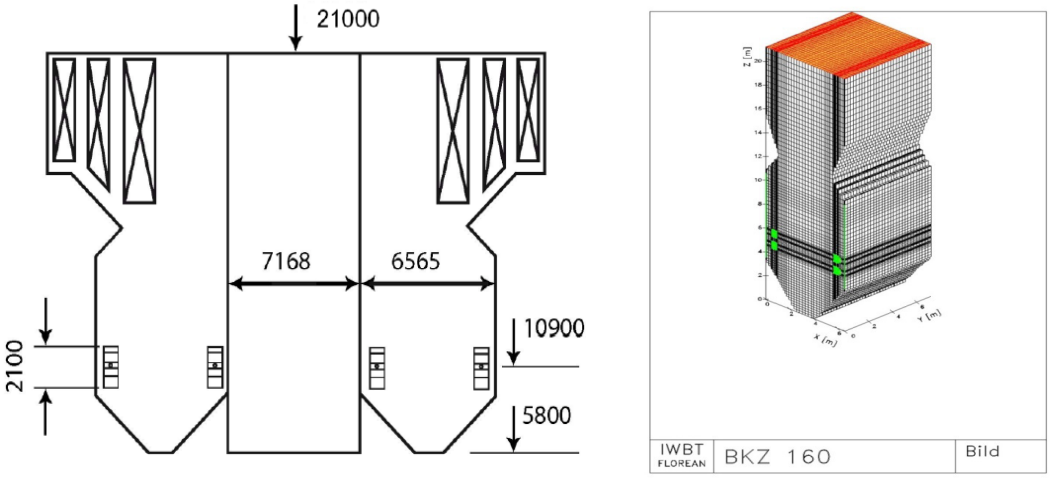

A) B)

Figure 1 – A) Scheme of the furnace,
B) General view of the camera, broken down into control volumes

For a qualitative description of combustion processes in a real three-dimensional physical and chemical system (combustion chamber of Thermal power plant) in the present work a numerical calculation of a turbulent pulverized coal flame was carried out taking into account the dispersion of coal. The percentage distribution of carbon particles

in size: dp=10 μm– 10%; dp=30 μm– 20%; dp=60 μm– 40%; dp=100 μm– 20%; dp=120 μm– 10% corresponds to a polydisperse flame, dp=60 μm– 100% – is the averaged diameter, which corresponds to a monodisperse flame. Numerical calculation in the work was carried out for the two cases listed above.

Results of numerical simulation

Let us consider the profiles of aerodynamics combustion of a turbulent pulverized flame in different sections along the length of the flame. Fig. 2 shows the distribution of the full-velocity vector in the longitudinal section of the furnace during combustion of a monodisperse and polydisperse flames. Obtained velocity fields allow us to visually analyze the aerodynamics of reacting flows in the combustion chamber. The fields of the full-velocity vector show the value of the flow velocity of the medium and its direction at each point.

In the Fig. 2 the area of fuel and oxidizer is clearly visible: counter dust and gas streams from opposing tangential burners create a vortex in the central part on the location of burners and level of active burning zone. Clearly visible is the recirculation zone with reverse gas currents [15]. Part of the flow is directed down to the funnel, forming two symmetrical vortex in the area below the burner arrangement, it is typical both for burning of a monodisperse flame and for burning of a polydisperse flame. However, in a longitudinal section of the combustion chamber symmetry is broken relative to the vertical axis of the chamber when burning polydisperse flame (Fig. 2b). It means that burning of dust and gas streams with different particle sizes affects to the character of the flow stream.

In cross-section chamber at a level between the lower and upper tiers of burners there is a clear picture of the current (Fig. 3). The pulverized coal streams flowing into the chamber deviate from the direction of the burner axes (located tangentially) towards the adjacent walls, with which they make up a smaller angle. Fusing into the total flow, the jets create a volumetric vortex with a vertical axis of rotation, which, as it rises, untwists and then moves along the axis, as can be seen clearly in Fig. 2.

The central vortical motion of the pulverized coal stream leads to uniform heating of the combustion chamber walls, to a decrease in the slagging of the heat shields and heat losses, which prolongs the life of individual elements of the boiler plant, and also increases the heat removal surface, which speaks of the advantages of the furnaces with the tangential arrangement of the burners. The aerodynamics of flow in the combustion of monodispersed and polydispersed flames has some differences; however, if it is necessary to make quick estimates, in numerical simulation of the aerodynamic characteristics of the coal combustion process, one can use the model of burning a particle of averaged size, which in turn reduces the expenditure of computer time [1, 16-21].

Being the UNFCCC framework (the United Nations Framework Convention on Climate Change) since 1995 and the Kyoto Protocol since 2009, Kazakhstan has a principled position and pursues a consistent policy in the field of preventing global climate change, in the field of reducing the carbon intensity of the economy and in the field increasing energy efficiency, creating conditions for the transition to technologies for environmentally "pure" burning of energy fuel [22]. In this connection, the study of the concentration characteristics of greenhouse gases is an urgent task.

Fig. 4,5,7 show a comparative analysis of carbon oxide concentration distributions for the case of a polydisperse and monodisperse flare. Analyzing the Fig. 4 it can be argued, the nature and pattern of carbon monoxide CO and carbon dioxide CO_2 are different from each other. Concentration of carbon oxide reaches area of the maximum values in a zone of active burning, unlike carbon dioxide which concentration increases as it moves out of the combustion chamber.

Concentrations of poly- and monodisperse flames in the field of an arrangement of burners do not differ. The average value of the concentration of carbon monoxide for polydisperse flame in the first tier of burners (z= 4,81m) is $0{,}184 \cdot 10^{-2}$ kg/kg, for monodisperse is $0{,}185 \cdot 10^{-2}$ kg/kg, in the second tier (z = 5,79m) is $0{,}279 \cdot 10^{-2}$ kg/kg both for poly- and for monodisperse flames (Fig. 4A). In the area of active burning the concentration of carbon monoxide CO reaches the maximum value, chemical processes of formation of carbon monoxide CO fade to output from the combustion chamber, for polydisperse flame at the exit of the combustion chamber the mean value is $1{,}35 \cdot 10^{-4}$ kg/kg, for monodisperse is $0{,}61\ 10^{-4}$ kg/kg (Fig. 4A).

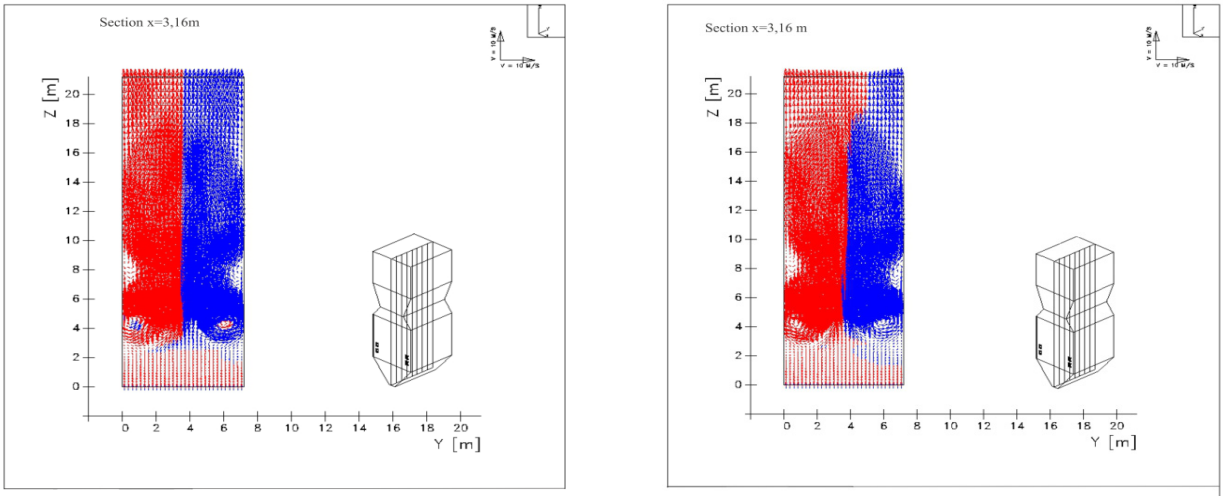

A) B)

Figure 2 – Field of a vector of full velocity in the longitudinal section of the combustion chamber (x = 3,16 m) for A) monodisperse flame; B) polydisperse flame

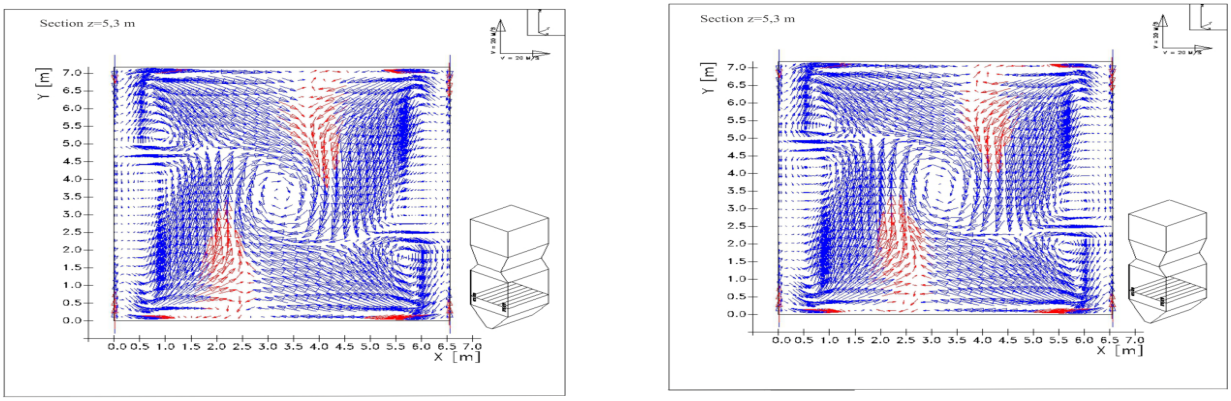

A) B)

Figure 3 – Field of a vector of full velocity in the cross-section of the combustion chamber (z = 5,3m) for A) monodisperse flame; B) polydisperse flame

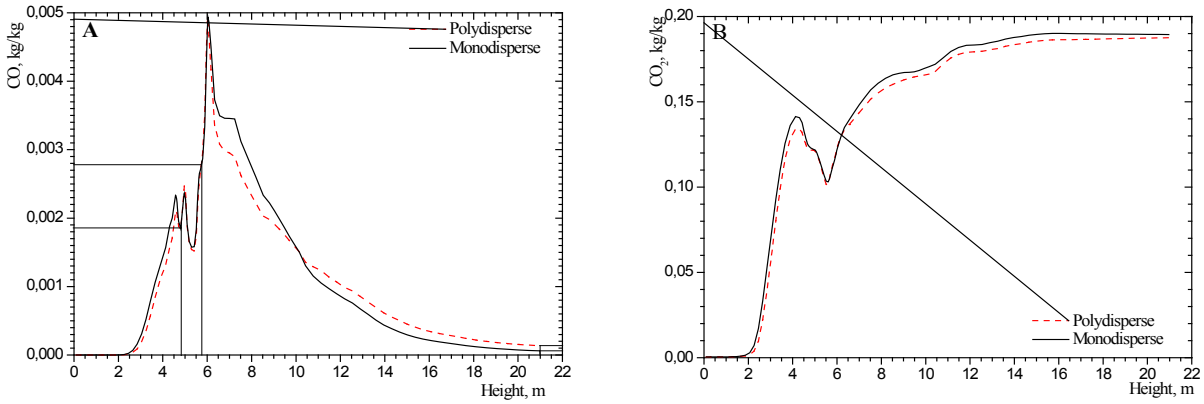

Figure 4 – Comparison of the average values of concentration A) CO, B) CO_2 for poly- and monodisperse flame on height of the combustion chamber

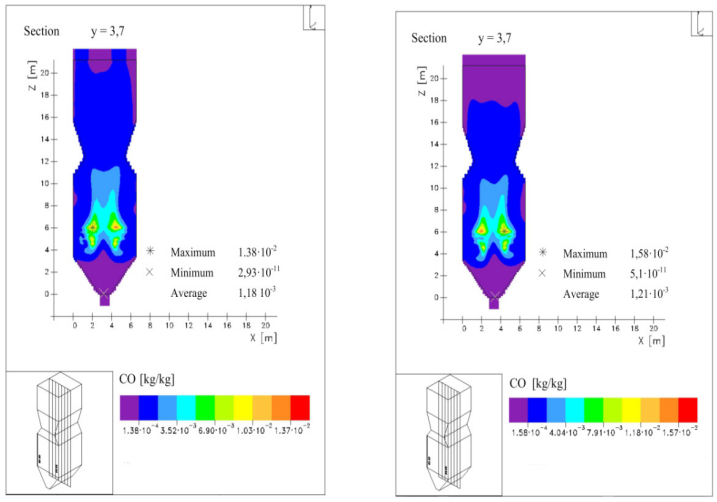

A) B)

Figure 5 – Distribution of the carbon oxide concentration in the longitudinal section of the furnace combustion chamber (y = 3,7m) for A) monodisperse flame; B) polydisperse flame

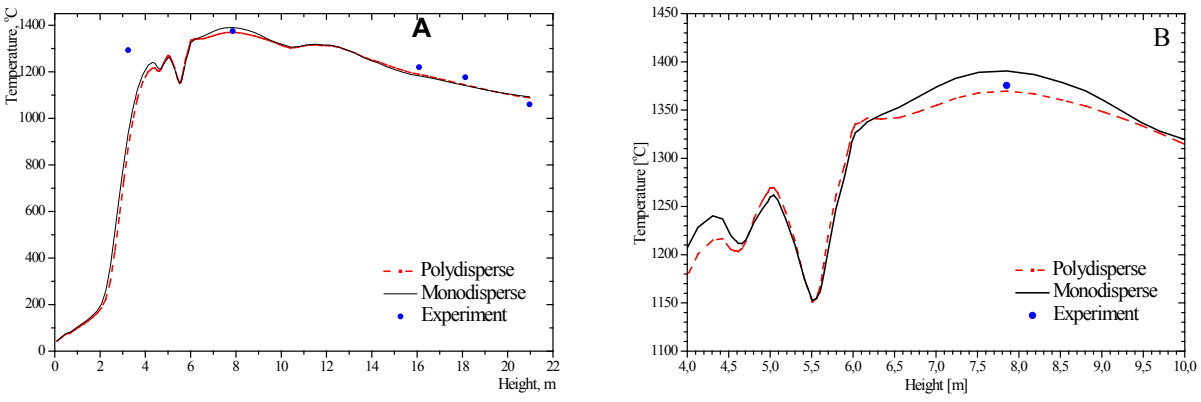

Figure 6 – Comparison of average temperature values for poly- and monodisperse flames and a comparison with the field experiment [23]: A) on height of the combustion chamber B) zone of active burning

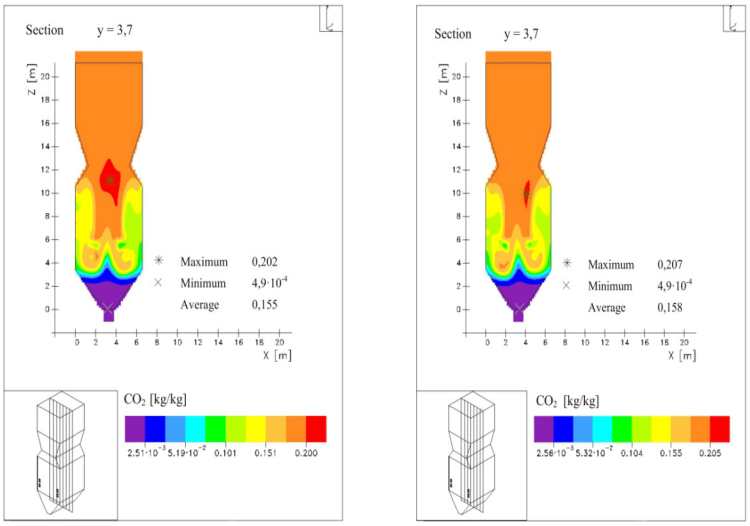

A) B)

Figure 7 – Distribution of carbon dioxide concentration in a longitudinal section of the combustion chamber of the combustion (y = 3,7m) for A) monodisperse flame; B) polydisperse flame

Analyzing the distribution of CO concentration in the longitudinal sections of the combustion chamber (Fig. 5), it can be said that in the active combustion zone, there is a clear difference in the formation of CO for a mono- and polydisperse flames, which indicates that the particle size has a significant effect on the formation of reaction products. The maximum values of carbon monoxide CO are explained by the intensive physical and chemical interaction between the fuel carbon and air oxygen, and with increased temperatures in this region (Fig. 6).

Fig. 6 shows the experimental points obtained directly from measurements at the thermal power plant [23]. It is confirmed that the numerical simulation results are in good agreement with the results of a natural experiment. It is leading to the conclusion of the applicability of the proposed physical-mathematical model of combustion processes, used in the present work. It should also be noted that the experimental data obtained directly from TPP-3 lie closer to the temperature curve of the polydisperse flame, from which it can be argued that the polydisperse flame model is more sensitive and reflects a more real process of burning pulverized coal at Almaty TPP-3.

Analyzing Fig. 4B and Fig. 7 it can be said that as flow moves out of the combustion chamber CO_2 is restored from CO, this regularity is fair both for monodisperse, and for polydisperse flames. It is possible to determine value of concentration in any point of furnace by a color scale of the received figures which is not always possible to obtain during the field experiments on the thermal power plant. So the average values of carbon dioxide CO_2 in the longitudinal section of the combustion chamber (y = 3,7m) for polydisperse flame is 0,155 kg/kg, for monodisperse flame is 0,158 kg/kg (Fig. 7). At the exit of the combustion chamber average concentration of carbon dioxide for polydisperse flame is 0,1876 kg/kg, for monodisperse flame is 0,1895 kg/kg.

Conclusion

In the present work, the calculation of aerodynamics, thermal and concentration characteristics of the combustion of mono- and polydisperse flames is performed; the results of the study can formulate the following conclusions:

– A detailed picture of the structure of the flame is obtained, which includes a developed recirculation zone with return currents of the combustion products;

– It is noted that the character of formation of the concentration fields CO and CO2 is different. The maximum concentration of carbon monoxide reaches in the zone of active combustion, and the formation of carbon dioxide CO2 increases as it moves towards the outlet from the furnace;

– The results of computer simulation of temperature T were compared with the results of field experiments, the analysis of which confirms the correctness of the chosen model of numerical experiment.

In conclusion, we note that the nature of combustion of mono- and polydisperse dust has differences, i.e. the influence of fineness of grinding has a significant influence on the processes of heat and mass transfer in the combustion chamber of CHPP boilers. The combustion model of polydisperse dust more accurately reflects the actual combustion process, which confirms the comparison with the full-scale experiment. However, the application of this model requires large computer, time resources. The results obtained in this study will give recommendations for optimizing the burning process of pulverized coal in order to reduce pollutant emissions and creations of power stations on 'pure' and an effective utilization of coal.

Also in the future, the authors of this work are planing to conduct a numerical experiment to determine other concentration characteristics of the turbulent combustion process (NO_x, SO_x, NH_3, NCN), taking into account the fineness of grinding fuel, which mutually complement each other and ensure the integrity of the entire study.

Acknowledgment

The work was carried out within the framework of the financing of the Ministry of Education and Science of the Republic of Kazakhstan. Grant No. 0115PK00599

References

1. Bekmukhamet A., Bolegenova S.A., Beketayeva M.T, et al. "Numerical modeling of turbulence characteristics of burning process of the solid fuel in BKZ 420 140-7c combustion chamber." International Journal of Mechanics 8 (2014): 112-122.

2. Askarova, Maximov, V., Ergalieva, A., et al. "3-D modeling of heat and mass transfer during combustion of solid fuel in Bkz-420-140-7C combustion chamber of Kazakhstan." Journal of Applied Fluid Mechanics 9, 2 (2016):699-709.

3. Pilipenko, N.V., Sivakov, I.A. "A method of determining nonstationary heat flux and heat conduction using parametric identification." Measurement Techniques 54 (2011): 318-323.

4. Pilipenko, N. V. "The systematic errors in determining the nonstationary heat-exchange conditions with parametric identification." Measurement Techniques 50 (2007): 880-887.

5. Askarova A. S., Bekmuhamet A., Maximov V. Yu., et al. "Mathematical simulation of pulverized coal in combustion chamber." Procedia Engineering 42 (2012):1259-1265.

6. Bolegenova, S. A., Maximov, V. Yu., A., Gabitova, Z. Kh., et al. "Computational method for investigation of solid fuel combustion in combustion chambers of a heat power plant." High Temperature 53, 5 (2015): 792-798.

7. Beketayeva M., Ospanova Sh., Gabitova Z. K. "Investigation of turbulence characteristics of burning process of the solid fuel in BKZ 420 combustion chamber." WSEAS Transactions on Heat and Mass Transfer 9 (2014): 39-50.

8. Müller, H. Numerische Berechnung dreidimensionaler turbulenter Strömungen in Dampferzeugern mit Wärmeübergang und chemischen Reaktionen am Beispiel des SNCR-Verfahrens und der Kohleverbrennung: Fortschritt–Berichte VDI–Verlag, 1992 (in German).

9. Bolegenova, S., Bolegenova, S., Bekmukhamet, A., et al. "Numerical experimenting of combustion in the real boiler of CHP." International Journal of Mechanics 7, 3 (2013): 343-352.

10. Askarova, A., Beketeyeva, M., Safarik, P. et al. "Numerical modeling of pulverized coal combustion at thermal power plant boilers." Journal of Thermal Science 24, 3 (2015): 275 282.

11. Lavrichsheva, Ye. I., Leithner, R., Müller, H., Magda, A., et al. "Combustion of low-rank coals in furnaces of Kazakhstan coal-firing power plants." VDI Berichte 1988 (2007): 497-502.

12. Karpenko, Yu. E, Messerle, V. E., Ustimenko A.B, et al. "Mathematical modelling of the processes of solid fuel ignition and combustion at combustors of the power boilers." 7th International Fall Seminar on Propellants, Explosives and Pyrotechnics, Xian 7 (2007): 672-683.

13. Leithner, R., Numerical Simulation. Computational Fluid Dynamics CFD: Course of Lecture, Braunschweig. – 2006. – 52 p.

14. Vockrodt, S., Leithner, R, Schiller, A., et al. "Firing technique measures for increased efficiency

and minimization of toxic emissions in Kasakh coal firing." 19th German Conf. on Flames, Germany 1492 (1999): 93-97.

15. Askarova, A. S., Bolegenova, S.A., Maximov, V.Y., et al. "Numerical research of aerodynamic characteristics of combustion chamber BKZ-75 mining thermal power station." Procedia Engineering 42 (2012): 1250-12-59.

16. Buchmann M. A., Askarowa A. "Structure of the flame of fluidized-bed burners and combustion processes of high-ash coal." Gesellschaft Energietechnik, Combustion and Incineration – Eighteenth Dutch-German Conference on Flames, VDI Berichte 1313 (1997): 241-244.

17. Karpenko, E. I., Messerle V. E., Ustimenko, A. B. "Plasma enhancement of combustion of solid fuel." Journal of High Energy Chemistry 40, 2 (2006): 111-118.

18. Messerle, V. E., Ustimenko, A. B., Maksimov, V. Yu., et al. "Numerical simulation of the coal combustion processinitiated by a plasma source." Thermophysics and Aeromechanics 21, 6 (2014): 747 754.

19. Askarova, A. S., Messerle, V. E., Ustimenko, A. B., et al. "Numerical simulation of pulverized coal combustion in a power boiler furnace." High Temperature 53, 3 (2015): 445 452.

20. 2Gorokhovski, M., Chtab-Desportes, A., Voloshina, I., Askarova, A. "Stochastic simulation of the spray formation assisted by a high pressure." AIP Conference Proceedings, Xian 1207 (2010): 66-73.

21. E. I. Heierle, S. A. Bolegenova, V. Ju. Maximov, S. A. Bolegenova, R. Manatbayev, M. T. Beketaeva, A. B. Ergalieva. "CFD Study of harmful substances production in coal-fired power plant of Kazakhstan." Bulgarian Chemical Communications Special Issue E (2016): 260-265.

22. Pilipenko, N. V., Gladskikh, D. A. "Determination of the Heat Losses of Buildings and Structures by Solving Inverse Heat Conduction Problems." Measurement Techniques 57 (2014): 181-186.

23. Alijarov, B. K., Alijarova, M. B. Combustion of Kazakh Coals in Thermal Power Stations and Large-Power Boiler Houses, Almaty, 2011 (in Russian).

IRSTI 29.03.85

[1,2]B.A. Iskakov, [1,2]Y.M. Tautayev, [1,2]T.X. Sadykov,
[3,4]A.L. Shepetov, [3,5]N.M. Salikhov

[1]Satbayev University, Institute of Physics and Technology, Almaty, Kazakhstan
[2]Al-Farabi KazNU, Almaty, Kazakhstan.
[3]Tien Shan Scientific Station, Almaty, Kazakhstan
[4]P.N. Lebedev Institute of Physics of RAS, Moscow, Russia
[5]Institute of Ionosphere, Almaty, Kazakhstan

Development and creation of a software system for the monitoring system mac1

Abstract. A special system of acoustic detectors was created to search for possible correlations between wide air showers and the signal of elastic oscillations from the depths of the earth's crust. They are intended for joint synchronous work with storm installation.
Key words: microphone, signals, microcircuit, program, acoustics.

A preliminary search for short-term acoustic emission signals in events related to the group passage of high-energy muons was carried out in a special experiment at the Tien-Shan high-altitude station in 2012. Upon completion of the modification of the Tien-Shan stormwater installation and the transition to regular recording of wide atmospheric showers, experiments of this kind it is expected to continue in full.

A highly sensitive microphone with a sensitivity of 20 mV/Pa in the acoustic frequency range of 500-1000 Hz is located at a depth of 50 m from the ground surface inside a well drilled in the rocky soil. The distance between the well and the storm detector system is approximately 200 m. The circuit of electronic equipment which provides registration is shown in Figure 1. The transmission of electrical signals from a microphone from the depth of a well is made over a cable line formed by a twisted pair of wires through a transformer junction. The microphone and the signal-carrying intermediate small-sized transformer are a single building block, which is completely lowered into the well. A constant voltage of ± 3V for powering the microphone is produced by an independent power source, which is built on the basis of a separate transformer with an ungrounded secondary winding and does not have direct electrical contact with the rest of the electronic circuit or the power lines of the external electrical network. From the power source to the microphone, this voltage is applied through the second pair of twisted wires. Thus, the microphone node of the measuring system is electrically isolated from all common ground lines and power supply to the electronic circuits.

Acoustic detector signals are recorded in a special room, which is located directly at the upper edge of the well. In the room are the other nodes forming the signal equipment. The differential amplifier (element D1 in Figure 1) provides 100 times the amplification of the useful signal while simultaneously suppressing common mode noise that occurs on a long link. The common mode rejection ratio of this type of amplifier is ~70 dB. At the output of the differential amplifier, bipolar sinusoidal signals are formed, belonging to the acoustic range (~102 – 104Hz) and ready for digitization by means of an ADC system. The low-frequency selector built on the operational amplifiers D2 and D3 serves to highlight the modulating amplitude of the acoustic signal of the low-frequency envelope, which is provided for registration through a separate ADC channel.

A special small-scale low-power ADC system has been developed for recording acoustic detector signals. It is placed together with the formation schemes directly at the upper edge of the well. The ADC system is based on the Raspberry PiB+ single-board computer on a Broadcom BCM2835 type microprocessor with a clock frequency of 700 MHz. This computer, through the lines of a general-purpose digital I/O port embedded in it, controls two ADC elements with AD7887 chips manufactured by Analog Devices. The clock sequences C (clock) and CS required for the operation of the microcircuits are generated by a computer microprocessor running a special driver program. The same program accepts the results of converting the input signals that come from the DO outputs of the ADC chips in the form of a serial binary code and converts them into binary data bytes. A schematic diagram of the connection of the ADC elements to the Raspberry PiB+ microcomputer is shown in Figure 2.

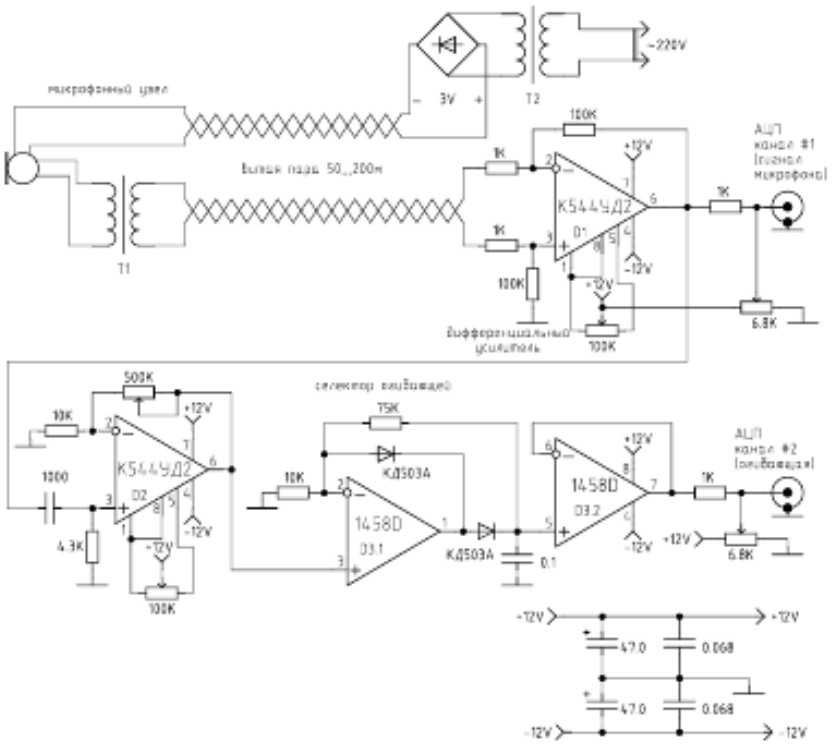

Figure 1 – Connection diagram of a microphone in an acoustic detector

The signals of the ADC microcircuits are connected to the pins of the GPIO port of the microcomputer through the buffer elements of the TTL logic. They are part of the K155LN1 chip and through resistive dividers, which are necessary for matching the level of logic signals from the microprocessor with the level of the AD7887 chip. The input analog signals are recorded over two information channels of the small-sized ADC system continuously with a period of 2 ms. Measured data is collected for subsequent on-line analysis in a file on a local disk that connects to the Raspberry PiB+ microcomputer via its built-in USB interface.

The block diagram of the software package that is used to record the data of the acoustic detector is shown in Figure 3. As can be seen in this diagram, the program interacts directly with the hardware registers built into the Raspberry PiB microcomputer parallel I/O port, to the lines of which the control signals of the ADC chip are connected k09raspi.c driver. This program is written in the compiled programming language C and is responsible for the formation, in accordance with the corresponding temporal characteristics, of two clock sequences C and CS. They provide the necessary synchronization of the ADC chips. In response to each clock cycle of

the synchronization sequence C, the next bits of the data code are received from the microcircuits, which are registered by the k09raspi.c program. on the two input lines of the parallel port. The received data bits are processed by the driver software, and parallel bytes of the 12-bit ADC code are formed from them, which are placed by this driver into a segment of shared memory that is readable by other programs.

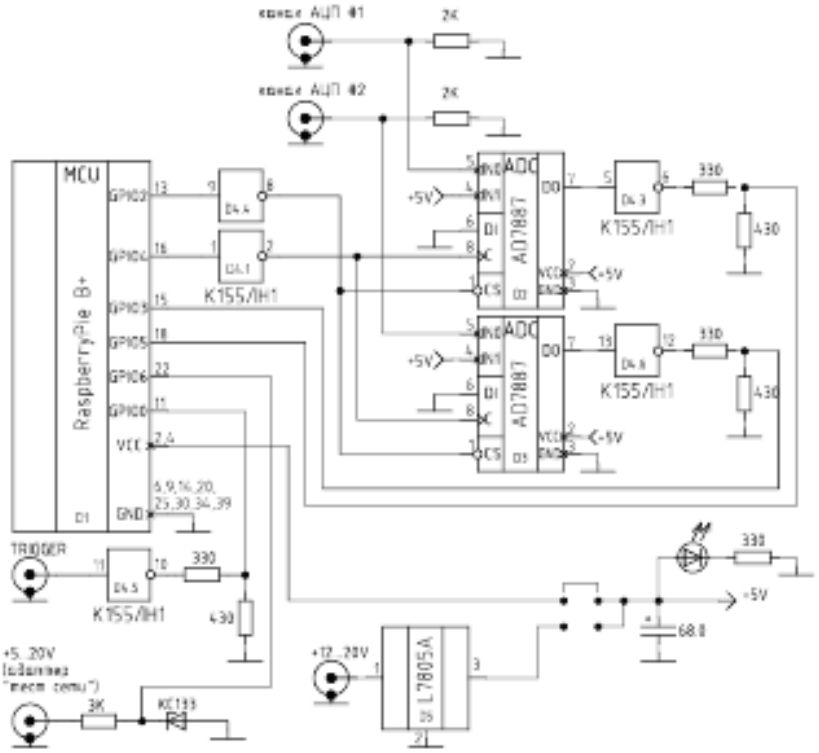

Figure 2 – Compact ADC system

Responsible for sampling the data generated by the driver from shared memory and further processing this information is the measurement management program k09001. This program performs the standard functions of supporting the measurement process, reads, immediately after launch, a set of configuration parameters from the input file k09in. It adjusts the algorithm of its work to the specifics of a specific measurement setup, tracks the appearance of new information packages in the shared memory segment, generates an array of binary data with measurement results from these packages, and writes this array to a file with the .zdat extension on the local disk. Before writing to the disk, the array is compressed by the archiver integrated into the program k09001, which reduces the total amount of output data and shortens the information exchange with the disk. Since the files recorded in this way directly during the measurements are packed in an irregular way, before they are sent for permanent storage they are processed once again by a special program – the utility k09006. It converts them into regular archive files .dat.gz, which can be read by standard archivers such as zip, gzip and the like. After the conversion, the data archive files are automatically sent to the general processing center via wireless communication lines.

Measurement management program k09001 is written in C ++ compiled programming language, which allows to satisfy rather stringent requirements for its speed. In addition, the required processing speed of incoming information is achieved due to double buffering and parallelization of operations in this program. When it starts, it creates two buffer arrays in the computer's memory to write data, at each moment of time one of these arrays is filled with current data. Information from the second at the same time is being written to the computer disk in

a separate stream of execution. The Raspberry PiB + microcomputer, which provides the process of digitizing the signals of an acoustic detector, runs on a specially adapted version of the Linux operating system. The programs included in this system ensure the performance of normal operations to support the normal operation of the entire measurement process: automatic start of the necessary utility programs, monitoring and automatic correction of the system clock, the ability to remotely connect via communication lines to monitor the system operation on-line and etc.

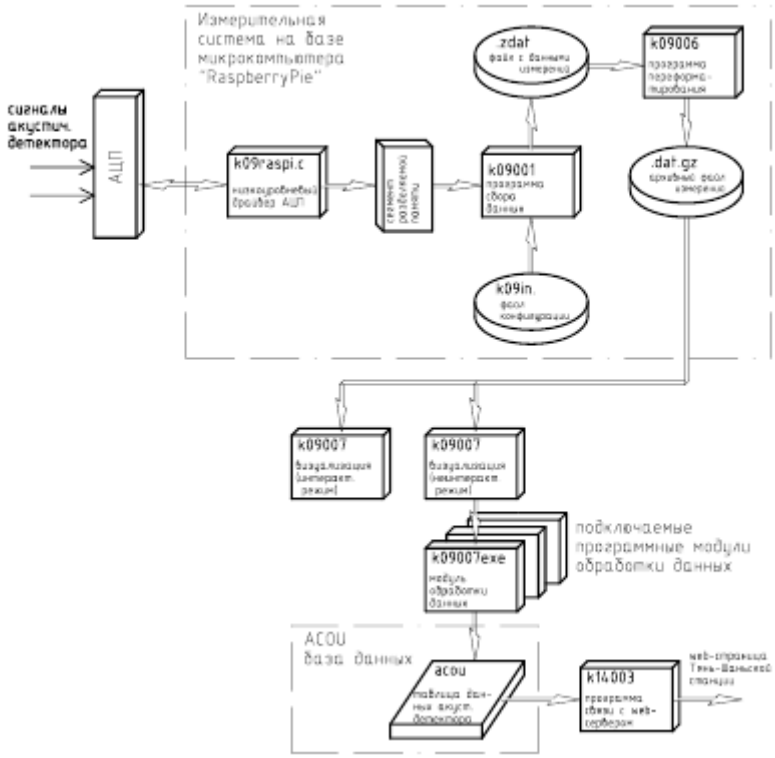

Figure 3 – Block diagram of the software system for the monitoring system

One of the specialized programs designed to work with the archived data files of the acoustic detector is the visualization program k09007, which, when launched in graphical mode of operation, allows you to view the measurement results stored in these files in the form of interactive graphs. The program k09007 is written in Python, and its graphical window interface is implemented using the Tkinter library, which is included in the standard distribution of this language. Graphs are drawn in the program window by means of the Python graphical library Matplotlib.

In addition to the interactive user mode of direct interaction with the user, the k09007 program also supports a non-interactive mode, in which information from archive files with measurement results, instead of directly displayed in the graphics window, is transmitted to external plug-in modules k09007exe, which implement various data processing algorithms, search for short peaks of intensity, etc. In particular, one of these modules is used to calculate the averaged parameters of the recorded signals: the rms values of the ADC codes, which are calculated both for the analog signal removed from the microphone and for its low-frequency envelope, as well as the number of events recorded per minute with ADC codes exceeding a number of threshold values.

Conclusion

As shown in the block diagram (Figure 3), the averaged parameters of the acoustic signal calculated in this way are loaded by the program k09007 into the special table for the acou database of the same name. The information stored in this table can be requested

by the web server to be displayed in text or graphic form on the Tian-Shan station web page. Processing requests from the web server and preparing for it the necessary information is made through an auxiliary program "CGE-general-purpose script k14003.

References

1. Berger Ch. et al. (Frejus Collab.). "Experimental study of muon bundles observed in the Fréjus detector. " Physical Review D, 40, 7 (1989): 2163.

2. Beringer, J., Arguin, J. F., Barnett, R. M., Copic, K., Dahl, O., Groom, D. E., ... & Yao, W. M. "Review of Particle Physics. " Physical Review D 86 (2012): 1-22.

3. Young, J.B., Presgrave, B.W., Aichele, H., Wiens, D.A. and Flinn, E.A. "The Flinn-Engdahl Regionalisation Scheme: the 1995 revision. " Physics of the Earth and Planetary Interiors 96, 4 (1996): 223-297.

4. Shepetov, A. L., Sadykov, T. K., Mukashev, K. M., Zhukov, V. V., Vil'danova, L., Salikhov, N. M., ... & Argynova, A. K. "Seismic signal Registration with an acoustic detector at the Tian Shan Mountain Station. " News of the National Academy of Sciences of the Republic of Kazakhstan – Series of geology and technical sciences 3, 429 (2018): 47-56.

5. Ambrosio M. et al. (MACRO Collab.). "Vertical muon intensity measured with macro at the Ggran Sasso laboratory. " Physical Review D 52, 7 (1995): 3793-3802.

6. Gusev G. A., Zhukov V. V., Merzon G. I. et al. "Cosmic rays as a new instrument of seismological studies." Bull. Lebedev Phys. Inst. 38, 12 (2011): 374–379.

7. Tribedy P. Journal of Physics: Conference Series Ser. 832 (2017) 012013.

8. Kroemer O. 2009 Proceedings of the 31st ICRC.- p. 25

9. Adamson P. et al. 2007 Phys. Rev. –Vol. D76. –P. 052003.

10. Beisembayev U., Dalkarov O.D., Sadykov T.Kh. et.al. Nuclear Instruments and Methods in Physics Research A. V.832 2016 – p.158–178.

11. G. V. Kulikov and G. B. Khristiansen. 1959 Soviet Physics JETP 35(8):441-444.

12. J. Abraham, Pierre Auger Collaboration 2010 Physics Letters B – V685. – p. 239–246.

13. M. Witek 2017 EPJ Web of Conferences 141, 01007.

Contents